

**SYNTHESIS, CHARACTERIZATION AND POSSIBLE  
APPLICATIONS OF PROTEIN LIPID AND PROTEIN  
GOLD COLLOID BIOCOMPOSITE MATERIALS**


THESIS SUBMITTED TO  
**THE UNIVERSITY OF PUNE**  
FOR THE DEGREE OF  
**DOCTOR OF PHILOSOPHY**  
IN  
**PHYSICS**

BY

**Mr. Anand M Gole**

**PHYSICAL CHEMISTRY DIVISION  
NATIONAL CHEMICAL LABORATORY  
PUNE 411 008  
INDIA**

**FEBRUARY 2002**



***Dedicated  
to my  
Parents and  
Teachers***

## CERTIFICATE

This is to certify that the work discussed in the thesis entitled "**SYNTHESIS, CHARACTERIZATION AND POSSIBLE APPLICATIONS OF PROTEIN LIPID AND PROTEIN GOLD COLLOID BIOCOMPOSITE MATERIALS**" by **Mr. Anand M. Gole**, for the degree of Doctor of Philosophy was carried out under my supervision in the Physical Chemistry Division of National Chemical Laboratory, Pune. Such material as has been obtained by other sources has been duly acknowledged in this thesis. To the best of my knowledge, the present work or any part thereof, has not been submitted to any other University for the award of any other degree or diploma.

Date:

Dr. Murali Sastry

Place: Pune

( Research Guide)

# TABLE OF CONTENTS

## CHAPTER I: Introduction

	Page Nos
1.1 Understanding Nature	2
1.2 The Changing Tradition: Need for Interdisciplinary Work	4
1.3 Different Types of Interactions	7
1.4 Protein-Lipid Interactions	9
1.5 Biomolecule-Colloidal Nanoparticle Interactions	11
1.6 Different Protocols for Protein Immobilization	11
1.7 Method Described in this Thesis	20
1.8 References	22

## CHAPTER II: Experimental Techniques

2.1 Thermal Evaporation of Fatty Lipids	31
2.2 Langmuir Blodgett (LB) Technique	33
2.3 Quartz Crystal Microgravimetry	35
2.4 UV-visible Spectroscopy	38
2.5 Fourier Transform Infrared Spectroscopy (FTIR)	41
2.6 Fluorescence Spectroscopy	44
2.7 X-Ray Diffraction	45
2.8 Scanning Electron Microscopy	46
2.9 Transmission Electron Microscopy	47
2.10 X-ray Photoelectron Spectroscopy	48
2.11 Ellipsometry	49
2.12 Contact Angle Measurements	52
2.13 Biocatalytic Activity Measurements	53
2.14 References	53

## CHAPTER III: Formation of Protein-Lipid Biocomposite Films

3.1 Introduction	58
3.2 Self - Organized Multilayers (SOMs)	59
3.3 Entrapment of Heme-Proteins into Thermally Evaporated Fatty Lipids	59
3.4 Methods for Enhancing the Protein Diffusivity in the Lipid Matrix	66

<b>3.5</b>	<b>Diffusion of Protein into Fatty Lipids: Role of Protein Charge: Mass (e/m), Total Protein Charge and Protein Hydrodynamic Radii</b>	<b>71</b>
<b>3.6</b>	<b>Monitoring Cyt c Redox Activity</b>	<b>74</b>
<b>3.7</b>	<b>Protein Native Structure Studies</b>	<b>75</b>
<b>3.8</b>	<b>Summary</b>	<b>76</b>
<b>3.9</b>	<b>References</b>	<b>77</b>

#### **CHAPTER 4: Immobilized Biocatalysis: Stability and Biological Activity**

<b>4.1</b>	<b>Introduction</b>	<b>81</b>
<b>4.2</b>	<b>Deposition of lipid films</b>	<b>83</b>
<b>4.3</b>	<b>Quartz Crystal Microgravimetry</b>	<b>84</b>
<b>4.4</b>	<b>Native Structural Studies</b>	<b>88</b>
<b>4.5</b>	<b>Chemical Analysis of Enzyme-Lipid Composites</b>	<b>92</b>
<b>4.6</b>	<b>Biocomposite Formation: Intercalation or Surface Adsorption?</b>	<b>93</b>
<b>4.7</b>	<b>Biocatalytic Activity Measurements</b>	<b>94</b>
<b>4.8</b>	<b>Summary</b>	<b>105</b>
<b>4.9</b>	<b>References</b>	<b>105</b>

#### **CHAPTER 5: Formation of Patterned Assemblies of Nanobiocomposites**

<b>5.1</b>	<b>Introduction</b>	<b>109</b>
<b>5.2</b>	<b>Different Strategies Used for Patterning</b>	<b>109</b>
<b>5.3</b>	<b>Patterned Protein-Lipid Biocomposites</b>	<b>112</b>
<b>5.4</b>	<b>Formation of Patterned Nanoparticle Thin films</b>	<b>121</b>
<b>5.5</b>	<b>Summary</b>	<b>124</b>
<b>5.6</b>	<b>References</b>	<b>125</b>

#### **CHAPTER 6: Formation of Protein-Gold Colloid Bioconjugates**

<b>6.1</b>	<b>Introduction</b>	<b>132</b>
<b>6.2</b>	<b>Immobilization of Biomolecules onto Polymer Microspheres</b>	<b>132</b>
<b>6.3</b>	<b>Immobilization of Biomolecules onto Inorganic Particles</b>	<b>134</b>
<b>6.4</b>	<b>Synthesis of Bioconjugates</b>	<b>137</b>
<b>6.5</b>	<b>UV-Vis Spectroscopy Studies</b>	<b>138</b>
<b>6.6</b>	<b>Morphology of the Bioconjugates</b>	<b>140</b>

<b>6.7</b>	<b>Determination of Size of Colloidal Gold in the Bioconjugate System</b>	<b>141</b>
<b>6.8</b>	<b>Native Conformation of the Enzyme in Bioconjugate Systems</b>	<b>143</b>
<b>6.9</b>	<b>Biocatalytic Activity Measurements</b>	<b>147</b>
<b>6.10</b>	<b>Summary</b>	<b>150</b>
<b>6.11</b>	<b>References</b>	<b>151</b>

## **CHAPTER 7: Conclusions**

<b>7.1</b>	<b>Summary of the Work</b>	<b>156</b>
<b>7.2</b>	<b>Scope for Future Work</b>	<b>157</b>
<b>7.3</b>	<b>References</b>	<b>158</b>

## ACKNOWLEDGEMENTS

*It gives me great pleasure to express my deep sense of gratitude and sincere thanks to my research guide Dr. Murali Sastry, Physical Chemistry Division, National Chemical Laboratory, Pune. His encouragement and scientific temperament furthered my interest in physics and chemistry and its relevance to biological systems. His tireless enthusiasm was always a source of inspiration. I am most indebted to him for encouraging and motivating me for a career in science.*

*I would like to acknowledge in a special way my parents who were extremely patient and tolerant towards my erratic hours of work and constantly encouraged me to excel in whatever I did. A special mention of thanks goes to my dear sister, brother in law and nephew who have always extended their help whenever I needed the most.*

*I wish to thank Dr. P. Ganguly and Dr. S. K. Date, former and present Heads, Physical chemistry Division, for their constant support and encouragement.*

*It gives me pleasure to thank Dr. (Mrs.) Mala Rao for her valuable suggestions and making the facilities available for the biological characterization done in this work. Her constant support was invaluable and went a long way towards the completion of this thesis.*

*My sincere thanks also goes out to Dr. Anil Lachke for his timely help and advice during the course of this work.*

*I would also like to thank Drs. K Vijayamohanan, Anil Kumar, D V Paranjape, I S Mulla, S D Sathye, K R Patil and N Iyer.*

*Working under a single roof, it was a pleasant company of Mr. Natarajan and Ms S. Adyanthaya who have always helped me in one way or the other.*

*My sincere thanks to Dr. S. Sivaram, Head, Polymer Division, NCL, and Dr. Ms. Aditi Pant, Head, Biochemical Sciences, NCL for making available the UV-vis spectrophotometers. I would also like to thank Dr. K.N. Ganesh, Head, Organic Chemistry Synthesis, NCL for providing the Fluorescence Spectroscopy facility. I take this opportunity to place on record my sincere thanks to Drs. Gopinathan for the FTIR characterization, S. R. Sainkar for SEM measurements, Ms. N. R. Pavaskar and Mrs. A. Mitra for the XRD characterization, and A.B. Mandale for XPS measurements. I'm thankful to Dr. M. Bhadbhade, Mr. Rajesh Gonnade and Ms. Renu Parischa for helping with TEM measurements.*

*This page would be incomplete without the mention of my seniors Drs. K.S. Mayya and Vijaya Patil who have gone out of their way to help me in various capacities and in*

*getting me familiarized with all the lab facilities and making me feel at home during my initial days of Ph.D. Also a special thanks to Mr. Milind Bargaje for his constant support and motivation. I would like to take this opportunity to thank my labmates who have helped me in all possible ways and have been my extended family during the tenure of my work at NCL. Thank you Madhu, Neeta, Ashavani, Vidya, Saikat, Sumant, Chinmay Damle, Reddy, Debabrat, Jaspreet, Kannan, Shankar, Anita, Chinmay Soman, Maya, Juilee, Prajakta, Anamika, Avantika, Trupti, Deepti, Rahul and Sarita.*

*I would like to give a special thanks to my colleagues Chandravanu Dash, Sudeep George and Santosh Vyas for their constant help.*

*A special mention of thanks to my friends in NCL, Varsha, Aslam, Kholam, Avinash and Shrojal.*

*My heartfelt thanks to my friends Amol, Srinivasan, Ajit, Vaibhav, Vshal, Satish, Rakesh, Shiva, Sanjay, Sanju for their invaluable companionship.*

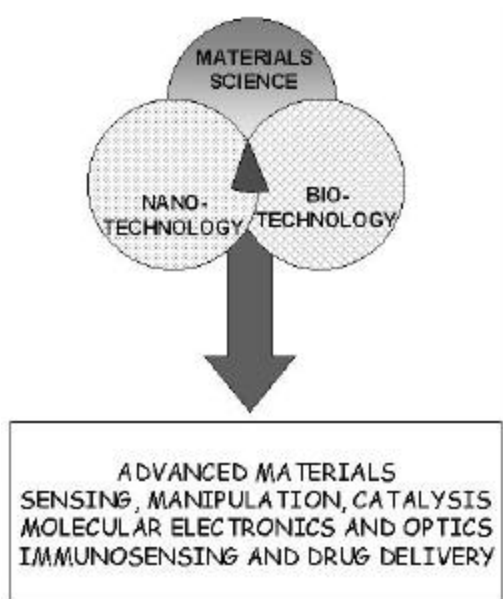
*I'm grateful to the director Dr. P. Ratnasamy, NCL, for giving me the opportunity to work in this institute and making most of the facilities available for carrying out research.*

*Dr. Murali Sastry's Young Scientist Award project and CSIR, New Delhi is gratefully acknowledged for valuable support in the form of Research Fellowships.*



# CHAPTER I

## INTRODUCTION



---

This chapter explains the complexities involved in understanding nature and drawing inspiration from nature for studying and developing novel materials. It emphasizes the need for studying protein-lipid interactions, need for immobilization of proteins/enzymes onto 2-D and 3-D supports. The different protocols currently in vogue for immobilization of biomolecules, their advantages/disadvantages have been discussed. This chapter also briefly describes immobilization of enzymes onto colloidal gold. The role of different interactions between proteins and 2-D and 3-D templates has also been discussed.

---

## 1.1 UNDERSTANDING NATURE.

Nature abounds with variety, beauty, specificity and complexity. The main purpose of all sciences is to understand nature, how things work, and try to mimic nature for the development of new materials. Prof. Henri Poincaré comments *"Science is facts; just as houses are made of stones, so is science made of facts; but a pile of stones is not a house and a collection of facts is not necessarily science."* Observation, reason and experiment make up the scientific method, which was devised to answer questions and understand natural processes. The real charm and complexity of nature is brought out when one starts studying biology, the science of life. The human body or for that matter any living organism, can be described as a community of molecules wherein individual molecules scurry about like ants, each performing its designated task so as to ensure the well-being of the society as a whole. Some gather food, some build structures in which they all dwell, others seek out and repel foreign invaders. Of course, each of these molecular workers is driven not by some autonomous consciousness but by the principles of physical and chemical sciences.<sup>1</sup> One can enumerate several examples in this direction, wherein one can admire how beautiful the things work in harmony and in symbiosis, yet very little is understood about them. The very fundamental question about the origin of life on earth is still disputed.<sup>1</sup> Some believe that the reaction between elements present in the primordial era led to the generation of basic building units for life. Some dispute the origins of life to be extraterrestrial when meteorites deposited organic molecules on earth. Another such puzzling aspect is the origin of chirality. Why natural amino acids prefer the 'L' form to the 'D' form and the reverse for the sugars in carbohydrates.<sup>1</sup> The very basic entity on which all the life depends, water, is an interesting molecule. The unusually high dielectric constant, high boiling point, its anomalous behavior at 4 °C, its solvent properties, hydrogen bonding etc are some of the novel properties it possesses.<sup>2a</sup> Hydrophobicity, which is related to organization of molecules in presence of water, is a key factor responsible for the biomolecule structure. The 'choosy' behavior of the individual biomolecules about whom to interact with is a very interesting fact and widely known as the 'molecular recognition phenomena'. How biomolecules are able to pick out their designated targets amidst a vast horde of other molecules, many of which look almost identical is a question still unanswered.<sup>1</sup> Protein folding is another such area, where research is

still in progress to determine the driving forces. It is thought provoking to reason out why any lyophilized protein added to aqueous solutions (under appropriate conditions) would fold in the same structures all the time and within very short intervals of time! Molecular self-assembly or self-organization is the key to unravel such processes. Another interesting example as to how nature develops strategies to sustain life is that of anti-freeze proteins (AFPs).<sup>2b,c</sup> The extreme low temperature conditions faced by the fishes and insects living in the polar regions could freeze the serum in their blood. This is avoided by AFPs, which are structurally diverse class of proteins that inhibit the growth of ice, by binding to its surface and avoiding nucleation and growth.<sup>2b</sup> The mechanism of ice growth inhibition is still unclear. Some believe it to be due to the specific amino acid residue matching with the spacing of water molecules in ice along appropriate planes.<sup>2b</sup> Others argue that the origin of this inhibition is possibly due to hydrophobic effect.<sup>2c</sup> Furthermore, the formation of biological minerals that make up bones, teeth, or shells, is one of the most intriguing examples of Nature's unique capabilities to program the genesis of macroscopic forms genetically.<sup>2d</sup> In such processes, nanometer-sized building blocks of mineral crystals are deposited in an organized fashion in the cellular or extracellular matrix of living organisms to build a macroscopic structure. Magnetotactic bacteria, is a good example wherein Nature uses inorganic materials for navigation.  $\text{Fe}_3\text{O}_4$  nanoparticles coated with a magnetosome membrane (which prevents agglomeration) are present in these bacteria, which are used for migration along the geomagnetic field lines.<sup>2e</sup> The real beauty of how nature can do interesting chemistry in very small regions of space can be seen in biological cells.<sup>1</sup> Cells are the fundamental units of life and are exceedingly complex and refined machines, with a variety of complex chemical reactions occurring simultaneously and symbiotically, that are far beyond those of current man-made machines. Proteins, which are synthesized by DNA, are the very fabric of which cells are made. Some proteins also act as enzymes, the molecular workhorses that drive the chemical reactions of life. Now, what happens when proteins are no longer needed or fail to fold correctly? Nature has an answer for this too! Structures called proteasomes inside cells continuously destroy proteins, break them down to the basic building blocks-amino acids-which are eventually recycled to make new proteins.<sup>2g</sup> There are other big proteins called molecular chaperons, that assist the folding of an

awkwardly unfolded protein or a protein 'stuck' in an unfavorable confirmation. All this interesting and complicated chemistry has a boundary or a wall known as a membrane that provides compartments of defined sizes, shapes and microenvironments. They organize living matter in the cell, create a fluid two-dimensional matrix, and allow for the controlled transport of solutes.<sup>1</sup> Such cellular functions as recognition, fusion, endocytosis, exocytosis, intercellular interaction, excitability, translocation, transport, and osmosis are all membrane mediated processes. Membrane of plant and animal cells is typically composed of 40-50% lipids and 50-60% proteins. Proteins bound to this lipid membrane act as signal transducers, transmitting signals from the *world outside* the cell to its interior. Studies on protein-lipid interactions are thus an area of great interest for addressing a number of fundamental issues. A part of this thesis is devoted to the study of protein-lipid interactions.

To summarize, understanding nature is surely interesting and a tough job on hands. Prof. Richard Feynman<sup>3</sup> makes one very interesting remark on the process of understanding nature. He describes understanding nature similar to amalgamating pieces in a jigsaw puzzle wherein some fit and some don't. He describes: "*Whether there are a finite number of pieces, and whether there is even a border to the puzzle, is of course unknown. It will never be known until we finish the picture, if ever.*" In spite of the difficulties encountered, the field of science is fascinating and researchers plunge into this field due to pure passion. Prof. Albert Einstein quotes "*If we knew what it was we were doing, it would not be called research, would it?*"

## **1.2 THE CHANGING TRADITION: NEED FOR INTERDISCIPLINARY WORK.**

Early years in understanding nature was divided into different branches of basic sciences.<sup>1</sup> Physics was concerned in the deepest mysteries of the universe, issues such as where did everything come from? What will happen to it all? What is matter? What is time? etc. Chemistry dealt with creating new substances, compounds with varying properties and applicability for industrial processes, enhancing rates etc. Biology was involved in studying life, diseases, and as to how we evolved from sea.<sup>1</sup> Science is changing and now it pays little regard to the disciplines into which it had been traditionally divided. Though, at college level, science is still taught as distinct traditional disciplines. But researchers believe that novel concept, ideas and views are emerging through interdisciplinary work which is changing the entire overview. To

find solutions in different branches of science requires a collective effort of researchers working in various areas of the basic sciences.

The two areas of tremendous current interest and applications are that of biotechnology and nanotechnology, where inputs from physics, chemistry and biology are of great value. This may be called the area of "*The colloidal Domain*" or that of "*nanobiotechnology*" where physics, chemistry, biology and technology meet. At the mesoscopic scale, (sizes of typically nanometer to micrometer range) the properties of materials are completely different from that of individual atoms or that of the bulk. This so called area of nanotechnology was first thought of by Prof. Feynman and talked of in his famous talk at Caltech : "*There is plenty of room at the bottom.*"<sup>4</sup> Since then, tremendous research and search for application potential for this new state of matter has been observed. As has been shown in the scheme on the title page, the combination of different branches of colloid chemistry for the research and design of completely new class of materials with tremendous applications has been a major goal of researchers during the recent past.<sup>5</sup> With the advent of nanobiotechnology, which is the bioconjugation of different chemicals/ biomolecules onto efficient nano templates has resulted in early detection of diseases, toxic gases, glucose monitoring, food testing etc.<sup>5a</sup> Nanobiotechnology has also helped in studying different aspects of design and development of molecular motors.<sup>5d</sup>

Although nature has provided us with a tremendous selection of substances with which to construct civilizations and improve the lives of its citizens, their range and abundance appears insufficient to meet our every need. The great variety of complex substances found in the living world, particularly in plants, has proved to be immensely valuable to physicians throughout the ages, but there are ailments for which natural cures are rare, ineffective or nonexistent. Many chemists are therefore engaged in the enterprise of creating purely artificial substances that provide cheaper or more potent alternatives, or which can fill the gaps.<sup>1</sup>

Another such area where insights from different branches of basic science are valuable is the area of materials science.<sup>1</sup> The dawn of the plastic age has unambiguously demonstrated that we are no longer forced to manage as best we can with the materials that the natural world provides-we can design new ones that better suit our purposes. Plastics show a variety of properties: they show tensile strengths comparable to steel, can be biodegradable, conduct

electricity, change color or contract and flex like muscles.<sup>1</sup> Control over the growth of materials atom by atom, opens up new possibilities in semiconductor microelectronics (nanotechnology and molecular electronics) and mimicking the design of natural substances like bone and shells (biomineralization). Furthermore, the ultimate dream in electronic industry, which is achievable, is to build circuits from individual molecules, using conducting molecular wires to link up atomic-scale components into incredibly compact "molecular devices".

Instrumentation technology has also advanced in the recent years. The interaction between two molecules may take place in less than a few thousandths of seconds. In the past, attempts to discover exactly what goes on when molecules get together, had been a problem. Of late, pulsed lasers that pump thousands of discrete light pulses often in picoseconds, has enabled researchers to capture "snap shots" of incredibly fast events, even those of protein folding. Furthermore, the art of "seeing" has improved from the micron level (ordinary optical microscope) to atomic level (electron and tunnelling microscopes).

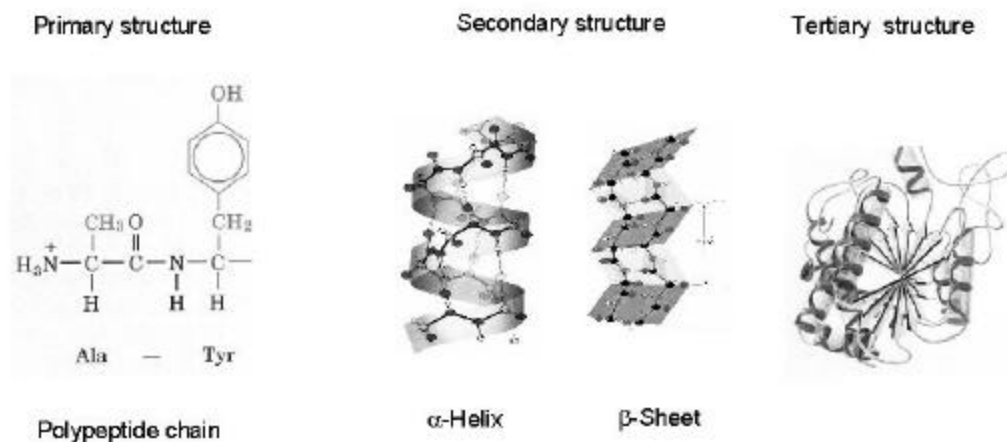
Energy generation is another area where research is currently focussed. We receive millions of megawatts of energy for free everyday by courtesy of the Sun, but have few efficient means of capturing this energy and converting it to more useful forms. Solar cells are the answer, wherein materials that absorb light and convert it to electricity are used. The trend is also changing from the use conventional direct band gap semiconductors for this purpose, to the more useful nanoparticles or quantum dots.

All the above examples stress the necessity of interdisciplinary work for the betterment of life as a whole and towards generation of advanced materials. Nanobiotechnology is one such area of interdisciplinary work, wherein contributions from physical sciences (quantum mechanical inputs, microscopy and explanation of physical phenomena), chemistry (efficient synthetic/fabrication protocols, electrochemistry, novel reactions) and biology (enzymology and protein science, molecular biology, drug delivery etc) come together to offer synergetic opportunities. Furthermore, the main driving force in nanobiotechnology comes from understanding nature, how it works and following the principles nature uses, for the development of self organizing, self replicating and self assembling advanced materials. If we want to build molecular structures one molecule at a time, we will need much more precision

and speed at manipulation than is available to today's engineers of the microworld.<sup>1</sup> But there is an alternative to this: get the molecules to assemble themselves. This might seem like expecting a house to suddenly leap together from a pile of bricks, but molecules are much more versatile than bricks. The better we understand the way the molecules interact, the more able we would be to design them so that they assemble themselves into these intricate structures. Here, again, there is much to be learned from nature, which abounds with molecules that can recognize and team up with others in very specific and organized ways.<sup>1</sup> Replication is another area, where we can have clues from nature. Small synthetic molecules can replicate even in a test tube and these molecules represent the first step towards a kind of artificial life.<sup>1</sup> Specificity is another issue where biology can help. In a chemical reaction, extracting one's intended product from a whole host of substances produced in side reactions, is usually a messy affair. This does not happen in the biochemistry of the body, where each reaction generally gives just the one desired product, and we are now learning from this to make chemistry more specific. Synthetic molecules that mimic enzymes have been designed for more specificity in a chemical reaction. So in all, nanobiotechnology, which is in essence the topic of this thesis, comprises an interdisciplinary work involving the combination of different basic sciences, exploiting principles nature uses to organize things, combined usage of different non-covalent interaction towards the realization of advanced materials. The famous artist Leonardo da Vinci once quoted: "*When Nature finishes producing its own species, man begins, using natural things and with the help of this nature, to create an infinity of species.*"

### **1.3 DIFFERENT TYPES OF INTERACTIONS.**

Proteins/enzymes are macromolecules, which are extremely sensitive to the environmental conditions. A number of interactions are therefore responsible for the stability of biomolecules and various processes that occur through them. The primary, secondary and the tertiary structure of proteins have been shown in Scheme 1.3 below. Nature has devised several strong and weak interactions, which impart overall structure and stability to the protein.



**Scheme. 1.3:** The various structures of the protein have been displayed. Primary structure: simple polypeptide chains. Secondary structure:  $\alpha$ -Helices,  $\beta$ -pleated sheets or random coils; Tertiary structure: weak interaction between  $\alpha$ -Helices,  $\beta$ -pleated sheets or random coils forming the overall structure of the protein.

Covalent interactions in particular gives rigidity to the structure of a biomolecule, viz. the peptide bonds and S-S bond cross linking the cysteine residues which defines stable protein primary, secondary and tertiary structures respectively. These directional, short-range forces are of the order of interatomic separations (0.1 - 0.2 nm), with energy of the order 100-300 kT. Secondary interactions such as electrostatic, dipolar, van der Waals forces, hydrogen-bonding interactions, hydrophobic and hydrophilic interactions, and steric interactions play a key role in the various interactions associated with biomolecules and impart overall stability and structure to the biomolecule. Indeed, the phenomenon of self-organization may have been responsible for the emergence of life itself.<sup>6</sup> The processes such as, the formation of the DNA double-helix,<sup>7a</sup> the process of protein and ribonuclease folding,<sup>7a,b</sup> and protein aggregation,<sup>7b</sup> as well as molecular recognition events (antigen-antibody interactions),<sup>7a,b</sup> formation of lipid bilayers,<sup>7c-e</sup> vesicles (liposomes) and micelles,<sup>7c-e</sup> self-assembled monolayers,<sup>8</sup> are all driven by self-assembly of molecules. In such a self-assembly, the interactions are governed, at a molecular level, by the combination of covalent, hydrophobic, ionic, hydrogen bonding, van der Waals and steric contributions.<sup>3,7</sup> In a broad sense, self-assembly can be defined as a process in which humans are not actively involved, and atoms, molecules, aggregates of molecules and components arrange themselves into ordered, functioning entities without human intervention.<sup>7b</sup>



The kind of self-assembly embodied by life is called coded self-assembly wherein instructions for the design of the system are built into its components.<sup>7b</sup> Drawing inspiration from nature, material scientists have successfully used these concepts to understand and design novel materials.<sup>3,7a,b</sup>

The area of interest of this thesis is to use weak secondary interactions to form efficient biocomposite materials by immobilization of proteins and enzymes onto 2-D and 3-D supports. The 2-D supports used are the thin films of thermally evaporated fatty lipids, and hence protein-lipid interactions have also been studied. The nanoscale-curved surface of colloidal gold particles forms the 3-D template for organization of enzymes.

#### **1.4 PROTEIN-LIPID INTERACTIONS.**

Proteins are polypeptides with primary, secondary, tertiary and sometimes a quaternary structure. The type of protein a cell produces depends on which of its genes are active at any given time. Genes encode how the 20 basic amino acids are assembled into chains of various combinations. The chains fold into compact coils and loops to become different kinds of proteins, each with a specific structure-function relationship, determined by its shape and chemistry. The complex structure of a protein is stabilized by covalent and other secondary interactions. There are different types of proteins such as transmembrane proteins (for transmembrane signaling), heme proteins (oxygen transport), enzymes (specific functions), chaperons (assisting protein refolding), proteosomes (destroying unwanted proteins) etc. Lipids are basically amphiphiles containing a hydrophobic moiety, generally an aliphatic double chain/single chain, phosphate or carboxylate ester polar headgroup, and in some cases, an intermediate region where hydrogen bonding can occur. The interaction between protein and lipids is an intricate problem, with a number of different interactions working in conjunction. All scientists involved in membrane and lipoprotein research have not come to the same "logically uniform system of thought", but it is from attempts to reconcile divergent interpretations of observations that general principles finally emerge. Thus, one hopes that exposure of differing views to discussion and criticism will lead to a reduction in the current state of 'chaos'.<sup>9</sup>

The studies on protein-lipid interactions have fundamental as well as technological importance. Lipid-protein interactions are probably the single most crucial factor that determines

the action of protein molecules in biological membranes.<sup>10</sup> Furthermore, protein-Lipid interactions are central to understanding structure-function relationships in various diverse fields such as ion transport, photosynthesis, cell recognition, cell division. Surfactant-protein interactions have also been extensively investigated. In the simplest form, there is competition between surfactant self-association (micelle formation) and surfactant protein binding. The latter may lead to denaturation and/or conformational changes in the proteins. Investigations of the effects of surfactants on protein stability and conformational changes have provided insight into the structure of proteins.<sup>11</sup> It is extremely difficult, if not impossible, to study the protein-lipid interactions *in-vivo* in membranes, hence micelles, microemulsions, monolayers, bilayers, vesicles, host-guest systems, and polyions have been used as membrane mimetic agents.<sup>12</sup> Arrangement of lipids and proteins in membranes are best considered in terms of fluid-mosaic model, proposed by Singer *et al.*<sup>13</sup> According to this model, the matrix of the membrane, a lipid bilayer composed of phospholipids and glucolipids, incorporates proteins, either on the surface or in the interior, and acts as a permeability barrier. Molecules are free to diffuse laterally in the plane of the membrane. This often produces selective ordering and segregated domain formation.<sup>12,13</sup> There are some other models, but no model is perfect or is able to mimic faithfully all aspects of complex membrane assemblies. There is however a more important objective in studying membrane models such as to develop novel chemistry of practical utility based on mimicking membrane mediated processes in relatively simple systems.<sup>12</sup>

From a technological perspective, protein-lipid interactions also help in designing matrixes for efficient immobilization of biomolecules, with enhanced temporal, temperature and pH stability, protection against degradation and intactness of natural confirmation of the immobilized biomolecule.<sup>14a-c</sup> This is especially useful for enzymes, due to the tremendous applicability of immobilized biocatalysts for industrial applications.<sup>14a-c</sup> Immobilized proteins have potential use in biosensors, biomaterials, and the design of solid-phase catalysts.<sup>14d,e</sup> Enzyme electrodes and immunosensors, are used in clinical diagnostics, food analysis, and environmental monitoring applications.<sup>14f</sup> In biomaterials, immobilized biomolecules may be used for controlling cellular adhesion or increasing biocompatibility of implants.<sup>14g,h</sup>

### 1.5 BIOMOLECULE-COLLOIDAL NANOPARTICLE INTERACTIONS.

The area of nanotechnology and molecular electronics requires synthesis and programmed assembly of nanostructures to compete the drive towards miniaturization. The interest also arises due to the unusual physicochemical and optoelectronic properties of nanoparticles arising primarily due to confinement of electrons within particles of dimensions smaller than the bulk electron delocalization length, this process being termed quantum confinement.<sup>15</sup> The unusual size dependent properties of nanoparticles, find applications in various fields such as non-linear optics, optoelectronic devices, lasers, LEDs, sensors and catalysis to name a few.<sup>15</sup> Furthermore, the utility of nanoscale curved surfaces for immobilizing biomolecules for immunoassays has been recognized in the early 1980's.<sup>16a</sup> Immunomicrospheres, which Rembaum *et al*<sup>16a</sup> defined as specially designed microscopic particles that have antibodies or similar molecules chemically bound to their surfaces that react in a highly specific way with target cells, viruses, or other antigenic agents. The high surface-to-volume ratio offered by colloidal particles result in the concentration of the immobilized entity being considerably higher than that afforded by protocols based on immobilization on planar, 2-D surfaces, resulting in enhanced detection signals. Furthermore, the conjugation of biomolecules with nanoparticles has tremendous potential in immunosensing, bio-labeling, biocatalysis and sensors for biomedical diagnostics.<sup>16</sup>

### 1.6 DIFFERENT PROTOCOLS FOR PROTEIN IMMOBILIZATION.

Biomolecules can be readily attached to solid surfaces, but they may easily denature and lose their activity. In the study of immobilization of biomolecules the principles of protein adsorption play a dominant role, because the initial step of immobilization of a protein is always the adsorption process. Uncontrolled adsorption at a surface can adversely affect the activity and stability of the biomolecule, which leads to a less optimal biomaterial.<sup>17</sup> A number of different interactions prevail or can be utilized between the protein and the matrix for its immobilization. One of the two ways to immobilize a biomolecule is either to modify it (so as to suit the matrix) or modify the matrix for ease of immobilization. The latter method is more effective as the immobilized biomolecule does not lose its biological activity. Immobilization of biomolecules can be generally defined as a procedure leading to its restricted mobility. The

various methods for protein immobilization that currently prevail in the literature are adsorption/attachment to prefabricated carriers, covalent binding, ionic binding, biospecific binding (use of specific interactions), crosslinking, encapsulation/inclusion in membranes, polymers, gels, microcapsules, liposomes/reversed micelles etc.<sup>14b</sup>

**Immobilization by adsorption.** Adsorption of enzymes to water-insoluble supports, whether organic or inorganic has been the simplest insolubilization technique.<sup>18a</sup> It has been attractive because it requires merely exposing the enzyme in solution to the support material. The ease of adsorption, however, is offset by the corresponding ease of desorption. The immobilization method typically involves mixing together the enzyme and support material under appropriate conditions and following a period of incubation, separating the insoluble material from the soluble material by centrifugation or filtration. The support material used can be inorganic matrixes such as porous alumina, titania or zirconia, calcium carbonate, calcium phosphate gel, cellulose, clay, porous glass, ion-exchange resins, or silica gels.<sup>18a,b</sup> Immunoassays made their breakthrough with the sandwich-ELISA technique, which was initially based predominantly on the passive adsorption of antibodies onto polymer surfaces by Engvall *et al.*<sup>18c</sup> Polystyrene (PS) has shown to be a most suitable adsorption matrix for antibodies. A number of researchers have demonstrated the adsorption of model proteins such as BSA onto PS as a function of pH, ionic strength, charge on the matrix, hydrophobicity of the protein etc.<sup>18d-i</sup> Physical adsorption of antibodies onto gold results usually in large aggregated structures, comprising randomly oriented antibodies.<sup>18j</sup>

**Covalent immobilization.** The general purpose of a covalent binding method is to get more stable attachment of the antibody to a surface and better preservation of its activity in long term, particularly for regeneration purposes. Proteins contain several lysine or thiol groups, which can be utilized for its immobilization onto noble metal surfaces. During such an immobilization, it is important that the amino acids essential to the catalytic activity of the enzyme are not involved in the covalent linkage to the support. Typical water-insoluble support materials used for the covalent attachment of enzymes are agarose (Sephacrose), cellulose, dextran (sephadex), glass, polyacrylamide co-polymers, polyaminostyrene.<sup>18b</sup> Natan and co-workers have demonstrated the use of lysine rich pockets of cytochrome *c* for covalent immobilization onto colloidal

gold/silver surfaces.<sup>16g</sup> Sasaki *et al* <sup>19a</sup> demonstrated that the functional protein, myosin subfragment 1, binds to gold thin film surfaces through a Au-S bond involving cysteine residues in the protein. In this direction, we have also demonstrated the immobilization of enzymes such as pepsin, fungal protease (F-prot) and endoglucanase to colloidal gold particles. The immobilization is believed to occur via the thiols (cysteine) or amine groups (lysine).<sup>19b-d</sup> Immunosensing is a major area where antibody/antibody- fragments are immobilized onto surfaces for efficient and early detection of disease. In these procedures glutaraldehyde, carbodiimide and other reagents such as succinimide esters, maleinimides and periodate are widely used. Proteins such as IgG, Fab' fragments of antigens, glycoproteins etc have been immobilized by a number of workers in this area for efficient and early detection of disease.<sup>19e-k</sup>

**Directed immobilization via specific interactions.** The high affinity of avidin or streptavidin for biotin ( $K_a \sim 10^{15}$ ) forms the basis of an immobilization system in which binding partners can be linked by specific interaction. The use of the system has expanded gradually into medical diagnostics systems, particularly in DNA immobilization.<sup>5a,20a</sup> The system is nowadays particularly useful for localization and patterning of biomolecules on surfaces. Patterned immobilization of biomolecules on surfaces has also been shown by DNA-directed immobilization.<sup>20b,c</sup> Coupling of Fab' via a thiol-reactive biotin derivative to nitrobiotin has also been demonstrated.<sup>20d</sup> Edmiston *et al* have studied the molecular orientation in asymmetric protein bilayers assembled on planar glass substrates. To a biotin capped phospholipid bilayer, streptavidin was bound, to which biotinylated yeast cytochrome *c* was attached.<sup>20e</sup> A number of researchers have studied such specific interaction systems and suggest these systems to be a model for the development of efficient biosensors.<sup>20f-h</sup>

**Entrapment into polymer matrices.** The ability to entrap drugs or biomolecules within, and subsequently release them from polymers has led to new treatments for a number of diseases.<sup>21a,b</sup> Appropriate type of polymers and formulation techniques could be used to release molecules of any size and charge for over 100 days.<sup>21c</sup> Applications such as immunology wherein a single-shot vaccine delivery system capable of pulsate dosing to immunize against multiple disease could be possible.<sup>21d</sup> Local delivery of inhibitors at the tumor site or tissue engineering, where growth factors are released from polymer scaffolds at appropriate times to

promote tissue regeneration can also be achieved.<sup>21e</sup> While early studies focused on the kinetics of protein release from the matrices, lately, the field began to focus on maintaining protein integrity and the factors that affect it throughout the lifetime of the produce.<sup>21f</sup> Schwendeman *et al* have recently used poly(DL-lactide-co-glycolide; PLGA)-based delivery system for entrapment of proteins. The rise in acidity upon immobilization of BSA led to denaturation of the protein and hence was co-immobilized along with  $Mg(OH)_2$ , which acts as an antacid and reduces the acidity.<sup>21g</sup> A number of researchers have immobilized proteins onto polymer microspheres as a function of pH, ionic strength and overall charge.<sup>18d-j</sup> Mateo *et al* have coated porous supports such as agarose, silica, polymeric resins by polyethylenimine via covalent immobilization. Crude extracts from E-coli and industrially important enzymes could be reversibly immobilized onto such supports.<sup>21h</sup> The photo-block-graft-copolymn. method using an iniferter, benzyl N,N-diethyldithiocarbamate, was utilized to design a biomedically functional surface for fabricated devices.<sup>21i</sup> Recently, Gill *et al* have reviewed the formation of biocomposite materials with polymers such as non-hydrogel epoxy resins, polyurethanes, polyvinyl plastics and silicones for the formation of biocatalysts and biosensor applications.<sup>21j</sup> The use of electropolymers such as poly(pyrrole), poly(pyrrole-2-carboxylate), poly(aniline), and poly(*o*-phenylenediamine) for the generation of protein-containing thin film architectures for biosensors have been covered by a recent comprehensive review.<sup>21k</sup>

**Sol-Gel matrix.** Since its inception a decade ago, sol-gel encapsulation has opened up an intriguing new way to immobilize biological materials such as enzymes, DNA, RNA, antigens, live bacteria, fungal, plant and animal cells and whole protozoa.<sup>22a</sup> The sol-gel matrices often used are silica, metal-oxide, organosiloxane and hybrid sol-gel polymers.<sup>22a</sup> The technique for bioencapsulation in sol-gel, is similar to traditional sol-gel technique, essentially doped with biologicals. The starting point is a precursor which is typically an alkyl silicate, an alkoxymetallate or an alkoxysilane or a mixture of these. The precursor is hydrolyzed by water, either spontaneously or under acid or base catalysis, to form hydroxy derivatives (silicic acids, hydroxometallates, hydroxysilanes, etc). A cascade of condensation reactions give rise to soluble, colloidal and ultimately phase-separated polymers (polysilicates, hydrous metal oxides, polysiloxanes etc), which produce the final matrices (silica, metallosilicate, metal oxide and

siloxane). Using the basic technique and specific fabrication processes (e.g. block casting, reverse emulsion polymerization, screen or contact printing, fluid-bed coating and dip or spin coating), one can obtain bio-doped hydrogels or xerogels in various configuration (e.g. monoliths, sheets, granulates, microparticles and thick and thin films).<sup>14a,22</sup> The groups of Avnir, Ottolenghi and Ellerby made significant contributions to the sol-gel encapsulation method by immobilizing various proteins and enzymes. The groups of Zink, Brown, and Stevens focussed their work on the use of sol-gel technique for the formation of efficient optical and electrochemical biosensors.<sup>221-n</sup> Heller *et al* have shown that by co-immobilizing polyelectrolytes with enzymes, their active site could be prevented from binding to the sol-gel matrix, and thus gives comparable biological activity.<sup>220</sup>

**Cross-linked Crystals.** Enzyme cross-linking was investigated thoroughly during the pioneering phase of enzyme immobilization.<sup>14c</sup> However because of low mechanical and hydrodynamic stability interest turned to other methods. The use of enzyme crystals is one example of a non-chemical binding method in which the crystallized protein is both the carrier and the catalyst. Multiple non-covalent forces form and stabilize the crystals and make them more rigid. Additional chemical bonding via cross-linkers is also required to stabilize the crystals against dissolution in an aqueous medium. A huge variety of homo or hetero-functional cross-linking agents have been developed, some of which are group specific. In biotechnology most often bis-epoxides, bis- or trifunctional aziridines, or dialdehydes (e.g glutardialdehyde) are used. Direct cross-linking of enzymes produces biocatalysts with poor characteristics concerning mechanical rigidity, compressibility, and hydrodynamic behaviour. Improvement is achieved by co-cross-linking with other inert materials like polyamines or by combination with other methods (sol-gels). Cross linked enzyme/protein crystals (CLE/P S) display high catalytic activity at high temperature and in organic solvents because the cross-linking prevents the denaturation of enzymes, through unfolding, dissociation or aggregation.<sup>23a</sup> Thermolysin-CLEC was used for synthesis of aspartame precursor in pure ethyl acetate at 55 °C, and the enzyme was reusable.<sup>23b</sup> The enantioselectivity of *Candida rugosa* lipase (CRL)-CLECs in the hydrolysis of the esters of (R,S)-2-arylpropionic acids is 3-50 times higher than that of a crude enzyme preparation in solution.<sup>23c</sup> Significant enhancement in enantioselectivity of CRL-CLECs in the

resolution of acids is especially important in the preparation of optically pure drugs.<sup>23c</sup> CLPCs have also been demonstrated as novel microporous materials.<sup>23d</sup> A distinct advantage of protein crystals over other porous materials is the inherently chiral nature of protein molecules. A number of researchers have demonstrated similar work using cross linked protein/enzyme crystals.<sup>23e-g</sup>

**Inorganic materials.** Inorganic templates such as layered zirconium phosphates, zeolites and mesoporous materials such as MCM-41 have been used for the immobilization of biomolecules. Kumar *et al* <sup>24a,b</sup> have studied in detail the encapsulation of different proteins and enzymes in the galleries of  $\alpha$ -zirconium phosphate  $[\text{Zr}(\text{HPO}_4)_2 \times n\text{H}_2\text{O}; \alpha\text{-ZrP}]$  and  $\alpha$ -zirconium phosphonate  $[\text{Zr}(\text{PO}_3\text{-CH}_2\text{COOH})_2 \times n\text{H}_2\text{O}; \alpha\text{-ZrPAA}]$ . Amino acids have also been intercalated within  $\alpha$ -ZrP matrices by a number of groups as a function of acidity/basicity of the amino acids.<sup>24c-e</sup> Kanzaki *et al* have studied the intercalation of various enzymes with molecular weights ranging from 23,000 (papain) to 2,40,000 (catalase) into layered inorganic compounds  $\gamma$ -Titanium (IV) phosphate  $(\text{Ti}(\text{HPO}_4)_2) \times 2\text{H}_2\text{O}$ .<sup>24f</sup> Mesoporous inorganic materials such as MCM-41 and zeolites have also been used for the immobilization of various proteins and enzymes.<sup>24g-i</sup>

**Polyelectrolytes and polyions.** A layer by layer (LBL) technique for the formation of layers of polyelectrolytes/polyions onto solid supports was proposed in 1991 by Decher, which works on the principle of charge overcompensation.<sup>25a,b</sup> This technique was successfully extended towards the realization of polyelectrolyte-nanoparticle/biomolecule multilayer films onto 2-D and 3-D supports by the groups of Caruso, Lvov, Kunitake, and Rusling.<sup>25c-j</sup> Different nanoparticles, proteins, enzymes and also DNA could be immobilized in polyelectrolyte multilayers using this method. Excellent biological activity of the immobilized enzyme was achieved. Multi-enzyme catalysis was also demonstrated using this technique. Crooks<sup>25k</sup> and co-workers have shown the use of a hyperbranched polyelectrolyte film for the electrostatic entrapment of glucose oxidase.

**Langmuir-Blodgett films.** Ordered multilayer protein films have been constructed using the Langmuir-Blodgett (LB) deposition method.<sup>26</sup> Most of the methods use Langmuir-Schaefer method for the deposition method instead of the conventional vertical lifting method. This is due



to the bulkyness of the protein, which does not allow uniform multilayer deposition. Leblanc *et al* study the LB films of Cyt *c* on graphite electrode by AFM and cyclic voltammetry measurements. The protein in the LB films forms an ordered monolayer in which the individual proteins pack into a quasi-hexagonal structure.<sup>26a</sup> Nicolini *et al* have investigated the formation of supramolecular architectures from LB technique for numerous electronic and biotechnological applications. They have studied the formation of LB films of metalloproteins and antibodies.<sup>26b-f</sup> Damodaran *et al* <sup>26g-i</sup> have studied in detail the energetics of protein-interface interactions and its effect on protein adsorption at air-water interface. They observe that the positively charged proteins exhibit adsorption diffusion rates an order of magnitude slower than their bulk diffusivities. On the other hand, negatively charged proteins exhibit diffusion rates higher than their bulk values. A number of researchers have formed LB films of different proteins.<sup>26j-p</sup>

**Self-assembled monolayers (SAMs).** Whitesides and co-workers have extensively investigated the role of SAMs terminating into different functional groups that resist protein/cells adsorption.<sup>27a-f</sup> By selecting specific functional groups with varying hydrophobicity, they achieve targeted assembly of various proteins/enzymes, and biological cells. The main driving forces behind this work are applications in cell biology, biosensing, tissue engineering, and screening genomic libraries. They have used the technique of surface plasmon resonance (SPR) and contact angle titrations to investigate protein adsorption behaviour. They have extensively used the method of microcontact printing ( $\mu$ -CP) for the formation of patterned SAMs for patterned and specific immobilization of biologicals.<sup>27g</sup> Crooks and co-workers have used this technique of  $\mu$ -CP to study the patterned immobilization and growth of biological cells. A number of other researchers have used SAMs to immobilize different biomolecules.<sup>27l-q</sup>

**Stacks of Lipid bilayers.** Kunitake and coworkers, in 1991, intercalated the heme protein myoglobin (Mb) in specific orientation into a multilayered cast film of phosphate/ammonium/zwitterionic bilayer membrane.<sup>28a,b</sup> Orientation of the protein was studied by ESR spectroscopy and it was found that the heme group in Met-Mb is oriented at an angle of 15-20° against the bilayer surface. Absorption spectroscopy was used to confirm the integrity of the immobilized protein. They also find that the protein occupies 10% of the overall bilayer surface indicating a large amount of empty space in the cast films.<sup>28a,b</sup> The utility of lipid bilayers

in enhancing the biological activity of the intercalated protein versus that of free protein has also been demonstrated.<sup>28c</sup> Rusling and co-workers have extensively studied the electrochemical applications of proteins/enzymes intercalated within lipid bilayers.<sup>28d-j</sup> A number of different researchers have used fatty lipids to organize/intercalate biomolecules and studied the orientation, salt and pH effects of the process.<sup>28k-n</sup>

**Immobilization onto 3-D curved surfaces.** The advantages of using 3-D curved surfaces are the high surface-to-volume ratio offered by colloidal particle resulting in the concentration of the immobilized entity being considerably higher than that afforded by protocols based on immobilization on planar, 2-D surfaces, resulting in enhanced detection signals. Generally antibodies, proteins, enzymes and DNA have been immobilized onto polymer and metallic colloidal particles. Drug delivery, immunosensing are some of the applications wherein polymer colloids are of great use. Metallic colloids such as that of gold, silver and quantum dots of semiconductors have applications in bio labeling, immunosensing etc.<sup>16</sup>

All the above mentioned biomolecule immobilization protocols have their own advantages/disadvantages. The simplest technique is immobilization by adsorption, but biomolecules can easily desorb by this method and hence cannot be reused. Covalent immobilization protocol is useful for limited biomolecules with cysteine or lysine residues in specific sequences such as those offered by immunoglobulins. Hence this technique is not applicable for a wide range of biomolecules, although the technique is powerful for antibody immobilization and detection of antigens. Directed immobilization using specific interactions such as biotin-avidin, DNA directed etc, which involve molecular recognition events, is a powerful technique for site-specific immobilization. But this technique suffers from the problem of a lot of maneuvering and protein modification, which may result in loss of biological activity of the protein to be immobilized. Entrapment into polymer matrix is a good tool when applications such as drug delivery are of use, and this technique is of great commercial and biomedical value. The sol-gel methodology often involves harsh experimental conditions, which may degrade the biomolecules. Cross-linked enzyme crystals (CLECs) find tremendous applications in organic synthetic chemistry when one wants to enzymatically resolve enantiomers of compounds. Inorganic layered materials such as zirconium phosphates, zeolites and MCM-41

are rigid matrices, but the time taken for protein immobilization is often too long which may degrade the protein. The use of polyelectrolytes/polyions either as monolayers or by the LBL technique, is a promising technique and currently finds a significant research activity. The LB technique also promises a lot of technological applications and is being pursued by a number of researchers. The use of SAMs for the immobilization of biologicals is an attractive approach for developing strategies in cell culture growth, although the amount of protein adsorbed is less. Lipid bilayer is a relatively simple tool for biomolecule immobilization. The amount of protein immobilized can be controlled by variation of the amount of lipid multilayers. Weak interactions are used for protein immobilization, which does not denature the protein. We believe that, among all the immobilization protocols, the protocols involving biomimetic systems such as lipids in the form of mono or bilayers, polyelectrolytes/polyions are more suitable for biomolecule immobilization as they are bio-friendly, more flexible or soft, relatively inert, and convenient. Sastry *et al* have developed a methodology for entrapment of ions,<sup>29</sup> colloidal nanoparticles,<sup>30</sup> and biomolecules<sup>31</sup> wherein secondary interactions such as electrostatic, hydrophobic and hydrogen bonding are responsible for intercalation/immobilization.

As far as immobilization of biomolecules onto 3-D surfaces is concerned, we feel that metallic nanoparticles offer more advantages. The choice of colloidal gold comes from its striking colorimetric properties which forms a model system to study immobilization. Colloidal gold has been extensively used by Mirkin and co-workers<sup>16e</sup> for immobilization of oligonucleotides and detection of complementary base sequences by changes in the visible spectra. The surface of colloidal gold does not require modification for chemisorption of proteins/enzymes as required in the case of organic colloids. The ease of characterization by observing colorimetric changes upon immobilization of analytes from solution, the biocompatibility, the stability of enzymes on colloidal gold surface (as also observed by Stonehuerner *et al*),<sup>16f</sup> the simplicity of bio-conjugate formation by just addition of proteins/enzymes to the colloidal gold solution with the fact that the surface does not require modification has led to the choice in our case for bio-conjugate formation.

### 1.7 Method described in this thesis.

The motivation for the study was from the earlier work developed in this laboratory. In 1996, it was demonstrated that thermally evaporated fatty acid films when immersed in electrolyte solutions such as  $\text{PbCl}_2/\text{CdCl}_2$  lead to the electrostatic entrapment of the metal cations in the acid matrix, formation of metal salts of the fatty acid and a consequent spontaneous organization of the film into a c-axis oriented lamellar structure similar to that observed in LB films.<sup>29a-c</sup> Recognizing that the principle of ion exchange is quite general, this approach has been extended to the reorganization of fatty amine films as well, via anion incorporation using  $[\text{PtCl}_6]^{2-}$ ,  $[\text{TiO}(\text{C}_2\text{O}_4)]^{2-}$  and keggion anions  $[\text{PW}_{12}\text{O}_{40}]^{29a-c}$ . The use of thermally evaporated fatty lipid films in such an immobilization protocol is exciting for the reason that patterned films may be readily deposited by suitable masking procedures. The entrapment of metal ions followed by their chemical treatment in patterned fatty lipid films has been used to grow organized assemblies of  $\text{CdS}^{29d}$  and gold<sup>29e</sup> nanoparticles. This approach has been recently extended to sequential entrapment of metal ions, formation of hetero-nanoparticle assemblies/core-shell nanoparticle structures and studied their low-temperature alloying behavior.<sup>29f,g</sup> This protocol was further extended in 1997 to the incorporation of negatively charged carboxylic acid derivatized colloidal nanoparticles of silver, gold and  $\text{CdS}$  into thermally evaporated fatty amine films.<sup>30</sup> The density of clusters incorporated into the organic matrix could be controlled by simple variation of colloidal solution pH, thereby leading to variation of charge on these particles as well as in the ionized lipid films.<sup>30</sup> The important question was whether this protocol could be successfully extended to intercalation of proteins/enzymes with negligible distortion to their three-dimensional (tertiary) structure, thus enabling them to perform their biological functions without hindrance. The successful attempt in this direction has been presented in this thesis.

The technique described in the thesis makes use of electrostatic interactions between oppositely charged proteins and the ionized multilayer films of amphiphilic molecules. The variation in the ionization of these entities enables "pumping out" of the entrapped proteins. Other secondary interactions such as hydrophobic and hydrogen bonding also contribute to intercalation process. The biocatalytic activity of the immobilized enzymes has been studied and

compared with free solution-form enzymes. The utility of such thermally evaporated lipid films in the generation of patterned protein assemblies has also been demonstrated. Immobilization of enzymes onto 3-D curved surfaces such as colloidal gold has also been studied.

The thesis has been divided into seven chapters. Chapter I gives a brief introduction to the thesis, followed by chapter II, which describes different characterization techniques used for characterization of the protein-lipid and protein-nanoparticle biocomposites. Chapter III focuses on the interaction of heme proteins such as cytochrome *c* (Cyt *c*) and hemoglobin (Hb) with oppositely charged thermally evaporated amphiphilic films. The effect of degree of swelling of the lipid films, thickness of the lipid films, role of buffers, pH and preordering the lipids on the diffusion of the proteins in these films is also discussed. The role of secondary interactions in the protein diffusion process has also been investigated. The kinetics of diffusion has been analyzed in terms of 1-D Fickian type diffusion model. The biocomposite films have been characterized by UV-vis, Fourier Transform Infrared (FTIR) and Fluorescence Spectroscopies.

Enzymes are biocatalysts and find applications in various biomedical and industrial applications. The utility of these enzymes is greatly enhanced upon immobilization due to the general applicability and advantages of immobilized biocatalysts. Chapter IV describes the immobilization of two industrially important enzymes, fungal protease (F-prot) and endoglucanase. The comparable biological activity of these immobilized enzymes as compared to their solution counterparts, the enhanced temporal and pH stability and the role of entrapped water in the lipid films have also been discussed.

The advantage of our protocol has been demonstrated by the formation of patterned nanocomposites and has been described in detail in chapter V. Selective entrapment of four different proteins/enzymes, two cationic and two anionic into oppositely charged lipid matrices has been demonstrated, by a simple masking and immersion protocol. FTIR has been used as a tool to study the intermixing of proteins into other regions of the lipid matrix. The generality of this technique has been demonstrated by patterned assembly of nanoparticles such as gold, silver and CdS into thermally evaporated octadecylamine (ODA) films by masking has been studied. UV-vis and spot-profile EDAX has been used to demonstrate the faithfulness of the masking procedure.

The formation of bioconjugates of enzymes fungal protease (F-prot) and endoglucanase with colloidal gold particles has been dealt with in chapter VI. The bioconjugates so formed have been characterized by a host of techniques such as UV-vis, fluorescence, FTIR, Transmission electron microscopy (TEM), Scanning electron microscopy (SEM), X-ray photoelectron spectroscopy (XPS), EDAX, and biocatalytic activity measurements.

The thesis concludes with a short summary of the work and its importance to nanobiotechnology. The scope for future work has also been discussed.

## 1.8. REFERENCES.

1. Ball, P. *Designing the Molecular World : Chemistry at the frontier.*, **1994**, Princeton University Press, New Jersey, USA.
2. a) Conn, E.E.; Stumpf, P.K.; Bruening, G.; Doi, R.H. *Outlines of biochemistry*, **1987**, John Wiley & sons, Inc, USA; b) Davies, P.L.; Sykes, B.D. *Curr opin struct biol.* **1997**, *7*, 828; c) Haymet, A. D. J.; Ward, L.G.; Harding, M.M. *J. Am. Chem. Soc.*, **1999**, *121*, 941; d) Mann, S. *Angew. Chem. Int. Ed.*, **2000**, *39*, 3392; e) Sarikaya, M. *Proc. Natl. Acad. Sci.*, **2000**, *97*, 14183; f) Goldberg, A.L.; Elledge, S.J.; Harper, J.W. *Sci. Am.*, **2001**, Jan, 68; h)
3. Feynman, R. P.; Leighton, R. B.; Sands, M. *The Feynman Lectures on Physics* Vol. 1, Addison-Wesley Publishing Co. Inc., USA. **1996**.
4. The classic talk by Richard Feynman entitled "There's plenty of room at the bottom" delivered at the annual meeting of the American Physical Society at the California Institute of Technology in 1959 is possibly the first serious exposition on the problem of manipulating nanoscale objects (the talk is available on the web at <http://www.zyvex.com/nanotech/feynman.html>).
5. a) Niemeyer, C.M. *Angew. Chem. Int. Ed.*, **2001**, *40*, 4128; b) Gilardi, G.; Fantuzzi, A. *Trends. Biotechnol.*, **2001**, *19*, 468; c) Merkle, R.C. *Trends. Biotechnol.*, **1999**, *17*, 271; d) A complete issue dedicated to molecular motors: *Acc. Chem. Res.*, **2001**, *34* ; e) A complete issue dedicated to nanotechnology: *Sci. Am.*, **2001**, 15<sup>th</sup> Sept.
6. Kuhn, H.; Waser, J. *Angew. Chem. Int. Ed.*, **1981**, *20*, 500.
7. a) Philip, D.; Stoddart, J.F. *Angew. Chem. Int. Ed.*, **1996**, *35*, 1155; b) Whitesides, G. M. *Sci. Am.*, **1995**, Sept, 114; c) Israelachvili, J. N. *Intermolecular and surface forces*, **1997**,

- Academic Press, San Diego, CA, USA; d) Tanford, C. *The hydrophobic effect: Formation of micelles and biological membranes*, **1980**, Wiley Interscience, USA; e) Evans, D.F.; Wennerstrom, H. *The Colloidal Domain*, **1999**, Wiley-VCH, New York, USA.
8. a) Nuzzo, R.G.; Allara, D.L. *J. Am. Chem. Soc.*, **1983**, *105*, 4481; b) Sunder, V.A.; Liedberg, B.; Allara, D.L. *Langmuir* **1995**, *11*, 3882; c) Bain, C.D.; Biebuyck, H.A.; Whitesides, G.M. *Langmuir* **1989**, *5*, 723.
9. Jost, P. C.; Griffith, O. H. *Lipid-Protein Interactions*, **1982**, Vol. 2, John Wiley & Sons, USA,
10. Mouritsen, O. G.; Bloom, M. *Biophys. J.*, **1984**, *46*, 141.
11. a) Nemethy, G. *Angew. Chem. Int. Ed.*, **1967**, *6*, 195; b) Reynolds, J.A.; Gallagher, J.P.; Steinhardt, J. *Biochemistry* **1970**, *9*, 1232; c) Steinhardt, J.; Krijn, J.; Leidy, J.G. *Biochemistry* **1971**, *10*, 4005.
12. Fendler, J. H. *Membrane mimetic chemistry*, **1982**, Wiley-Interscience, USA.
13. Singer, S. J.; Nicolson, G. L. *Science* **1972**, *175*, 720.
14. a) Avnir, D.; Braun, S. **1996**, *Biochemical Aspects of Sol-Gel Science and Technology*, Kluwer: Hingham, MA.; b) Tischer, W.; Wedekind, F. *Top. Curr. Chem.* **2000**, *200*, 95; c) Tischer, W.; Kasche, V. *Trends. Biotechnol.*, **1999**, *17*, 326; d) Mosbach, K., *Meth. Enzymol.*, **1988**, 137; e) Shabat, D.; Grynszpan, F.; Saphier, S.; Turniansky, A.; Avnir, D.; Keinan, E. *Chem. Mater.* **1997**, *9*, 2258; f) Turner, A.P.F.; Karube, I.; Wilson, G.S. *Biosensors: Fundamentals and applications*, **1987**, Oxford university press, Oxford; g) Ortenwall, P.; Wandenwick, H.; Kutti, J.; Risberg, B.; *J. Vasc. Surg.*, **1987**, *6*, 17; h) Singhvi, R.; Kumar, A.; Lopez, G.P.; Stephanopoulos, G.N.; Wang, D.I.C.; Whitesides, G.M.; Ingber, D.E. *Science*, **1994**, *264*, 696.
15. a) Henglein, A. *Top. Curr. Chem.* **1988**, *143*, 113; b) Mulvaney, P. *Langmuir* **1996**, *12*, 788; c) Steigerwald, M.L.; Brus, L.E.; *Acc. Chem. Res.*, **1990**, *23*, 183; d) El-Sayed, M.A. *Acc. Chem. Res.*, **2001**, *34*, 257; e) Alivisatos, A. P. *Science* **1996**, *271*, 933; f) Ahmadi, T.; Wang, Z.L.; Green, T.C.; Henglein, A.; El-Sayed, M.A. *Science* **1996**, *272*, 1924; g) Haruta, M.; Ueda, A.; Tsubota, S.; Torres Sanches, R.M. *Catal. Today.*, **1996**, *29*, 443.
16. a) Rembaum, A.; Dreyer, W.J. *Science* **1980**, *208*, 364; b) Caruso, F.; Mohwald, H. *J. Am. Chem. Soc.*, **1999**, *121*, 6039; c) Niemeyer, C.M. *Angew. Chem. Int. Ed.*, **2001**, *40*, 4128; d)

- Bruchez, M. Jr.; Moronne, M.; Gin, P.; Weiss, S.; Alivisatos, P.A. *Science* **1998**, *281*, 2013;
- d) Chan, W.C.W.; Nie, S. *Science* **1998**, *281*, 2016-2018; e) Mirkin, C. A. *Inorg. Chem.*, **2000**, *39*, 2258; f) Crumbliss, A.L.; Perine, S.C.; Stonehuerner, J.; Tubergen, K.R.; Zhao, J.; O'Daly, J.P. *Biotech. Bioeng.*, **1992**, *40*, 483; g) Keating, C.D.; Kovaleski, K.M.; Natan, M.J. *J. Phys. Chem. B.*, **1998**, *102*, 9404; h) Alivisatos, A. P.; Johnsson, K. P.; Peng, X.; Wilson, T. E.; Loweth, C. J.; Bruchez, M. P., Jr.; Schultz, P. G. *Nature* **1996**, *382*, 609.
17. Albers, W.M.; Vikholm, I.; Viitala, T.; Peltonen, J. *Interfacial and materials aspects of the immobilization of biomolecules onto solid surfaces*, Handbook of surfaces and interfaces of materials, Vol. 5, Chapter 1, **2001**, Academic Press, San Diego, USA.
18. a) Johnson, J.C. *Immobilized enzymes: Preparation and engineering, Recent advances*, **1979**, Noyes data corporation, New Jersey, USA; b) Woodward, J. *Immobilised cells and enzymes: a practical approach.*, **1985**, IRL press, Oxford, UK; c) Engvall, E.; Perlmann, P. *Immunochemistry*, **1971**, *8*, 871; d) Schmitt, A.; Fernandez-Barbero, A.; Cabrerizo-Vilchez, M.; Hidalgo-Alvarez, R. *Prog. Colloid Polym. Sci.* **1997**, *104*, 144; e) Elgersma, A. V.; Zsom, R. L. J.; Norde, W.; Lyklema, J. *J. Colloid Interface Sci.* **1990**, *138*, 145; f) Kamyshny, A.; Magdassi, S. *Coll.Surf.B.*, **1997**, *9*, 147; g) Peula, J.M.; de las Nieves, F.J. *Coll. Surf. A.*, **1993**, *77*, 199; h) Peula, J.M.; de las Nieves, F.J. *Coll. Surf. A.*, **1994**, *90*, 55; i) Molina-Bolivar, J.A.; Ortega-Vinuesa, J.L. *Langmuir* **1999**, *15*, 2644; j) Caruso, F; Rodda, E.; Furlong, D.N. *J. Colloid. Interface. Sci.*, **1986**, *178*, 104.
19. a) Sasaki, Y.C.; Yasuda, K.; Suzuki, Y.; Ishibashi, T.; Satoh, I.; Fujiki, Y.; Ishiwata, S. *Biophys. J.*, **1997**, *72*, 1842; b) Gole, A.; Dash, C.; Ramakrishnan, V.; Sainkar, S. R.; Mandale, A. B.; Rao, M.; Sastry, M. *Langmuir* **2001**, *17*, 1674; c) Gole, A.; Dash, C.; Sainkar, S. R.; Rao, M.; Sastry, M. *Bioconjugate Chemistry.*, **2001**, *12*, 684-690; d) Gole, A.; Vyas, S.; Phadtare, S.; Lachke, A.; Sastry, M. *Coll.Surf.B.*, In press; e) Bin, L.; Xie, J.; Lu, C.; Wu, C.; Wie, Y. *Anal. Chem.*, **1995**, *67*, 83; f) O' Brien, J.C.; Jones, V.W.; Porter, M.D.; Mosher, C.L.; Henderson, E. *Anal. Chem.*, **2000**, *72*, 703; g) O' Shannessy, D.J.; Hoffman, W.L. *Biotechnol. Appl. Biochem.*, **1987**, *9*, 488; h) Viitala, T.; Vikholm, I.; Peltonen, J. *Langmuir* **2000**, *16*, 4953; i) Nakanishi, K.; Mvguruma, H.; Karube, I. *Anal. Chem.*, **1996**,



- 68, 1695; j) Vikholm, I.; Albers, W.M. *Langmuir* **1998**, *14*, 3865; k) Prisyazhnoy, V.S.; Fusek, M.; Alakhov, Y.B. *J. Chromat.*, **1988**, *424*, 243.
20. a) Niemeyer, C. M.; Ceyhan, B.; Blohm, D. *Bioconj. Chem.*, **1999**, *10*, 708; b) Niemeyer, C. M.; Boldt, L.; Ceyhan, B.; Blohm, D. *Anal. Biochem.*, **1999**, *268*, 54; c) Hengsakul, M.; Cass, A.E.G. *Bioconj. Chem.*, **1996**, *7*, 249; d) Morag, E.; Bayer, E.A.; Wilchek, M. *Biochem. J.*, **1996**, 316; e) Edmiston, P.L.; Saavedra, S.S. *J. Am. Chem. Soc.*, **1998**, *120*, 1665; f) Spinke, J.; Liley, M.; Guder, H.J.; Angemaier, L.; Knoll, W. *Langmuir* **1993**, *9*, 1821; g) Muller, W.; Ringsdorf, H.; Rump, E.; Wildburg, G.; Zhang, X.; Angemaier, L.; Knoll, W.; Liley, M.; Spinke, J. *Science* **1993**, *262*, 1706; h) Zhao, S.; Reichert, W.M. *Langmuir* **1992**, *8*, 2785.
21. a) Fu, K.; Klibanov, A.M.; Langer, R. *Nat. Biotechnol.*, **2000**, *18*, 24; b) Langer, R. *Nature* **1998**, *392*, 5; c) Langer, R.; Folkman, J. *Nature* **1976**, *263*, 797; d) Gibbons, A. *Science* **1992**, *255*, 1351; e) Kim, B.S.; Mooney, D.J. *Trends. Biotechnol.*, **1998**, *16*, 224; f) Putney, S.D.; Burke, P.A. *Nat. Biotechnol.*, **1998**, *16*, 153; g) Zhu, G.; Mallery, S.R.; Schwendeman, S.P. *Nat. Biotechnol.*, **2000**, *18*, 52; h) Mateo, C.; Abian, O.; Fernandez-Lafuente, R.; Guisan, J.M. *Biotech. Bioeng.*, **2000**, *68*, 98; i) Nakayama, Y.; Matsuda, T. *Langmuir* **1999**, *15*, 5560; j) Gill, I.; Ballesteros, A. *Trends. Biotechnol.*, **2000**, *18*, 469; k) Cosnier, S. *Biosens. Bioelectron.*, **1999**, *14*, 443.
22. a) Gill, I.; Ballesteros, A. *Trends. Biotechnol.*, **2000**, *18*, 282; b) Ellerby, L. M.; Nishida, C. R.; Nishida, F.; Yamanaka, F. A.; Dunn, B.; Valentine, J. B.; Zink, J. I. *Science* **1992**, *255*, 1113; c) Gill, I.; Ballesteros, A. *J. Am. Chem. Soc.*, **1998**, *120*, 8587; d) Ji, Q.; Lloyd, C. R.; Ellis, W. R.; Eyring, E. M. *J. Am. Chem. Soc.*, **1998**, *120*, 221; e) Zheng, L.; Flora, K.; Brennan, J. D. *Chem. Mater.*, **1998**, *10*, 3974; f) Das, T. K.; Khan, I.; Rousseau, D. L.; Friedman, J. M. *J. Am. Chem. Soc.*, **1998**, *120*, 10268; g) Rao, M. S.; Dave, B. C. *J. Am. Chem. Soc.*, **1998**, *120*, 13270; h) Avnir, D.; Braun, S.; Lev, O.; Ottolenghi, M. *Chem. Mater.*, **1994**, *6*, 1605; i) Chen, Q.; Kenausis, G. L.; Heller, A. *J. Am. Chem. Soc.*, **1998**, *120*, 4582; j) Wang, J.; Pamidi, P.; Park, D. *Anal. Chem.*, **1996**, *68*, 2705; k) Lev, O.; Tsionsky, M.; Rabinovich, L.; Glezer, V.; Sampath, S.; Pankratov, I.; Gun, J. *Anal. Chem.*, **1995**, *67*, 23A; l) Peng, T.; Cheng, Q.; Stevens, R.C. *Anal. Chem.*, **2000**, *72*, 1611; m) Dave, B.C.; Dunn, B.; Valentine,

- J.; Selverstone; Z., Jeffrey I. *Anal. Chem.*, **1994**, *66*, 1120A; n) Lin, J.; Brown, C.W. *Trends Anal. Chem.*, **1997**, *16*, 200; o) Chen, Q.; Kenausis, G.L.; Heller, A. *J. Am. Chem. Soc.*, **1998**, *120*, 4582.
23. a) St. Clair, N.L.; Navia, M.A. *J. Am. Chem. Soc.*, **1992**, *114*, 7314; b) Zelinski, T.; Waldmann, H. *Angew. Chem., Int. Ed.*, **1997**, *36*, 722; c) Lalonde, J. J.; Govardhan, C.; Khalaf, N.; Martinez, A. G.; Visuri, K.; Margolin, A. L. *J. Am. Chem. Soc.*, **1995**, *117*, 6845; d) Vilenchik, L. Z.; Griffith, J. P.; Clair, N. St.; Navia, M. A.; Margolin, A. L. *J. Am. Chem. Soc.*, **1998**, *120*, 4290; e) Cao, L.; van Rantwijk, F.; Sheldon, R. A. *Org. Lett.*, **2000**, *2*, 1361. f) Partridge, J.; Halling, P. J.; Moore, B. D. *Prog. Biotechnol.*, **1998**, *15*, 373. g) Browne, J. K.; Mckervery, M. A.; Pitarch, M.; Russell, J. A.; Millership, J. S. *Tetrahedron Lett.*, **1998**, *39*, 1787.
24. a) Kumar, C. V.; Chaudhari, A. *J. Am. Chem. Soc.*, **2000**, *122*, 830; b) Kumar, C. V.; McLendon, G. L. *Chem. Mater.*, **1997**, *9*, 863; c) Ding, Y.; Jones, D.J.; Maireles-Torres, P.; Roziere, J. *Chem. Mater.*, **1995**, *7*, 562; d) Kijima, T.; Ueno, S.; Goto, M. *J.Chem.Soc., Dalton Trans.*, **1982**, 2499; e) Kijima, T.; Ueno, S. *J.Chem.Soc., Dalton Trans.*, **1986**, 61; f) Kanzaki, Y.; Abe, M. *Bull. Chem. Soc. Jpn.*, **1991**, *64*, 2292; g) Das, G.; Prabhu, K.A. *Enz. Microb. Technol.*, **1990**, *12*, 625; h) Liu, B.; Hu, R.; Deng, J. *Anal. Chem.*, **1997**, *69*, 2343; i) Diaz, J.F.; Balkus Jr, K.J. *J. Mol. Cat. B*, **1996**, *2*, 15.
25. a) Decher, G. *Science* **1997**, *277*, 1232; b) Schmitt, J.; Decher, G.; Dressik, W.J.; Brandow, S.L.; Geer, R.E.; Shashidhar, R.; Calvert, J.M. *Adv. Mater.*, **1997**, *9*, 61; c) Lvov, Y.; Ariga, K.; Ichinose, I.; Kunitake, T. *J. Am. Chem. Soc.*, **1995**, *117*, 6117; d) Caruso, F.; Niikura, K.; Furlong, D.N.; Okahata, Y. *Langmuir* **1997**, *13*, 3427; e) Caruso, F.; Mohwald, H. *J. Am. Chem. Soc.*, **1999**, *121*, 6039; f) Caruso, F. *Adv. Mater.*, **2001**, *13*, 11; g) Lvov, Y.; Munge, B.; Giraldo, O.; Ichinose, I.; Suib, S.L.; Rusling, J.F. *Langmuir* **2000**, *16*, 8850; h) Ma, H; Hu, N.; Rusling, J.F. *Langmuir* **2000**, *16*, 4969; i) Lvov, Y.M.; Lu, Z.; Schenkman, J. B.; Zu, X.; Rusling, J.F. *J. Am. Chem. Soc.*, **1998**, *120*, 4073; j) Franchina, J. G.; Lackowski, W. M.; Dermody, D. L.; Crooks, R. M.; Bergbreiter, D. E.; Sirkar, K.; Russell, R. J.; Pishko, M. V. *Anal. Chem.*, **1999**, *71*, 3133.

26. a) Boussaad, A.; Dziri, L.; Arechabaleta, N. J.; Tao, N. J.; Leblanc, R. M. *Langmuir* **1998**, *14*, 6215; b) Nicolini, C.; Erokhin, V.; Antolini, F.; Catasti, P.; Facci, P. *Biochim. Biophys. Acta.*, **1993**, *1158*, 273; c) Nicolini, C. *Thin Solid Films*, **1996**, *284-285*, 1; d) Riccio, A.; Lanzi, M.; Antolini, C.; De Nitti, C.; Tavani, C.; Nicolini, C. *Langmuir* **1996**, *12*, 1545; e) Erokhin, V.; Facci, P.; Nicolini, C. *Biosens. Bioelectronics.*, **1995**, *10*, 25; f) Erokhin, V.; Facci, P.; Kononenko, A.; Radicchi, G.; Nicolini, C. *Thin Solid Films*, **1996**, *284-285*, 805; g) Sengupta, T.; Razumovsky, L.; Damodaran S. *Langmuir* **1999**, *15*, 6991; h) Damodaran, S. *Langmuir*; **1998**, *14*, 6457; i) Rao, C.S.; Damodaran, S. *Langmuir*, **2000**, *16*, 9468; j) Berzina, T. S.; Piras, L.; Troitsky, V. I. *Thin Solid Films* **1998**, *327-329*, 621; k) Preininger, C.; Clausen-Schaumann, H.; Ahluwalia, A.; de Rossi, D. *Talanta* **2000**, *52*, 921; l) Kiselyova, O. I.; Guryev, O. L.; Krivosheev, A. V.; Usanov, S. A.; Yaminsky, I. V. *Langmuir* **1999**, *15*, 1353; m) Girard-Egrot, A. P.; Morelis, R. M.; Coulet, P. R. *Langmuir* **1997**, *13*, 6540; n) Loescher, F.; Ruckstuhl, T.; Jaworek, T.; Wegner, G.; Seeger, S. *Langmuir* **1998**, *14*, 2786; o) Chen, X.; Moser, C. C.; Pilloud, D. L.; Dutton, P. L. *J. Phys. Chem. B.*, **1998**, *102*, 6425; p) Turko, I. V.; Yurkevich, I.S.; Chashchin, V.L. *Thin. Solid. Films*, **1992**, *210/211*, 710.
27. a) Ostuni, E.; Chapman, R. G.; Liang, M.N.; Meluleni, G.; Pier, G.; Ingber, D.E.; Whitesides, G. M. *Langmuir* **2001**, *17*, 6336; b) Ostuni, E.; Chapman, R. G.; Holmlin, E.; Takayama, Shuichi.; Whitesides, G.M. *Langmuir* **2001**, *17*, 5605; c) Ostuni, E.; Kane, R. Chen, C.S.; Ingber, D. E. Whitesides, G.M. *Langmuir* **2000**, *16*, 7811; d) Chapman, R.G.; Ostuni, E.; Takayama, S.R.; Holmlin, E.; Yan, L.; Whitesides, G.M. *J. Am. Chem. Soc.*, **2000**, *122*, 8303; e) Roberts, C.; Chen, C. S.; Mrksich, M.; Martichonok, V.; Ingber, D. E.; Whitesides, G.M. *J. Am. Chem. Soc.*, **1998**, *120*, 6548; f) Sigal, G.B. Bamdad, C.; Barberis, A.; Strominger, J.; Whitesides, G.M. *Anal. Chem.*, **1996**, *68*, 490; g) Xia, Y.; Rogers, J.A.; Paul, K.E.; Whitesides, G.M. *Chem. Rev.*, **1999**, *99*, 1823; h) Ghosh, P.; Amirpour, M. L.; Lackowski, W. M.; Pishko, M. V.; Crooks, R. M. *Angew. Chem. Int. Ed.*, **1999**, *38*, 1592; i) Ghosh, P.; Crooks, R.M. *J. Am. Chem. Soc.*, **1999**, *121*, 8395; j) Aoki, A; Ghosh, P; Crooks, R.M. *Langmuir* **1999**, *15*, 7418; k) Amirpour, M.L.; Ghosh, P.; Lackowski, W.M.; Crooks, R.M.; Pishko, M.V. *Anal. Chem.*, **2001**, *73*, 1560; l) Fang, J.; Knobler, C. M. *Langmuir* **1996**, *12*, 1368; m) Ferretti, S.; Paynter, S.; Russell, D. A.; Sapsford, K. E.; Richardson, D. J.

- TrAC, Trends. Anal. Chem.*, **2000**, *19*, 530; n) Viitala, T.; Vikholm, I.; Peltonen, J. *Langmuir* **2000**, *16*, 4953; o) Guiomar, A. J.; Guthrie, J. T.; Evans, S. D. *Langmuir* **1999**, *15*, 1198; p) Gooding, J. J.; Hibbert, D. B. *TrAC, Trends. Anal. Chem.*, **1999**, *18*, 525; q) Yang, Z.; Yu, H. *Langmuir* **1999**, *15*, 1731.
28. a) Hamachi, I.; Honda, T.; Noda, S.; Kunitake, T. *Chem. Lett.*, **1991**, 1121; b) Himachi, I.; Noda, S.; Kunitake, T. *J. Am. Chem. Soc.*, **1990**, *112*, 6744; c) Hamachi, I.; Fujita, A.; Kunitake, T. *J. Am. Chem. Soc.*, **1994**, *116*, 8811; d) Rusling, J. F. *Acc. Chem. Res.*, **1998**, *31*, 363; e) Chen, X.; Hu, N.; Zeng, Y.; Rusling, J. F.; Yang, J. *Langmuir* **1999**, *15*, 7022; f) Nassar, A-E F.; Zhang, Z.; Hu, N.; Rusling, J. F.; Kumosinski, T. F. *J. Phys. Chem. B.*, **1997**, *101*, 2224; g) Lu, Z.; Huang, Q.; Rusling, J.F. *J. Electroanal. Chem.*, **1997**, *423*, 59; h) Tominaga, M.; Yanagimoto, J.; Nassar, A.F.; Rusling, J.F.; Nakashima, N. *Chem. Lett.*, **1996**, *7*, 523; i) Nassar, A. F.; Zhang, Z.; Chynwat, V.; Frank, H.A.; Rusling, J.F.; Suga, K. *J. Phys. Chem.*, **1995**, *99*, 11013; j) Zhang, Z.; Rusling, J.F. *Biophys. Chem.*, **1997**, *63*, 133; k) Ramsden, J. J. *Biosens. Bioelectron.*, **1998**, *13*, 593; l) Hianik, T.; Snejdarkova, M.; Passechnik, V I.; Rehak, M.; Babincova, M. *Bioelectrochem. Bioenerg.*, **1996**, *41*, 221; m) Burgess, J. D.; Rhoten, M. C.; Hawkridge, F. M. *Langmuir* **1998**, *14*, 2467; n) Salamon, Z.; Tollin, G. *Biophys. J.*, **1996**, *71*, 848.
29. a) Ganguly, P.; Pal, S.; Sastry, M.; Shashikala, M.N. *Langmuir* **1995**, *11*, 1078; b) Pal, S. Ph.D. Thesis, University of Poona, **1996**; c) Gole, A.; Sastry, M. *Inorg. Chem. Commun.*, **2001**, *4*, 568; d) Mandal, S.; Damle, C.; Sainkar, S.R.; Sastry, M. *J. Nanoscience Nanotech.* **2001**, *1*, 281; e) Mandal, S.; Sainkar, S.R.; Sastry, M. *Nanotechnology* **2001**, *12*, 358; f) Kumar, A.; Damle, C.; Sastry, M. *Appl. Phys. Lett.*, **2001**, *79*, 3314; g) Damle, C.; Kumar, A.; Sastry, M. *J. Phys. Chem. B.*, **2002**, *106*, 297.
30. a) Patil, V.; Mayya, K.S.; Sastry, M. *Langmuir* **1998**, *14*, 2707; b) Sastry, M.; Patil, V.; Mayya, K.S. *Langmuir* **1997**, *13*, 4490; c) Sastry, M.; Patil, V.; Sainkar, S.R. . *J. Phys. Chem. B.*, **1998**, *102*, 1404; d) Patil, V.; Sastry, M. *Langmuir* **2000**, *16*, 2207; e) Patil, V.; Sastry, M. *Langmuir* **1997**, *13*, 5511-5513; f) Patil, V.; Malvankar, R.B.; Sastry, M. *Langmuir* **1999**, *15*, 8197; g) Patil, V.; Sastry, M. *J.Chem.Soc., Faraday Trans.*, **1997**, *93*, 4347; h) Sastry, M. *Curr. Sci.*, **2000**, *72*, 1089; i) Sastry, M. *Nanoparticle thin films: An approach*

*based on self-assembly*, Handbook of surfaces and interfaces of materials, Vol. 3, **2001**, Academic Press, San Diego, USA.

31. a) Gole, A.; Dash, C.; Rao, M.; Sastry, M. *J.Chem.Soc., Chem. Commun.*, **2000**, 297; b) Gole, A.; Dash, C.; Mandale, A. B.; Rao, M.; Sastry, M. *Anal. Chem.*, **2000**, 72, 4301; c) Gole, A.; Sastry, M. *Biotech. Bioeng.*, **2001**, 74, 172; d) Gole, A.; Chaudhari, P.; Kaur, J.; Sastry, M. *Langmuir* **2001**, 17, 5646; e) Gole, A.; Vyas, S.; Sainkar, S. R.; Lachke, A.; Sastry, M. *Langmuir* **2001**, 17, 5964; f) Gole, A.; Kaur, J.; Pavaskar, N.; Sastry, M. *Langmuir* **2001**, 17, 8249; g) Sastry, M.; Ramakrishnan, V.; Pattarkine, M.; Ganesh, K.N. *J. Phys. Chem. B.*, **2001**, 105, 4409.

# CHAPTER II

## EXPERIMENTAL TECHNIQUES

---

The different experimental techniques used during the course of the present work are discussed in this chapter

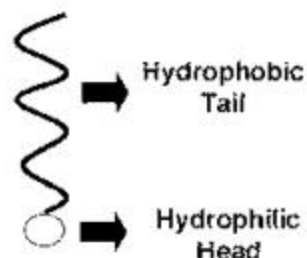
---

The main emphasis of this thesis is the formation of protein-lipid and protein-gold colloid biocomposites. These biocomposites have been characterized by a host of techniques such as QCM, UV-vis, FTIR, Fluorescence, XPS, SEM, TEM, and biocatalytic activity measurements. A lot of other techniques have also been used. This chapter is devoted in explaining the basic principles and techniques used for characterization. The basic requirement for the formation of protein-lipid biocomposite films is the preparation of lipid films. The ordered multilayer lipid films have been formed by two techniques: a) Thermal evaporation of the lipid and on subsequent immersion in protein/electrolyte solution leading to the formation of *self-organized multilayers* (SOMs); b) The classical c-axis oriented Langmuir-Blodgett films such as salts of fatty acids which when immersed in protein solution, leads to the formation of protein-lipid biocomposites.

## 2.1 THERMAL EVAPORATION OF FATTY LIPIDS.

The films used for protein/enzyme immobilization in this thesis have been deposited using an Edwards E306 coating unit. The coating unit consists of a rotary pump, which can pump upto  $10^{-3}$  Torr. Below this pressure, an oil diffusion pump is employed and can go upto  $10^{-7}$  Torr.<sup>1</sup> Both these pumps are used in conjunction for backing and roughing the deposition chamber. A liquid nitrogen trap was also used. Deposition of organic thin films is done under vacuum due to the following reasons: a) The quality of deposition is better due to the increased mean free path of a molecule under vacuum as compared to atmosphere. This results in a linear trajectory of the thermally evaporated molecule; b) The melting point is reduced under vacuum enabling low current requirements for thermal evaporation. The amphiphilic molecules required for deposition, were taken in a molybdenum boat and subjected to a low tension DC of about 20 amps under  $10^{-7}$  Torr vacuum. Different substrates such as Si(111), glass, quartz were kept at a suitable distance above the molybdenum boat. The molecules when heated evaporate and condense onto these substrates giving more or less same thickness uniform films on each substrate. The deposition was monitored *insitu* using an Edwards FTM5 quartz crystal microbalance. The films deposited were tested by IR for possible decomposition, and were found that the films did not decompose on deposition in vacuum.

**2.1.1 Amphiphilic molecules** An amphiphilic molecule has a hydrophobic and a hydrophilic part. The hydrophobic end is normally a long chain of hydrocarbons called the tail and the hydrophilic moiety is called the head and is polar in nature, as shown in Scheme. 2.1.1

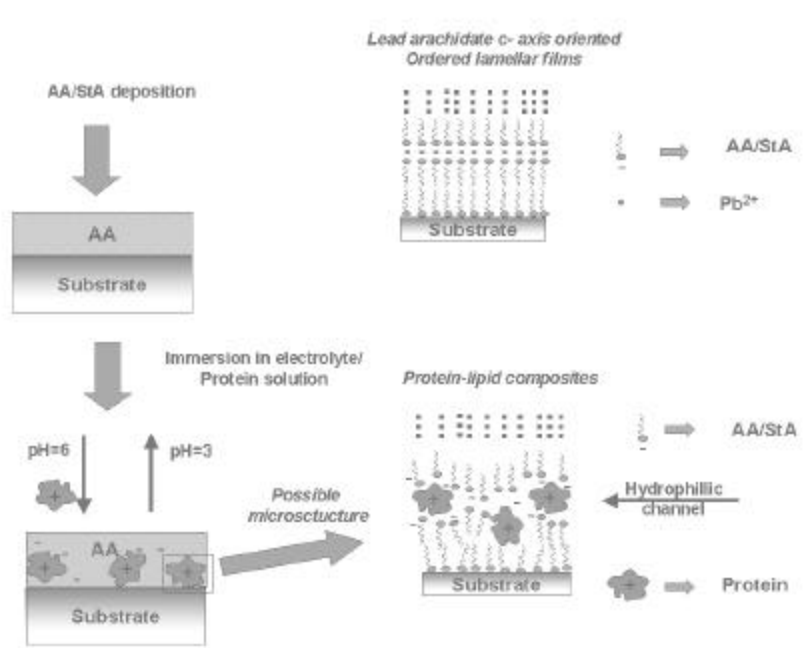


**Scheme 2.1.1.** A schematic of an amphiphilic molecule showing the hydrophobic (long chain hydrocarbons) and hydrophilic regions (polar groups).

Typical examples of amphiphilic molecules that we have used are: Arachidic acid [AA;  $\text{CH}_3\text{-(CH}_2\text{)}_{19}\text{-COOH}$ ], Stearic acid [StA;  $\text{CH}_3\text{-(CH}_2\text{)}_{17}\text{-COOH}$ ], octadecylamine [ODA;  $\text{CH}_3\text{-(CH}_2\text{)}_{17}\text{-NH}_2$ ], octadecanol [ODOH;  $\text{CH}_3\text{-(CH}_2\text{)}_{17}\text{-OH}$ ].

**2.1.2 Self-organized Multilayers (SOMs):** In earlier studies in this laboratory, it has been shown that the thermally evaporated films of fatty acids/amines can be spontaneously organized via selective ionic interaction of cations/anions by simple immersion of the film in a suitable electrolyte.<sup>2</sup> This leads to an organized lamellar film structure similar to c-axis oriented Y-type LB films, which is termed as self-organized multilayers (SOMs). Recognizing that this principle is general, this approach was extended to the electrostatic binding of surface modified colloidal nanoparticles<sup>3</sup> and in this thesis has been shown to intercalate proteins/enzymes.<sup>4</sup> The process has been explained in detail in Scheme 2.1.2





**Scheme 2.1.2.** Scheme showing the formation of fatty acid salts and protein-lipid composites by simple immersion protocol in the case of SOMs.

## 2.2 LANGMUIR BLODGETT (LB) TECHNIQUE.

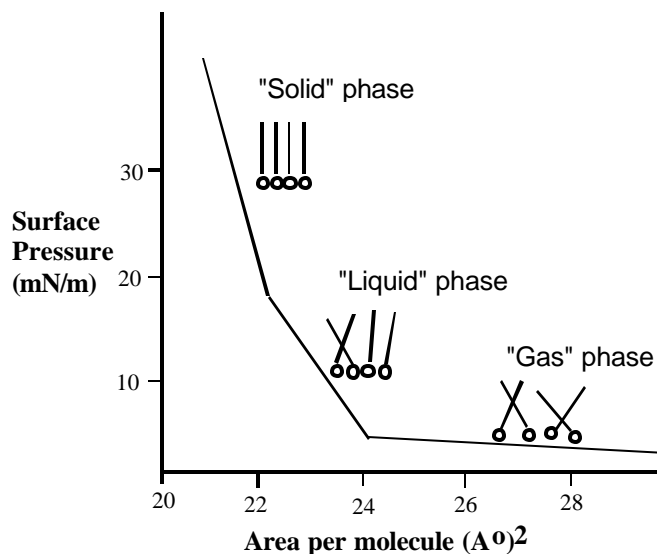
We have used the LB technique for the formation of lead arachidate films and thereafter simple immersion into protein solution leads to the formation of protein-lipid biocomposite films. It has also been shown that the use of such a 'preordered film' in protein intercalation enhances the protein diffusivity by an order of magnitude as compared to that of 'unordered films'.

### **Basic Principles:**

#### 2.2.1 Pressure-Area Isotherms (p-A isotherm)

Monolayers of amphiphilic molecules at an interface can exist in a number of different physical states, analogous to the gaseous, liquid and solid states of matter in bulk. Information regarding the transition between these states can be obtained by measuring the surface pressure of a monolayer as a function of the surface concentration.<sup>5</sup> *The surface pressure  $p$  is the lateral pressure that must be applied to prevent the film from spreading.* In the case under study in this thesis, where lead arachidate films were formed, pressure-area ( $\pi$ -A) isotherms were performed immediately after spreading the monolayer and after 30 min to allow

complexation of lead ions to the interface. Scheme 2.2.1 shows a typical  $\pi$ -A isotherm of stearic acid (StA) on the surface of water.



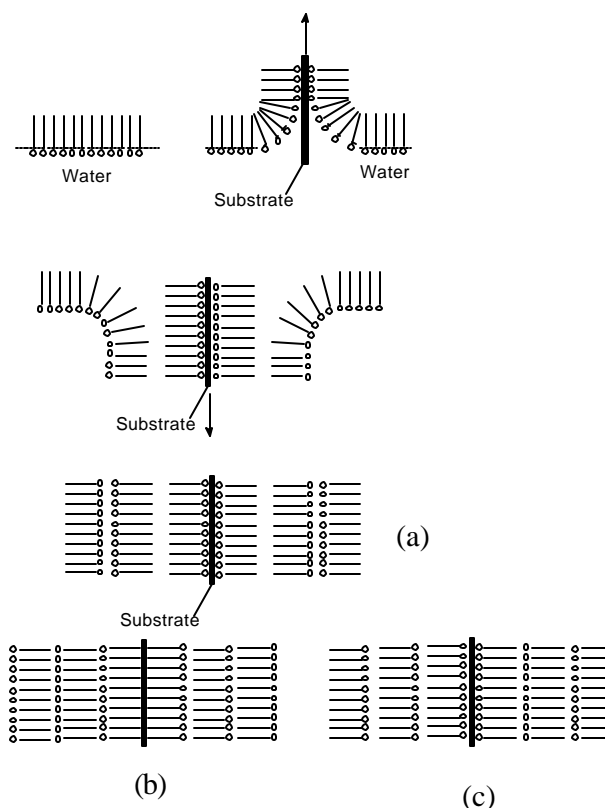
**Scheme 2.2.1:** A typical pressure-area ( $\pi$ -a) isotherm showing the various phase transitions of the floating monolayer.

$\pi$ -A isotherms give information about the stability of the molecules in the two-dimensional system, phase transitions and conformational transitions. The pressure-area isotherm also gives some idea of the amount of pressure that has to be applied to the film on the subphase, to enable deposition of the LB film in the solid-like phase. Thus at appropriate pressure, the film can be transferred to the substrate.

## 2.2.2 The LB film preparation technique.

The LB film preparation technique is shown in scheme 2.2.2. In a typical experiment, measured amount of appropriate surfactant is dissolved in a volatile solvent like chloroform ( $\text{CHCl}_3$ ), and this is spread on the air-water interface. Due to their amphiphilicity, the molecules orient themselves on the water surface with their heads in the water and their tails in the air. This film is then compressed until the molecules are in a solid-like phase with two-dimensional order. The two different methods used for film formation are: a) Vertical-lifting technique developed by Langmuir and Blodgett and b) the horizontal deposition method known as the Schaefer's method. We have used the vertical deposition Langmuir-Blodgett technique for the deposition of lead-stearate LB films. In this method, as shown in scheme 2.2.2 the deposition

occurs during both the upward and downward stroke of the substrate. The different type of LB films are also shown in the scheme.



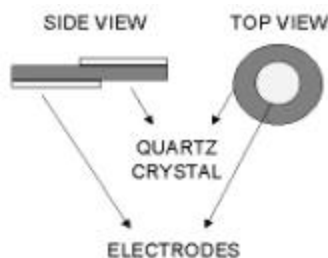
**Scheme 2.2.2:** Vertical deposition method showing the deposition of monolayer films on a solid substrate during dipping and retraction.. (a) y-type (b) x-type (c) z-type.

### 2.3 QUARTZ CRYSTAL MICROGRAVIMETRY.

Quartz crystal based microgravimetry is a powerful tool to study various adsorption processes and has been used to study adsorption of gases,<sup>6a,b</sup> self-assembled monolayers (SAMs),<sup>6c-e</sup> Langmuir-Blodgett films,<sup>6f,g</sup> nanoparticles,<sup>6f,j</sup> and biomolecules.<sup>6k-n</sup> For the work discussed in this thesis, QCM has been extensively used for calculating the exact amount of entrapped protein/enzyme. The knowledge of exact amount of the immobilized biocatalyst is important since one wishes to accurately compare the biocatalytic activity of free versus immobilized enzyme.

**Basic Principles:** In 1880, Jacques and Pierre Curie discovered that mechanical stress applied to the surfaces of various crystals such as quartz, rochelle and tourmaline, afforded a

corresponding electrical potential across the crystal whose magnitude was proportional to the applied stress.<sup>7</sup> This was referred to as the *piezoelectric effect*. It is a characteristic of materials that are acentric, i.e. those that crystallize in noncentrosymmetric space groups. A single crystal of an acentric material will possess a polar axis due to dipoles associated with the orientation of atoms in the crystalline lattice. When stress is applied across an appropriate direction, there is a shift of dipoles resulting from the displacement of atoms. This atomic displacement leads to a corresponding change in the net dipole moment. This will produce a net change in electrical charge on the faces of the crystal. The validity of the converse of this effect was also established wherein application of a voltage across these crystals afforded a corresponding mechanical strain. This inverse piezoelectric effect is the basis of the quartz crystal microgravimetry (QCM) technique. AT-cut quartz resonator, in which thin quartz wafer is prepared by slicing a quartz rod at an angle of  $35^\circ$  with respect to the X-axis of the crystal, resonates in the *thickness shear mode*. The scheme 2.3.1 shows a typical QCM crystal.



**Scheme 2.3.1:** Diagram showing details of a quartz resonator.

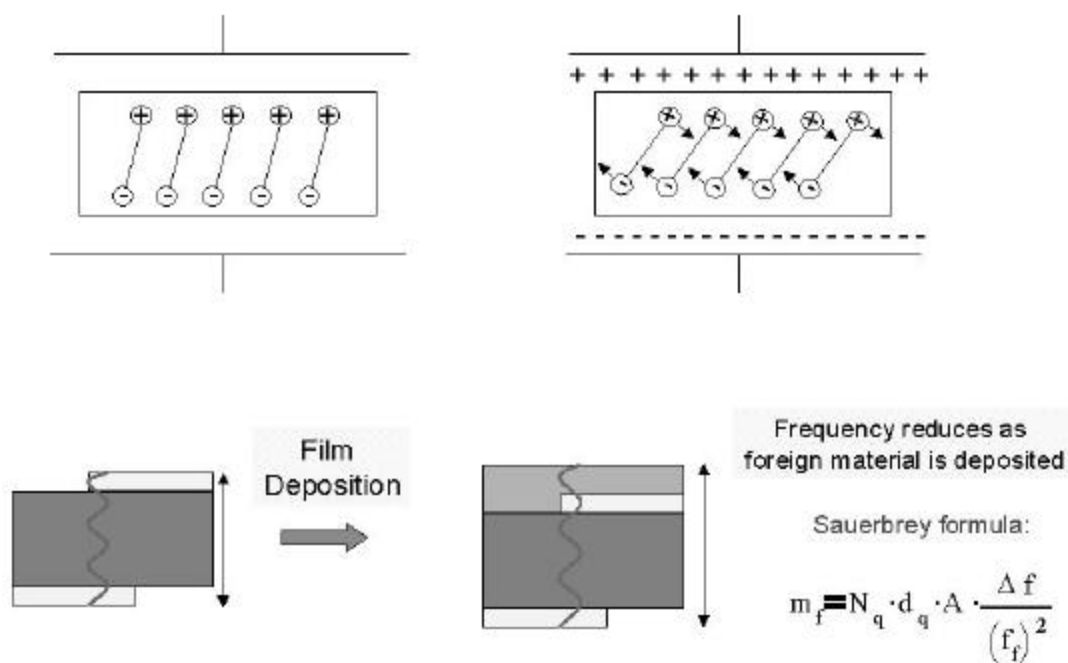
Application of electric field across the crystal causes a vibrational motion of the quartz crystal, with amplitude parallel to the surface of the crystal.<sup>6d</sup> The result of the vibrational motion of the quartz crystal is the establishment of a transverse acoustic wave that propagates across the thickness of the crystal, reflecting back into the crystal at the surfaces. When a uniform layer of foreign material is added to the surface of the quartz crystal, the acoustic wave will travel across the interface, and will propagate through the layer. This leads to decrease in the frequency of the crystal. The details have been depicted in the scheme 2.3.2 shown below. The

Frequency changes on deposition of the film can be converted to mass loading using the Saurbrey formula.<sup>8</sup>

**Saurbrey formula:**

$$\Delta f = -2 f_0^2 \times \frac{\Delta m}{A \times (\mu_q \times \rho_q)^{1/2}}$$

Where  $\Delta f$  - frequency shift,  $f_0$  - frequency of the crystal prior to a mass change,  $\Delta m$  - mass change,  $A$  - Piezo electrically active area,  $\rho_q$  - density of quartz,  $\mu_q$  - shear modulus for quartz. ( $\mu_q = 2.95 \times 10^{11} \text{ g cm}^{-1} \text{ s}^{-2}$ ,  $\rho_q = 2.65 \text{ g/cm}^3$ )



**Scheme 2.3.2:** Diagram showing the details of principles involved in qcm measurements.

In the work described in this thesis we have used a gold coated AT-cut 6 MHz quartz crystal. The frequency counter used was an Edwards FTM5 instrument operating at a frequency stability and resolution of  $\pm 1$  Hz. At this resolution and the type of quartz crystal used, the mass resolution would be  $12 \text{ ng/cm}^2$ . We have used QCM technique in the following way. Different

thickness films of lipids were thermally evaporated on the QCM crystals. These crystals were immersed into protein solutions for different time intervals and the frequency changes were measured *exsitu* after thorough washing (in deionized water) and drying (in flowing nitrogen) of the crystals. The frequency changes were converted to a mass uptake by using the standard Sauerbrey formula.<sup>8</sup> The "leaching out" of the proteins was also studied by QCM.

We would like to point out possible errors in the interpretation of the QCM data using the simple Sauerbrey formula. Most QCM investigations assume that the film layer shows rigid behaviour and no slip at the resonator-fluid boundary, while using Sauerbrey equation.<sup>6c,d</sup> These assumptions are valid when dealing with studies on inorganic thin films, wherein the film deposited is rigid enough to be considered "quartz like". However while dealing with lipid films that are being intercalated with biological molecules such as proteins and DNA, one would need to consider factors such as viscoelastic effects, high mass loadings, surface roughness, surface stress, interfacial slippage and non uniform mass distribution in any piezoelectric measurement.<sup>6c,d</sup> The thin films in our case (about 250 Å), low mass loadings (about 6-12 µg) as compared to total weight of the crystal, and assuming uniform mass distribution over the film surface supports the validity of the use of Sauerbrey equation in our case.

#### 2.4 UV-VISIBLE SPECTROSCOPY.

We have extensively used UV-vis spectroscopy for monitoring the proteins and colloidal gold particle signatures. The resonance at about 280 nm arising from the  $\pi$ - $\pi^*$  transitions in the tyrosine and tryptophan residues in proteins is a characteristic signature which has been probed by us. The heme-proteins give well-known signatures in the visible region of the electromagnetic spectrum, known as the Soret band (410 nm) and the Q band (520-550 nm) and have been used by us to study its redox activity. Furthermore, noble metal particles are ideal candidates for study with UV-vis spectroscopy, since they exhibit strong surface plasmon resonance absorption in the visible region, and are highly sensitive to surface modification.

**Basic principles:** Absorption spectroscopy in the visible region has long been an important tool to the analyst.<sup>9</sup> Color transitions arise due to molecular and structural changes in the substances being examined, leading to corresponding changes in the ability to absorb light in

the visible region of the electromagnetic spectrum. Appearance of color arises from the property of the colored material to absorb selectively within the visible region of the electromagnetic spectrum. Absorption of energy leads to a transition of electron from ground state to excited state. Most of the spectra are very broad, smooth curves and not sharp peaks. This is because any change in the electronic energy is accompanied by a corresponding change in the vibrational and rotational energy levels. A variety of energy absorption is possible depending upon the nature of the bonds within a molecule. For instance, strong  $\sigma$  bonds, in weaker  $\pi$ -bonds or non-bonding (n) and when energy is absorbed all of these types of electrons can be elevated to excited antibonding states represented as  $\sigma^*$ ,  $\pi^*$ . Most  $\sigma$  to  $\sigma^*$  absorptions for individual bonds take place below 200 nm in the vacuum ultraviolet region and compounds containing just  $\sigma$  bonds are transparent in the near UV/vis region.  $\pi \longrightarrow \pi^*$  and  $n \longrightarrow \pi^*$  absorptions occur in the near UV/vis region, and result from the presence in molecules of unsaturated groups known as *chromophores*.

The intensity of light passing through a sample is given by the relation:

$$I = I_0 \exp(-\alpha k x)$$

Where  $I$  = intensity of transmitted light;  $I_0$  = intensity of incident light;  $\alpha$  = molar absorption coefficient;  $k$  = constant;  $x$  = path length.

The combined Beer-Lambert law is used for quantification of exact concentration of "unknown" species in a mixture using UV-vis spectroscopy. This can be done by drawing a graph of intensities of absorption for different concentrations of the sample and comparing with a standard graph.<sup>9</sup>

The Beer-Lambert law is:

$$A = \epsilon c l$$

Where  $\epsilon$  = proportionality constant known as the absorptivity.

These laws can easily explain the absorption of proteins. On the other hand, light absorption by small metal particles is best described by Mie's theory.<sup>10</sup> The absorption spectrum of particles in a given solvent can be calculated from the optical constants of the bulk metal, although the absorption of the particles is often vastly different from that of the bulk metal

itself.<sup>10</sup> The simplest case is when the particles are spherical and their size is small compared to the wavelength of light, and the particles are well separated in solution. At particle sizes between about 3 and 20 nm, there is not a strong dependence of the absorption spectra on particle size. This is because the particles are below the size at which higher order terms in the Mie formula for the absorption constant become significant. Thus, one has to regard only the dipole term which depends only on the total metal concentration in the solution and not on particle size. The absorption coefficient in mol<sup>-1</sup>. L. cm<sup>-1</sup> is calculated from the relation<sup>10,11</sup>

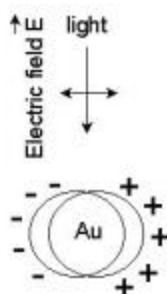
$$\alpha = \frac{18 \pi}{\ln 10} \frac{10^5}{\lambda} \frac{M n_0^3}{\rho} \frac{\epsilon_2}{(\epsilon_1 + 2 n_0^2) + \epsilon_2^2}$$

where  $\lambda$  is the wavelength of light in nanometers, M and  $\rho$  are the molecular weight and density of the metal,  $n_0$  is the refractive index of the solvent and  $\epsilon_1$  and  $\epsilon_2$  are the real and imaginary parts of the dielectric constant of the metal. When the size of the particles becomes smaller than the mean free path of the electrons, the absorption bands are broadened; this is accounted for by using size-corrected values of  $\epsilon_2$ .<sup>10,11</sup>

$$\epsilon_2 = \epsilon_{2(\text{bulk})} + (\omega_p^2 / \omega^3)(v_F/R)$$

where  $\omega$  is the light frequency, the plasmon frequency,  $v_F$  the electron velocity at the Fermi level and R the particle radius ( $R/v_F$ , mean time of the free movement of the electrons). Resonance with the incident light is reached at the wavelength, where the negative value of  $\epsilon_1$  of the metal is equal to twice the dielectric constant of the medium. Gold particles possess plasmon resonances in the visible range (~514 nm). Resonance is produced by a collective excitation of all the free electrons in the particles. As is shown in Scheme. 2.4.1, the movement of the electrons under the influence of the electric field vector of the incoming light leads to a dipole excitation across the particle sphere, the positive polarization charge acting as a restoring force, which makes the electrons oscillate.





**Scheme 2.4.1.** Polarization of a spherical metal particle by the electrical field vector of the incoming light

Thus, the electron density within a surface layer, the thickness of which is about equal to the screening length of a few angstroms, oscillate, whereas the density in the interior of the particle remains constant ("surface plasmon"). Therefore, any changes in the electron density of this surface layer will lead to changes in the plasmon absorption. This surface sensitivity of colloidal nanoparticles has been used to study adsorption/chemisorption of thiols,<sup>12a-c</sup> biomolecules etc.<sup>12d-g</sup> A colorimetric detection system using biomolecules and nanoparticles to detect antigen-antibody<sup>13</sup> and DNA mismatch detection<sup>14</sup> has also been studied.

## 2.5 FOURIER TRANSFORM INFRARED SPECTROSCOPY (FTIR).

FTIR is a powerful tool to study protein-lipid biocomposite films. The amide linkages between amino acid residues in polypeptides and proteins give rise to well-known signatures in the infrared region of the electromagnetic spectrum. The position of the amide I (the C=O band in amide linkage at ca. 1650 cm<sup>-1</sup>), amide II band (the N-H stretch mode of vibration in the polypeptide linkage at ca. 1546 cm<sup>-1</sup>) and the amide III (the C-N band in the polypeptide chain at ca. 1240 cm<sup>-1</sup>) bands in the FTIR spectra of proteins is a sensitive indicator of conformational changes in the protein secondary structure.<sup>15</sup> The lipids also show characteristic bands which can be monitored.

**Basic Principles:** The principles of IR can be explained by classical as well as quantum theories.<sup>16</sup> The classical model considers a simple ball and spring model wherein diatomic molecule with two masses  $m_1$  and  $m_2$  are connected by a spring. According to Hooke's law when spring is displaced,

$$F = -kx$$

Where  $F$  = opposing restoring force;  $k$  = force constant;  $x$  = displacement from equilibrium position. This is simple harmonic equation wherein the frequency of vibration is given by the relation:

$$\nu = \frac{1}{2\pi} \sqrt{\frac{k}{\mu}}$$

where  $\mu$  is the reduced mass. Using simple laws of mechanics, a system of masses joined by springs has a number of fundamental modes of vibration each of which has a particular natural frequency. Consider an oscillator such as the electric vector of electromagnetic radiation coupled to a system of masses such as a polyatomic molecule. By scanning through a range of frequencies some may be 'tuned' to the various fundamental modes of vibration by virtue of a change in dipole moment associated with that vibration. So, a series of absorption take place for a polyatomic molecule as we scan through a range of frequencies, radiation is absorbed each time we 'tune-in' or 'come into resonance' with the natural frequency of a fundamental mode which is capable of dipolar interaction.<sup>16</sup>

Many facts cannot be explained classically (one such fact is the  $\text{CO}_2$  splitting) and requires quantum mechanical treatment. This treatment considers the electronic change accompanied by vibration and rotation with discrete energy levels. The energy of quantised energy levels is derived by using Schrodinger wave equation. For polyatomic molecules, the position of each atoms can be described using coordinate geometry, and the degree of freedom are stated for linear molecules ( $3N-5$ ) and for non-linear molecules ( $3N-6$ ).  $N$  represents number of atoms.<sup>16</sup>

Most published work in this area has been for films deposited on silicon substrates, for variety of reasons. It is chemically very stable and generally not very reactive even at high temperatures. It is excellent for optical studies of deposited films in the visible region using reflection techniques. It does not have strong lattice absorption bands in the useful regions of the infrared and thus can be used for transmission studies in this region. To correct for the lattice absorption bands in silicon, a reference silicon sample is used as a reference. All FTIR data presented in the thesis been presented as obtained except for baseline correction.

Infra-red Spectroscopy (IR) affords an excellent insight into the organization of hydrophobic chain, transport and ion exchange properties of the LB film.<sup>17</sup> For ion exchange/protein incorporation discussed in this thesis, a 250 Å thick lipid was deposited onto a Si (111) wafer. The IR characterization of the film was carried out on a Shimadzu 8201 PC FTIR spectrometer operated in the diffuse reflectance mode at a resolution of 4 cm<sup>-1</sup>. A total of 250 scans yielded a good signal to noise ratio of the IR spectra.

### **Peak assignments for Fatty lipids:**

#### ***C-H Stretching region:***

The two bands at 2920 and 2850 cm<sup>-1</sup> have been assigned to the antisymmetric and symmetric methylene (CH<sub>2</sub>) stretching vibrations respectively and two weak bands at about 2960 and 2875 cm<sup>-1</sup> to the asymmetric/degenerate and symmetric methyl (CH<sub>3</sub>) stretching vibrations respectively. The position of the peaks and the increase in intensity of the methylene stretching vibrations relative to methyl stretching vibration with chain length indicates structural integrity of the molecule. More interestingly, actual peak values of the symmetric and antisymmetric CH<sub>2</sub> stretching vibrations, can be used as a sensitive indicator of the ordering of the alkyl chains. For example, Nuzzo *et al* reported that the d<sup>-</sup> and d<sup>+</sup> values for hexadecanethiolate monolayer on gold surface appear at 2920 and 2850 cm<sup>-1</sup> respectively and concluded that the number of gauche defects in the methylene chains was small.<sup>18</sup> Similarly Porter *et al*<sup>19</sup> reported that monolayers with chains longer than 6 carbon atoms in the alkyl chain, were highly ordered, whereas the smaller molecules resembled the liquid state, i.e., high density of gauche defects (d<sup>+</sup> and d<sup>-</sup> - 2855 and 2924 respectively).

#### ***N-H vibrations:***

Typical peaks for the free amine are seen at 3333 cm<sup>-1</sup>. This band shifts to 3198 cm<sup>-1</sup> on salt formation of primary amine.<sup>20a,b</sup> NH<sub>3</sub> symmetric deformation band is observed at 1487 cm<sup>-1</sup> in case of pure amine. The NH<sub>3</sub> antisymmetric deformation appears in the region of 1587 cm<sup>-1</sup>.<sup>20c</sup>

**The protein Amide bands:** The position of the amide I, II and III bands in the FTIR spectra of proteins is a sensitive indicator of conformational changes in the protein secondary structure<sup>15</sup> and we have used this to study the protein molecules in the lipid matrix as well as onto colloidal gold particles. The amide I band, which is assigned to the stretch mode of the carbonyl group

coupled to the amide linkage, occurs at  $1650\text{ cm}^{-1}$ . The amide II band, which arises due to the N-H stretching modes of vibration in the amide linkage, occurs at  $1546\text{ cm}^{-1}$ . The amide III band arises due to the C-N stretching vibration in the polypeptide chains of the protein and occurs at  $1240\text{ cm}^{-1}$ . These bands in the biocomposite films have been compared with drop dried proteins films on Si(111) substrates. Table 2.5.1 shows all these assignments.

**Table 2.5.1.** Peak assignment for lipid films and that for biocomposite films

BAND	VIBRATION	PEAK POSITION ( $\text{cm}^{-1}$ )
Methylene asymmetric stretch	$n_a(\text{CH}_2)$	2916
Methylene symmetric stretch	$n_s(\text{CH}_2)$	2850
Methylene Scissors	$d(\text{CH}_2)$	1463, 1472
Amine stretch	N-H	3333
Carbonyl stretch(from lipids)	$n(\text{C}=\text{O})$	1699
Carboxylate asymmetric stretch	$n_a(\text{COO}^-)$	1541, 1512
Carboxylate symmetric stretch	$n_s(\text{COO}^-)$	1420
Amide I (carbonyl stretch in proteins)	$n(\text{C}=\text{O})$	1650
Amide II (amine stretch in proteins)	N-H	1546
Amide III (C-N stretch in proteins)	C-N	1240

## 2.6 FLUORESCENCE SPECTROSCOPY.

The biocatalytic activity of the biocomposite films would, to a large extent, depend on the tertiary structure of the enzyme remaining unperturbed within the lipid/nanoparticle matrix. The tertiary structure of an enzyme can be checked by fluorescence measurements by exciting the sample at a particular wavelength and monitoring the fluorescence emission from the tryptophan or tyrosine residues in the enzyme. This is a standard procedure and we have used it to check the tertiary structure of proteins/enzymes in the lipid matrix as well as onto gold nanoparticles by excitation of the  $\pi - \pi^*$  transition in the tryptophan residues at  $295\text{ nm}$ .<sup>21</sup>

**Basic Principles:** The emission of light is always a response to an input of energy of some type and the different types of luminescence are distinguished by the prefix denoting the type of

energy involved.<sup>22</sup> Eg. Bioluminescence from glow-worms, chemiluminescence from luminous paint, radioluminescence from cold light sticks, photoluminescence from theatrical masks etc. The most widely used type of photoluminescence in analytical chemistry is fluorescence. Fluorescence was first observed as long ago as 1565 and gets its name from the fact that the mineral fluor spar was found to glow under UV radiation.

Initially, a molecule will be in its electronic ground state and lowest vibrational energy level. After the absorption of energy, the molecule will be in an excited electronic state, but depending on the energy absorbed, vibrational state will be different. In case of fluorescence, the lifetime of electron in excited state is  $10^{-8}$  s. A number of vibrations/rotations can occur during this time. Energy is dissipated, and the electron returns to lowest vibrational energy level in the excited state. This energy is dissipated to neighbouring solvent molecules. The transition to ground electronic state takes place, with a red shift in wavelength of emission.<sup>22</sup>

It is well known that the tryptophan fluorescence emission is very sensitive to changes in the local environment. This fact has been successfully used by a number of researchers to probe the changes in the local protein environment variation by exciting the sample at 295 nm and monitoring the emission spectra.<sup>23</sup> Significant red/blue shifts in the emission spectra are observed depending on the local tryptophan variation and indicates whether the protein is stable or in denatured form.<sup>23</sup>

## 2.7 X-RAY DIFFRACTION (XRD).

We have used XRD for the determination of the lamellar lipid bilayer structure. When lead ions are intercalated in the SOM films or LB films, XRD analysis gives a spectra of (0,0,l) reflections arising due to the layer-by-layer structure similar to the *c*-axis oriented LB films. The spacing between the reflections can be converted to the 'd' values using Bragg's law. This spacing gives us an idea whether the periodicity of the lipid bilayer stacks is maintained or if there is some tilt in the chains of the lipid stacks.

We have also used XRD for determining the size of nanoparticles in the enzyme-colloidal gold bioconjugates using the Debye-Scherrer formula.

$$d(\text{\AA}) = \frac{0.9 \lambda}{\beta_{1/2} \cos \theta}$$

## 2.8 SCANNING ELECTRON MICROSCOPY.

Scanning Electron Microscopy is extremely useful for the direct observations of surfaces because they offer better resolution and depth of field than optical microscope. The study of SEM in our case is important in order to rule out any surface adsorption of proteins on the lipid surface. SEM and EDAX were also used for characterization of the protein-colloidal gold bioconjugates. SEM and EDAX measurements were performed on a Leica Stereoscan-440 scanning electron microscopy (SEM) equipped with a Phoenix EDAX attachment.

**Basic Principles:** The instrument can be simplified into three major sections: a) electron-optical 'column'; b) vacuum system and c) electronics and display system.<sup>24</sup> A tungsten filament is heated to 2700 K, which produces electrons that are accelerated towards the anode disc. Electrostatic shaping of the electron beam under vacuum gives a beam diameter of about 50  $\mu\text{m}$ . Ultimate performance of the SEM is mainly limited by the diameter of the beam and hence two lenses and condensers demagnify the beam to around 5 nm. The scanning coils deflect this beam and sweep it over the specimen surface. A cathode-ray display tube is scanned synchronously with the electron beam. The brightness of the display tube is modulated by the signal, which arises from the interaction of the beam with the surface element, which is probed. The strength of this signal is translated into image contrast. Secondary electrons, which the beam probe liberates from the specimen surface, are collected and used as the contrast signal. The yield of collected electrons depends on the nature of the specimen surface and on its

inclination with respect to the probing beam. Consequently, one obtains pictures with a high perspective appearance.<sup>24</sup>

**2.71. Specimen-Beam interaction:** There are different types of interactions of the electron beam possible with the sample.<sup>24</sup> For thin samples ( $< 1\mu\text{m}$ ), with electron beam energy of 20-30 keV, one can have unscattered electrons, wherein the beam just passes through and does not contain any information about the sample. Most of the electrons are scattered at large angles (from 0 to  $180^\circ$ ) when they interact with the positively charged nucleus. These elastically scattered electrons usually called 'backscattered electrons' are used for SEM imaging. Some electrons scatter inelastically due to the loss in kinetic energy upon their interaction with orbital shell electrons. Due to electron bombardment, phonons are set up in the specimen resulting considerable heating of the specimen. Incident electrons may knock off loosely bound conduction electrons out of the sample. These are secondary electrons and along with backscattered electrons are widely used for SEM topographical imaging. If the electron beam knocks off an inner shell electron, the atom rearranges by dropping an outer shell electron to an inner one. This excited or ionised atom emits an electron commonly known as the Auger electron. Recently Auger electron spectroscopy (AES) is useful to provide compositional information. Instead of excited atom releasing Auger electron, it can release a photon of electromagnetic radiation. If the amount of energy released is high, the photon will be an X-ray photon. These electrons are characteristic of the sample and can be used for analysis. This type of analysis is known as Energy Dispersive analysis of X-rays (EDAX). We have used this for spot profile analysis to determine relative concentrations of the bioconjugate samples.

## **2.9 TRANSMISSION ELECTRON MICROSCOPY (TEM).**

We have used TEM analysis for the determination of particle size of gold colloids in the bioconjugate films. A drop of the protein-gold colloid bioconjugate solution was placed onto a carbon coated copper grid. After 5 minutes, the excess amount of the solution was removed using a blotting paper. TEM measurements were performed on a JEOL Model 1200EX instrument operated at an accelerating voltage of 120 kV.

**Working Principle:** Diffraction camera consists of an electron gun, an aperture to define a small beam cross section, a specimen holder and a fluorescent screen and plate camera. Measurements are usually carried out in diffraction mode and in the microscopy mode. The advantage of this arrangement is the possibility of directly viewing the area from which the diffraction pattern arises. The specimen is illuminated by a double-condenser system, which allows one to choose the divergence of the incident beam and the size of irradiated specimen area. After passing through the specimen, the beam traverses the objective lens. The specimen image generated by the objective lens is subsequently magnified in one or two more magnification stages by the intermediate and projector lens and projected onto a fluorescent screen or photographic plate.

## 2.10 X-RAY PHOTOELECTRON SPECTROSCOPY (XPS).

Photoelectron spectroscopy is a surface science technique used in understanding atoms, molecules & solids on the surface. We have used XPS for preliminary characterization of the presence of the enzyme fungal protease (F-prot) in the lipid matrix.

**Working Principle:** XPS is based on the well-known photoelectric effect first explained by Einstein in 1905. If photons of energy  $h\nu$  shined on a solid having the work function  $\phi$ , then the maximum kinetic energy  $E_k$  of photoemitted electron is given by the equation:

$$E_k = h\nu - E_b - \phi$$

where  $E_b$  is the binding energy of electron in solid. Employing photons with fixed energy  $h\nu$ , it is obvious that if kinetic energy  $E_k$  and work function  $\phi$  of the sample are measured, it is possible to measure binding energy of electron in solid. Binding energies being characteristic of atoms, different elements present in the sample under investigation are identified. Electrons traveling through a material have a relatively high probability of experiencing inelastic collisions with locally bound electrons as a result of which they suffer energy loss. Due to inelastic scattering process, the flux of photoelectrons emerging from the sample is much attenuated. While the exciting photons penetrate deep into the solid sample, the photoelectrons can escape from only a very short distance beneath the surface ( $< 100 \text{ \AA}$ ). Therefore photoelectron spectroscopy is a *surface sensitive technique*.



## 2.11 ELLIPSOMETRY.

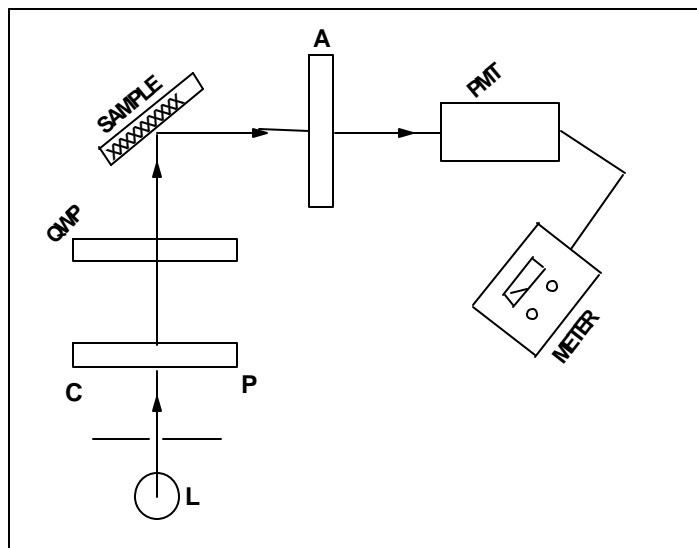
Ellipsometry is one of the most versatile techniques for the study of optical properties of thin films on either solid or liquid surfaces. We have used ellipsometry for the determination of refractive index and thickness of lipid films before and after protein intercalation. The increase in the thickness of the lipid film keeping refractive index constant can be co-related to the size of the intercalated protein.

**Working principle:** The technique is based on the principle that the state of polarization of light changes on reflection from an interface. This technique is also known as reflection polarimetry or polarimetric spectroscopy. In its broadest sense, ellipsometry is the measurement of the state of polarization of light. *Paul Drude* was the first to develop fundamental equations of ellipsometry, which demonstrated potential monolayer sensitivity for the detection and characterization of thin films on specular surfaces.<sup>25a</sup>

When a polarized light beam reflects from any specular surface, changes occur in both the amplitude and phase of the oscillating parallel and perpendicular vector components of the electric field associated with the beam. The main objective of an ellipsometry experiment is to measure these amplitude and phase changes, which provide us information about the reflecting surface through the Fresnel reflection coefficients.<sup>25b</sup> We have used a Gaertner L 118 manually operated null ellipsometer in the polarizer-compensator-sample-analyser (PCSA) mode to measure the ellipsometric angles of lipid films deposited on Si (111) substrate.

### 2.10.1 Measurement of ellipsometric angles $\Psi$ and $D$ - Calculation of thickness of film:

The basic experimental setup of the null ellipsometer used in the study of the optical properties of the lipid and the biocomposite films is shown in scheme 2.10.1.



**Scheme 2.10.1:** Scheme of the various optical elements and their configuration in the null-ellipsometry measurements.

The light source (L) is a monochromatic He-Ne laser ( $\lambda = 6328 \text{ \AA}$ ) with a collimator (scheme 2.10.1). The azimuths of the polarizer (P) in conjunction with a compensator (QWP, a quarter wave plate made of mica) determine the state of polarization of the light incident on the sample surfaces (S). The azimuth of the compensator was kept fixed at  $45^\circ$  with respect to the plane of incidence for all measurements reported in this thesis. In null ellipsometry, the state of polarization of the incident light is adjusted by changing the azimuth of the polarizer (P) such that the light reflected from the sample surface is linearly polarized. This can be checked using another polarizer, the analyzer (A) which would give extinction of light under crossed conditions. To obtain improved sensitivity a photo multiplier tube (PMT) is used to detect the null position. Under these null conditions, the ellipsometric angles  $\Psi$  and  $\Delta$  are related to the Fresnel coefficients of their reflecting surface and the azimuths of the analyzer and polarizer ( $A_0$  and  $P_0$  respectively) through equation (2.1).

$$\rho := \frac{r_p}{r_s} = \tan \psi \exp(i\Delta) \quad (2 - 1)$$

where  $r_p$  and  $r_s$  are Fresnel reflection coefficients<sup>26</sup>

In case where a uniform thin film of refractive index  $n_1$  and thickness  $d$  rests on a infinitely thick substrate of refractive index  $n_2 - i.k_2$  (the substrate may be absorbing at the wavelength used for the measurement, hence the imaginary component to the refractive index), the whole system being in an ambient of refractive index  $n_0$ , the Fresnel reflection coefficients are related to the system material properties through the equation (2-12). For the sample with multiple interfaces,  $r_p$  and  $r_s$  are given as follows<sup>27</sup>

$$r_{pj} := \frac{n_j \cdot \cos(\phi_{j-1}) - n_{j-1} \cdot \cos(\phi_j)}{n_j \cdot \cos(\phi_{j-1}) + n_{j-1} \cdot \cos(\phi_j)} \quad j := 1, 2, \dots (2 - 12a)$$

$$r_{sj} := \frac{n_{j-1} \cdot \cos(\phi_{j-1}) - n_j \cdot \cos(\phi_j)}{n_{j-1} \cdot \cos(\phi_{j-1}) + n_j \cdot \cos(\phi_j)} \quad j := 1, 2, \dots (2 - 12b)$$

In the case of the study under consideration in the thesis, there are only two interfaces and hence the range variable runs only up to 2. Reflection from the two interfaces (ambient-film and film-substrate) introduces a phase shift

$$\delta = 2\pi / \lambda n_1 d \cos(\phi_1) \quad (2 - 13)$$

With incorporation of Equation 2-12 in 2-10, the exact equation of ellipsometry now becomes

$$\tan(\psi) \cdot \exp(i \cdot \Delta) = \frac{(r_{p1} + r_{p2} \cdot e^{-2 \cdot i \cdot \delta}) \cdot (1 + r_{s1} \cdot r_{s2} \cdot e^{-2 \cdot i \cdot \delta})}{(1 + r_{p1} \cdot r_{p2} \cdot e^{-2 \cdot i \cdot \delta}) \cdot (r_{s1} + r_{s2} \cdot e^{-2 \cdot i \cdot \delta})} \quad (2 - 14)$$

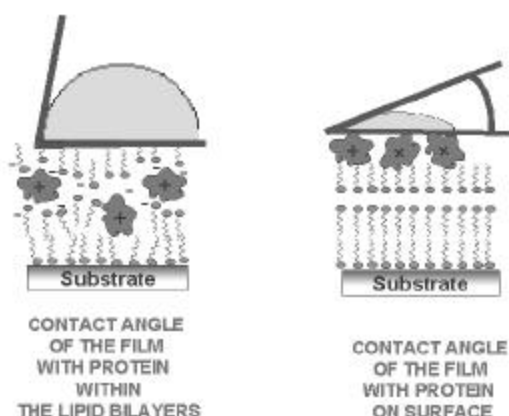
Equation (2-14) involves complex quantities and yields two equations on separating the real and imaginary parts: thus one set of measurements of  $\Psi$  and  $\Delta$  under certain experimental conditions can be used to determine two unknowns such as the thickness and refractive index of the film. Equation (2-14) cannot be inverted analytically and must therefore be solved

numerically. A small application written in Mathcad, written by Dr. Murali Sastry<sup>28</sup> was used to numerically solve these equations and calculate the thickness of the films.

We have assumed the refractive index of all films (before and after protein uptake) to be 1.5 and calculated the thickness of the lipid films before and after protein intercalation by using the exact equation of ellipsometry. After incorporation of the protein, it is possible that the refractive index could change due to the presence of highly polarizable functional groups in the amino acids of the entrapped proteins. This assumption together with possible contributions from scattering by the film should be considered when analyzing the ellipsometry results.

## 2.12 CONTACT ANGLE MEASUREMENTS.

We have performed contact angle measurements of our lipid films before and after protein intercalation using a Rame Hart 100 Goniometer. Contact angle measurements are sensitive to changes in the surface and one can probe any changes in surface hydrophobicity by this technique. Whitesides and co-workers have extensively studied the SAM formation, surface functionality etc using contact angle titrations.<sup>29</sup> We believe that protein molecules are intercalated *within the lipid bilayers* and not on the film surface. Contact angle measurements gives an indirect evidence for this assumption. If the protein were adsorbed on the film surface, the contact angle would be less as compared to the contact angle before protein intercalation. This is clearly shown in scheme 2.11.1 below.



**Scheme 2.11.1** Scheme showing the contact angle measurements of lipid film with protein on surface and the protein within the lipid bilayers.

### 2.13. BIOCATALYTIC ACTIVITY MEASUREMENTS.

The most significant aspect in protein-lipid/colloid bioconjugate systems is the immunoreactivity of the proteins after biocomposite formation. This is of vital importance because of the ultimate application potential of the biocomposites is in the areas of medical diagnosis, drug delivery, biocatalytic and biosensing applications. We have studied the biological activity of cyt *c*-StA biocomposite films, F-prot-StA and F-prot-colloidal gold, endoglucanase-ODA and endoglucanase-colloidal gold biocomposites. The reproducibility for biological activity of enzyme-lipid/colloidal gold particles as a function of reuse, temporal and temperature stability has been checked and compared with free form of the enzyme.

Cyt *c* is a redox protein, and we have checked its biological activity by studying the Q-band (band at 520-550 nm in the UV-vis spectra) as a function of immersion of the biocomposite films into reducing and oxidizing solutions.<sup>15b</sup> F-prot is a proteolytic enzyme and its biological activity has been tested by reaction with measured amount of hemoglobin (Hb) for standard time interval.<sup>30</sup> The tryptophan/tyrosine liberated due to the hydrolysis of Hb by F-prot is monitored after quenching the reaction and centrifugation.<sup>30</sup> Endoglucanase hydrolyzes carboxymethyl cellulose (CMC) to liberate sugar derivatives which are quantitated by standard Nelson-Somogyi method.<sup>31</sup> The role of lipid/colloidal matrix in stabilizing the enzyme against harsh environmental conditions has also been studied and compared with free enzyme in solution.

### 2.14. REFERENCES.

1. Maissel, L.I.; Glang, R. *Handbook of thin film technology*, McGraw Hill Book Company, NewYork, **1970**.
2. a) Ganguly, P.; Pal, S.; Sastry, M.; Shashikala, M.N. *Langmuir* **1995**, *11*, 1078; b) Pal, S. Ph.D. Thesis, University of Poona, **1996**; c) Gole, A.; Sastry, M. *Inorg. Chem. Commun.*, **2001**, *4*, 568.
3. a) Patil, V.; Mayya, K.S.; Sastry, M. *Langmuir* **1998**, *14*, 2707; b) Sastry, M.; Patil, V.; Mayya, K.S. *Langmuir* **1997**, *13*, 4490; c) Sastry, M.; Patil, V.; Sainkar, S.R. *J.Phys.Chem.B.* **1998**, *102*, 1404; d) Patil, V.; Sastry, M. *Langmuir* **2000**, *16*, 2207; e) Patil, V.; Sastry, M. *Langmuir* **1997**, *13*, 5511; f) Patil, V.; Malvankar, R.B.; Sastry, M. *Langmuir*

- 1999, 15, 8197; g) Patil, V.; Sastry, M. *J.Chem.Soc.,Faraday Trans.* **1997**, 93, 4347; h) Sastry, M. *Curr.Sci.* **2000**, 72, 1089.
4. a) Gole, A.; Dash, C.; Rao, M.; Sastry, M. *J.Chem.Soc.,Chem.Commun.* **2000**, 297; b) Gole, A.; Dash, C.; Mandale, A. B.; Rao, M.; Sastry, M. *Anal.Chem.* **2000**, 72, 4301; c) Gole, A.; Sastry, M. *Biotech. Bioeng.* **2001**, 74, 172; d) Gole, A.; Chaudhari, P.; Kaur, J.; Sastry, M. *Langmuir* **2001**, 17, 5646; e) Gole, A.; Vyas, S.; Sainkar, S.R.; Lachke, A. L.; Sastry, M. *Langmuir* **2001**, 17, 5964.
5. a) Langmuir, I.; *J. Am. Chem. Soc.*, **1917**, 39, 1848; b) Ulman, A. *An introduction to Ultrathin Organic Films: from Langmuir-Blodgett to Self-Assembly*, Academic Press, San Diego, CA, **1991**.
6. a) Burrell, M. C.; Armstrong, N.R. *Langmuir* **1986**, 2, 37; b) Cheek, G.T.; O' Grady, W.E. *J.Electroanal. Chem.*, **1990**, 277, 341; c) Wang, J.; Frostman, L.M.; Ward, M.D. *J.Phys.Chem.* **1992**, 96, 5224; d) Buttry, D. A.; Ward, M.D. *Chem. Rev.* **1992**, 92, 1356; e) Geddes, N.J.; Urquhart, R.S.; Furlong, D. N.; Lawrence, C.R.; Tanaka, K.; Okahata, Y. *J. Phys. Chem.*, **1993**, 97, 13767; f) Brust, M.; Etchonique, R.; Calvo, E.J.; Gordillo, G.J. *J.C.S. Chem. Commun.*, **1996**, 1949; g) Patil, V.; Mayya, K. S.; Pradhan, S. D.; Sastry, M. *J. Am. Chem. Soc.*, **1997**, 119, 9281; h) Bright, R.M.; Musick, M.D.; Natan, M.J. *Langmuir* **1998**, 14, 5695; i) Sastry, M.; Patil, V.; Sainkar, S. R. *J. Phys. Chem. B*, **1998**, 102, 1404; j) Gole, A.; Sainkar, S. R.; Sastry, M. *Chem. Mater.*, **2000**, 12, 1234; k) Caruso, F.; Niikura, K.; Furlong, D. N.; Okahata, Y. *Langmuir* **1997**, 13, 3427; l) Caruso, F.; Rodda, E.; Furlong, N.D.; Niikura, K.; Okahata, Y. *Anal. Chem.* **1997**, 69, 2043; m) Gole, A.; Dash, C.; Mandale, A. B.; Rao, M.; Sastry, M. *Anal.Chem.* **2000**, 72, 4301; n) Gole, A.; Chaudhari, P.; Kaur, J.; Sastry, M. *Langmuir* **2001**, 17, 5646.
7. Curie, P.; Curie, J. C. R. *Acad. Sci.* **1880**, 91, 294.
8. Sauerbrey, G. *Z.Phys. (Munich)* **1959**, 155, 206.
9. Denney, R.C; Sinclair, R. *Visible and Ultraviolet Spectroscopy. Analytical Chemistry by open learning series*, John Wiley and Sons, USA.
10. Mie, G.; *Ann. Phys.*, **1908**, 25, 377.
11. a) Mulvaney, P. *Langmuir*, **1996**, 12, 788; b) Henglein, A. *J.Phys.B.*, **1993**, 97, 5457.

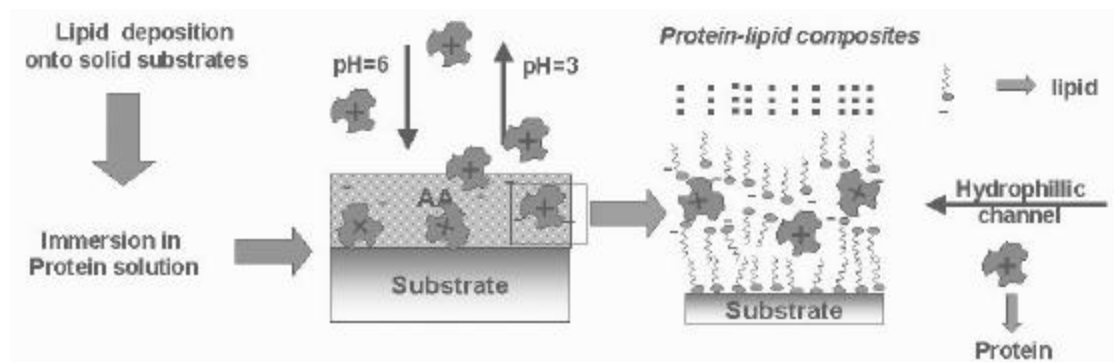
12. a) Brust, M.; Walker, M.; Bethell, D.; Schiffrin, D.J.; Whyman, R. *J.C.S. Chem Commun.*, **1994**, 801; b) Malinsky, M.D.; Kelly, K.L.; Schatz, G.C.; VanDuyne, R.P. *J.Am.Chem.Soc.*, **2001**, 123, 1471; c) Templeton, A.C.; Wvelfing, W.P.; Murray, R.W. *Acc.Chem.Res.*, **2000**, 33, 27; d) Keating, C.D.; Kovaleski, K.M.; Natan, M.J. *J. Phys. Chem. B.* **1998**, 102, 9404; e) Xu, H.; Bjerneld, E. J.; Kall, M.; Borjesson, L. *Phy Rev Lett.* **1999**, 83, 4357; f) Crumbliss, A.L.; Perine, S.C.; Stonehuerner, J.; Tubergen, K.R.; Zhao, J.; O'Daly, J.P. *Biotech.Bioeng.* **1992**, 40, 483; g) Gole, A.; Dash, C.; Ramakrishnan, V.; Sainkar, S.R.; Mandale, A.B.; Rao, M.; Sastry, M. *Langmuir* **2001**, 17, 1674.
13. a) Sastry, M.; Lala, N.; Patil, V.; Chavan, S.P.; Chittiboyina, A.G.; *Langmuir* **1998**, 14, 4138; b) Mann, S.; Shenton, W.; Li, M.; Connolly, S.; Fitzmaurice, D. *Adv.Mater.*, **2000**, 12, 147.
14. a) Storhoff, J.J.; Elghanian, R.; Mucic, R.C.; Mirkin, C.A.; Letsinger, R.L. *J.Am.Chem.Soc.*, **1998**, 120, 1959; b) Reynolds, R.A. III.; Mirkin, C.A.; Letsinger, R.L.; *Pure.Appl.Chem.*, **2000**, 72, 229; c) Mirkin, C. A. *Inorg.Chem.*, **2000**, 39, 2258.
15. a) Dong, A.; Huang, P.; Caughey, W.S. *Biochemistry* **1992**, 31, 182; b) Kumar, C. V.; McLendon, G. L. *Chem. Mater.* **1997**, 9, 863; c) Templeton, A.C.; Chen, S.; Gross, S.M.; Murray, R.W. *Langmuir* **1999**, 15, 66; d) Caruso, F.; Furlong, D. N.; Ariga, Katsuhiko.; Ichinose, I.; Kunitake, T. *Langmuir* **1998**, 14, 4559.
16. George, W.O.; McIntyre, P.S. *Infrared Spectroscopy: Analytical Chemistry by open learning*, John Wiley and Sons, USA, **1987**.
17. a) Marshbanks, T.L.; Ahn, D.J.; Franses, E.I. *Langmuir* **1994**, 10, 276; b) Marshbanks, T.L.; Ranses, E.I. *J.Phys.Chem.*, **1994**, 98, 2166.
18. a) Nuzzo, R.G.; Fusco, F.A.; Allara, D.L. *J.Am.Chem.Soc.*, **1987**, 109, 2358; b) Nuzzo, R.G.; Dubois, L.H.; Allara, D.L.; *J.Am.Chem.Soc.*, **1990**, 112, 558.
19. Porter, M.D.; Bright, T.B.; Allara, D.L.; Chidsey, C.E.D. *J.Am.Chem.Soc.*, **1987**, 109, 3559.
20. a) Bardosova, M.; Tregold, R.H.; Ali-Adib, Z. *Langmuir* **1995**, 11, 1273; b) Pal, S. *Ph. D thesis*, **1996**, University of Pune; c) Ning, G.; Guangfu, Z.; Shiquan, X. *J.Mol.Struct.*, **1992**, 275, 85.
21. Eftink, M.R and Ghiron, C. A. *Anal. Biochem.* **1981**, 199-227.

22. Rendell, D.; Mowthorpe, D. *Fluorescence and Phosphorescence Spectroscopy: Analytical Chemistry by open learning*. John Wiley & Sons, USA, **1987**.
23. a) Reynolds, J.A.; Gallagher, J.P.; Steinhardt, J. *Biochemistry* **1970**, *9*, 1232; b) Eftink, M.R and Ghiron, C. A. *Anal. Biochem.* **1981**, 199; c)
24. Lawes, G. *Scanning electron microscopy and X-ray microanalysis: Analytical chemistry by open learning*, John Wiley & sons, **1987**.
25. a) Hall, A.C. *Surf. Sci.* **1969**, *16*, 1; b) Azzam, R.M.A.; Bashara, N.M.; *Ellipsometry and Polarized Light.*; **1977**, North-Holland: Amsterdam.
26. Fresnel reflection coefficients are complex quantities describing the ratio of the reflected electric field component to the incident field component for the  $p$  and  $s$  directions, respectively. Thus, they are a measure of the amplitude ratio and phase difference upon reflection for the subscripted component. The Fresnel reflection coefficients,  $r_p$  and  $r_s$  are defined as ratios of the reflected and incident electric fields (including both the amplitude and complex phase factors) for the  $p$  and  $s$  components.
27. Granqvist, C.G.; Hunderi, O.; *Phys. Rev. B*, **1977**, *16*, 3513.
28. Dr. Sastry's ref on ellipsometry.
29. Lee, T. R.; Carey, R. I.; Biebuyck, H. A.; Whitesides, G. M. *Langmuir* **1994**, *10*, 741
30. Anson, M. *J.Gen.Physiol.* **1938**, *22*, 79
31. a) Nelson, N. *J. Biol. Chem.* **1944**, *153*, 376. b) Somogyi, M. *J. Biol. Chem.* **1952**, *195*, 19.



# CHAPTER III

## FORMATION OF PROTEIN-LIPID BIOCOMPOSITE FILMS



Formation of heme-protein-fatty lipid biocomposite films is demonstrated in this chapter. Analysis of the influence of protein solution pH, role of buffers and thickness of the lipid films on the diffusion process has been discussed. The role of protein charge: mass (e/m) ratio and overall protein charge on the rate and amount of protein entrapment has also been studied. Attempts at enhancing the diffusivity of the protein in the lipid matrix are successfully demonstrated. The kinetics of the protein diffusion process has been analyzed in terms of a one-dimensional (1-D) Fickian type diffusion model.

Part of the work presented in this chapter has been published: 1) Gole, A.; Chaudhari, P.; Kaur, J.; Sastry, M. *Langmuir* **2001**, *17*, 5646; 2) Gole, A.; Kaur, J.; Pavaskar, N.R.; Sastry, M. *Langmuir* **2001**, *17*, 8249; 3) Gole, A.; Thakar, J.; Sastry, M. *Langmuir* communicated.

### 3.1 INTRODUCTION.

Proteins are macromolecules or polymers in which the basic structural units are amino acids.<sup>1a</sup> Twenty varieties of amino acid have been identified in proteins. They possess both an acid (COOH) and basic or amine (NH<sub>2</sub>) functional group. These two groups can react together so as to become linked by a chemical bond, called a peptide bond.<sup>1a</sup> Chains of amino acids linked by peptide bonds are generally termed polypeptides; proteins are giant polypeptides that occur naturally. Many of the fibrous tissues of the body are made from proteins such as keratin (which forms skin, hair and nails), collagen (tendons) and myosin (muscle).<sup>1a</sup> In biological cells, there are different protein or enzymes which perform specific functions. The cell wall of a biological cell constitutes of about 50% proteins and 50% of lipids.<sup>1</sup> Lipids are amphiphilic molecules having a hydrophobic and a hydrophilic component in a single molecule, hence displaying dual character. Understanding protein-lipid interactions is one of the fundamental current research goals. The formation of biocomposites by interaction of proteins/enzymes with a number of membrane mimetic agents either in solution or by immobilization onto solid supports has fundamental as well as technological applications.<sup>1</sup> The study of nature of the interactions that prevail in proteins conjugated with lipids, helps one to estimate the protein orientation, accessibility and protein attachment to biomembranes.<sup>1</sup> Studies on binding of proteins to lipids, long-chain alkyl sulfates, sulfonates, n-octane and their derivatives have been studied in great detail in the past by Steinhardt *et al.*<sup>2</sup> The changes in the protein structure on binding to these fatty lipids and surfactants have been studied by monitoring binding isotherms, fluorescence and circular dichroism.<sup>2</sup> The role of pH, buffers, ions, polyelectrolytes and clay materials on the protein orientation, stability and biological activity has been probed thoroughly.<sup>3</sup> Whitesides and coworkers have extensively investigated the role of surface functionality of a self-assembled monolayer (SAM) to assist / resist protein adsorption.<sup>4</sup> This is crucial in developing protocols related to vascular grafting and tissue engineering.<sup>4</sup> The approaches closely related to the work described in this chapter are based on the use of lipid monolayers / bilayers for protein immobilization onto two dimensional (2-D) supports by virtue of a number of secondary interactions. Detailed investigations into a new approach for the formation of protein-

lipid biocomposites by an electrostatically controlled diffusion process has been described in this chapter. The chapter also points out the role of other secondary interactions responsible for the immobilization process. The role of protein charge: mass ( $e/m$ ) ratio on the protein diffusion process has also been demonstrated by studying a number of different proteins with varying charges, sizes and molecular weights. The biocomposite formation has been characterized by QCM, FTIR, Fluorescence and XRD measurements.

### **3.2 SELF-ORGANIZED MULTILAYERS (SOMs).**

In the earlier studies carried out in this laboratory (1996), it has been established that thermally evaporated fatty acid / amine films can be spontaneously organized via selective ionic interactions of cations / anions by immersion of the film in a suitable electrolyte solution.<sup>5</sup> This leads to an organized lamellar film structure similar to *c* - axis oriented Y-type LB films. The generality of this protocol was extended in the year 1997 to the incorporation of surface modified colloidal nanoparticles into thermally evaporated ionizable fatty lipid films.<sup>6</sup> It was demonstrated that both positively and negatively charged colloidal nanoparticles of silver, gold and cadmium sulfide (CdS) could be incorporated into fatty acid/amines via selective electrostatic interactions. It was found that the modulation of solution pH, film thickness and particle size, varied the amount of loading in the lipid films. The important question was whether the simple solution-based extraction protocol could work with more delicate guests such as proteins/enzymes? Would the entrapped proteins/enzymes be able to perform their biological functions without hindrance? We found the answer to be affirmative as has been explained in detail in this and forthcoming chapters. The encapsulated protein is accessible to external redox agents and substrates and protects the protein against harsh environmental conditions. In fact, the lipid host enhances the temporal, pH and temperature stability of the encapsulated enzyme as will be explained in the next chapter, thus making the protocol of self-organized multilayers (SOMs) suitable in biocomposite formation for industrial applications.

### **3.3 ENTRAPMENT OF HEME-PROTEINS INTO THERMALLY EVAPORATED FATTY LIPIDS.**

The model proteins Cyt *c* (cationic at pH 7) and Hb (anionic at pH 9) respectively have been shown to intercalate in oppositely charged matrices. The matrices used were arachidic

acid (AA,  $\text{CH}_3(\text{CH}_2)_{19}\text{COOH}$ ,  $\text{pK}_a \sim 3.5$ ), stearic acid (StA,  $\text{CH}_3(\text{CH}_2)_{17}\text{COOH}$ ,  $\text{pK}_a \sim 3.5$ ) and octadecylamine (ODA,  $\text{CH}_3(\text{CH}_2)_{17}\text{NH}_2$ ,  $\text{pK}_b \sim 10.5$ ). These lipids were thermally evaporated onto substrates such as gold-coated AT-cut quartz crystals, Si (111) substrates and quartz substrates. The deposition was done in an Edwards E 306A vacuum deposition unit at a pressure less than  $10^{-7}$  torr. The stability of the films was confirmed by FTIR measurements.

### 3.3.1 Quartz Crystal Microgravimetry.

1000 Å thick AA and 250 Å thick ODA films were thermally evaporated (using an Edwards E 306 A coating system) onto Si (111) wafers (for FTIR studies), quartz substrates (for UV-vis studies) and gold coated AT-cut quartz crystals (for QCM studies) respectively. The experimental details are explained in chapter 2.  $10^{-5}$  M concentrated solutions of Cyt *c* (in water) and Hb (in buffer) at different pH values were prepared. The lipid-coated quartz crystals were immersed into the protein solutions for different time intervals and frequency changes were measured *exsitu* after thorough washing (in de-ionized water) and drying (in flowing nitrogen) of the crystals. The frequency changes were converted to mass uptake using the standard Saurbrey formula.<sup>7</sup>

**Cyt-*c* - AA system:** Fig. 3.3.1 shows a plot of the QCM mass uptake data of Cyt *c* intercalation into a 1000 Å thick AA film during immersion in  $10^{-5}$  M concentrated Cyt *c* solutions at pH 3 (circles), pH 6.8 (squares) and pH 9 (triangles). The protein solution pH and equilibrium Cyt *c* : AA molar ratios are indicated next to the respective curves. It can be seen that complete incorporation of the protein in this case takes place within 70 hours of immersion of the AA film. It is observed from Fig.3.3.1 that maximum Cyt *c* intercalation occurs at close to physiological pH due to maximum electrostatic interactions at this pH ( $\text{pI}$  of Cyt *c*  $\sim 9$ ;  $\text{pK}_a$  of AA  $\sim 4.5$ ). At the other two pH values, either the matrix is not charged (pH 3) or the protein is not charged (pH 9). At these pH values, other secondary interactions such as hydrophobic and hydrogen bonding contribute to the protein intercalation process. The error bars shown in Fig. 3.3.1 for the Cyt *c*-AA film are based on an analysis of five QCM experiments at all the pH values mentioned and indicate roughly a 10 % standard deviation to the data.

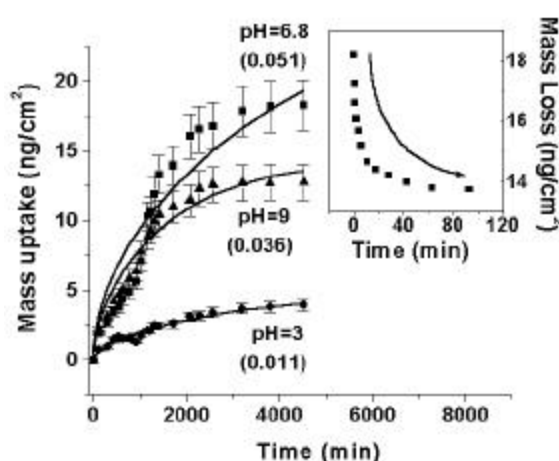


**Figure. 3.3.1:** QCM mass uptake of Cyt *c* with time during immersion of 1000 Å thick AA films in  $10^{-5}$  M Cyt *c* solutions at different pH values. The pH values are indicated next to the respective mass uptake curves together with the equilibrium Cyt *c* : AA molar ratios in parenthesis. The solid lines are fits to the data using a 1-D diffusion model (see text for details). The error bars to the data are roughly 10% deviation of the data from the mean values (see text for details). The inset shows the loss of Cyt *c* from the 1000 Å thick biocomposite film formed at pH = 6.8 during immersion in water at pH = 3.

**Hb-ODA system :** Fig. 3.3.2 shows a plot of the QCM mass uptake data of Hb intercalation into 250 Å thick ODA films during immersion in  $10^{-5}$  M concentrated Hb in buffer solutions at three different pH values (pH 3, 0.05 M glycine – HCl, circles; pH 6, 0.05 M sodium – phosphate, squares; pH 9, 0.05 M Tris – HCl, triangles). The protein solution pH and the equilibrium Hb : ODA molar ratios are indicated next to the respective curves. At pH 9, there is maximum electrostatic interaction between the protein and the lipid ( $pI$  of Hb  $\sim 7$ ,  $pK_b$  of ODA  $\sim 10.5$ ) leading to maximum mass uptake at this pH as compared to the other two pH values. The mass uptake at other two-pH values is attributed to other secondary interactions responsible for protein diffusion process. It can also be seen from Fig.3.3.2 that complete protein intercalation is achieved within a period of 30 minutes of immersion and is considerably better than that reported for other techniques. The error bars shown in Fig.3.3.2 for the Hb-ODA film are based on an analysis of five similar QCM experiments at the three-pH values and show a 5 % deviation to the data. A control experiment was also performed wherein a 250 Å thick ODA film was immersed for different time intervals in a buffer solution (0.05 M Tris – HCl , pH 9) and the mass uptake measured for this film is shown in Fig. 3.3.2 (crosses) indicating no significant mass uptake due to the buffer salts as compared to the actual protein uptake.

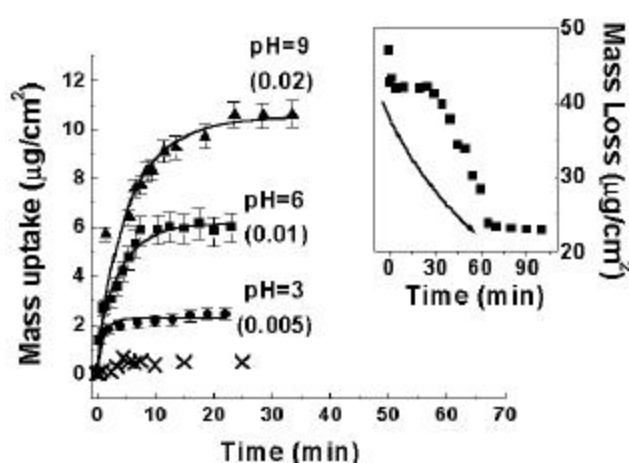


**Figure. 3.3.2** QCM mass uptake of Hb with time during immersion of 250 Å thick ODA films in  $10^{-5}$  M Hb solutions at different pH values. The pH values are indicated next to the respective curves while the equilibrium molar ratios of Hb : ODA listed in parenthesis. The error bars shown in the curves are ca. 5 % deviation of the data from the mean values (see text for details). The inset shows the loss of Hb from a 250 Å thick biocomposite film formed at pH = 9 during immersion in water at pH = 3. A control experiment of mass uptake measured as a function of immersion of 250 Å thick ODA deposited quartz crystal for different time intervals into 0.05 M tris-HCl, pH=9 buffer (crosses; see text for details).

**Reversibility of the diffusion process:** The fact that electrostatic interactions dominate the protein incorporation in the lipid films implies that the adsorption process should be reversible. After the formation of the protein-lipid biocomposite films (Cyt *c*-AA film at pH 6.8, and Hb-ODA film at pH 9) the films were immersed in pH 3 aqueous solution. The inset of Fig. 3.3.1 and 3.3.2 shows the QCM kinetics of leaching out of Cyt *c* and Hb respectively. At this pH either the lipid is uncharged (AA) or the charge on the protein (Hb) is similar to the matrix (ODA). It can be seen that the release of both the proteins is not complete – ca. 76 % of the Cyt *c* molecules and 28 % of Hb molecules are retained in the matrix and this agrees with earlier inferences that interactions other than electrostatic interactions contribute to the protein immobilization process. It may be possible that Cyt *c* being a membrane protein, hydrophobic interactions also contribute to its immobilization thereby giving rise to a significant amount of protein retention in the matrix as compared to Hb. This feature of reversible adsorption/desorption is possible in very few techniques currently in vogue.<sup>8</sup> Such an approach has been used for the electrostatically controlled reversible adsorption/desorption of glucose oxidase in a weak amine, polyelectrolyte hyperbranched thin film by Crooks and co-workers.<sup>8a</sup> Dave and Rao<sup>8b</sup> have also shown the selective intake and release of proteins by organically-modified silica sol-gels,

wherein the gel porosity is adjusted such that large biomolecules can freely diffuse in and out of the bulk of the material. They observe selective release of Cyt *c* from an encapsulated mixture of Myoglobin (Mb) and Cyt *c* or Hb and Cyt *c* when the material is immersed in water, which they attribute to the repulsive electrostatic interaction between the Cyt *c* and the amino groups in the sol gel material.<sup>8b</sup>

### One-dimensional (1-D) Diffusion Model:

Recently, Frances *et al*<sup>9</sup> have studied the process of ion exchange and water transport in Langmuir Blodgett (LB) films of calcium stearate using infrared spectroscopy. An analysis of the ion diffusion process in terms of a 1-D diffusion model was done taking into account a reaction term (due to salt formation) and it was shown that the model did not adequately account for the IR intensity variations observed. A possible explanation put forward was that ion (and water) diffusion could occur through defects such as pores in the film as well as through the hydrophilic lamellar spaces present in the LB films studied resulting consequently in two simultaneous 1-D diffusion processes. In the present situation, the thermally evaporated lipid films are disordered (as evidenced by the complete lack of Bragg peaks in the XRD patterns)<sup>6</sup> and therefore, a 1-D model may be appropriate. To simplify the calculations, we have omitted the reaction term in the diffusion equation. We feel this is justified given that the electrostatic interaction between the proteins/enzymes and the lipid molecules is weak when compared to the energies involved in salt formation.

The equation for simple 1-D diffusion is written as:

$$\frac{\partial C(x,t)}{\partial t} = D \frac{\partial^2 C(x,t)}{\partial x^2} \quad \dots (1)$$

where  $C(x,t)$  is the time and distance dependent protein concentration in the film and  $D$  is the protein diffusivity. Scheme 3.3.1 shows the physical situation in this protein incorporation study and leads naturally to the following boundary conditions:

$$C(L,t) = \begin{cases} 0 & t < 0 \\ C_0 & t \geq 0 \end{cases} \quad \dots (2a)$$

$$\partial C(0, t) / \partial x = 0 \quad \dots (2b)$$

where  $C_0$  is the protein concentration at the film/protein solution interface (Scheme 3.1.1,  $x = L$ ) and condition (2b) is a consequence of the fact that the quartz crystal substrate is impervious to protein diffusion (at  $x = 0$ , the film/quartz substrate interface, scheme 1). The solution of Eq.1 subject to the above boundary conditions (Eq.2) is given by<sup>10</sup> :

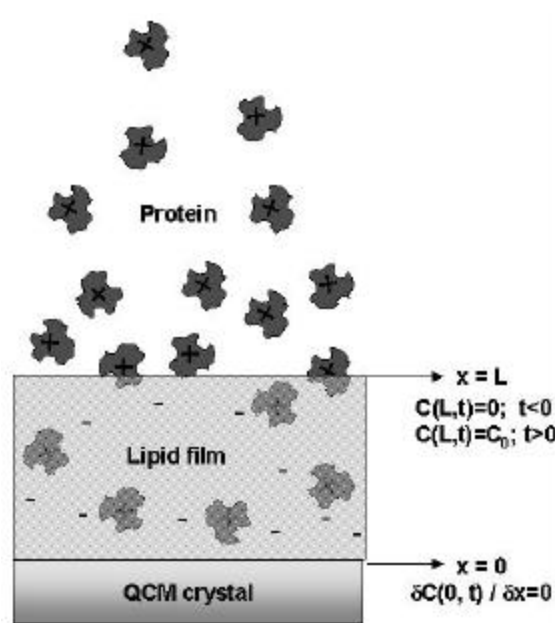
$$C(x, t) = C_0 \left[ 1 + 4 \cdot \sum_{n=0}^{\infty} e^{-D \cdot \left[ (2 \cdot n + 1)^2 \cdot \frac{\pi^2}{4 \cdot L^2} \right] \cdot t} \cdot \cos \left[ \frac{(2 \cdot n + 1) \cdot \pi \cdot x}{2 \cdot L} \right] \cdot \frac{(-1)^{n+1}}{(2 \cdot n + 1) \cdot \pi} \right] \quad \dots(3)$$

In QCM studies, one observes a mass uptake over the whole length of the film covering the sensing electrode. The total mass uptake recorded as a function of time,  $M(t)$ , is therefore :

$$M(t) = m_0 \cdot \int_0^L C(x, t) dx \quad \dots(4)$$

where  $m_0$  is the mass per protein molecule. Ellipsometry was used to determine the film thickness before and after protein incorporation. The final thickness values thus determined ( $L$ ) were used in Eq.3 and the QCM kinetics results fitted to Eq.4 using a non-linear least squares procedure using an application written in Mathcad by Dr. Murali Sastry. Mathcad is a commercial mathematical software package for the PC available from Mathsoft Inc., Cambridge, Ma 02142, USA.





**Scheme 3.3.1.** Scheme (not to scale) showing protein incorporation in a thermally evaporated lipid film during immersion in the protein solution. The boundary conditions are shown.

### Analysis of the QCM data using 1-D diffusion model:

The solid lines in Fig. 3.3.1 and 3.3.2 are the 1-D diffusion fits to the QCM mass uptake data for Cyt *c* and Hb respectively. The parameters obtained from fits are listed in Table 3.3.1 for the cyt *c*-AA and Hb-ODA systems respectively. It is seen that for the cyt *c*-AA case the diffusivities of the cyt *c* molecules into the AA matrix are almost identical at pH 6.8 (pH at which maximum incorporation takes place) and at pH 3 (pH at which minimum mass uptake is observed). At pH 9, it is observed that the diffusivity is much higher than that at the other two-pH values. In the case of Hb-ODA system, the diffusivity of the Hb molecules into the ODA matrix is highest under conditions where the host and guest repel one another (pH 3). The diffusivities at pH 6 and 9 are nearly identical but less than at pH 3, as mentioned above. The concentration at the film- solution interface, however, does show a physically meaningful trend in both the cases, wherein  $C_0$  is higher when there is more electrostatic interaction between the host and the guest. We do not know whether the discrepancies observed in the diffusivity values in both the systems is a consequence of the very simple model being used to describe the protein incorporation process or whether it is due to assumption of a primitive electrostatic picture for

the process. We would like to emphasize that this model is highly idealized and represents a first step in the analysis of the kinetics of the protein incorporation process. We would like to mention that we do not stress on the absolute values of the diffusivities of the protein from this model. We have used a simple model, wherein the diffusivity values are used for comparison of the same system under different pH conditions. Hence we also would not like to compare our diffusivity values with that of other models. Herein we are interested only in the trends for diffusivities. It is clear that a purely electrostatic picture of the process is not correct and supports earlier studies of polyion-ionized lipid monolayer interactions where a Poisson-Boltzmann electrostatic model was clearly shown to be inadequate in explaining the complexation observed.<sup>11</sup> The situation on hand regarding protein-lipid interactions is expected to be far more complex. Later in this chapter the studies on different protein intercalation, dependence of diffusivity on protein charge: mass ( $e/m$ ) and total charge has been explained.

#### 3.4. METHODS FOR ENHANCING THE PROTEIN DIFFUSIVITY IN THE LIPID MATRIX.

One of the prerequisites for biocomposite formation is that the process should be relatively fast thereby avoiding denaturation of the biomolecules being used. The importance of this factor in commercialization of such enzyme immobilization protocols cannot be overemphasized. In the case of Cyt *c* entrapment in thermally evaporated AA films, the diffusion of the protein into the lipid is extremely slow, often requiring 40-72 h of immersion in the protein solution to achieve equilibration in the lipid matrix. This may prove to be detrimental to the immobilized protein/enzyme and prompted us to investigate means of enhancing the diffusion rate of cyt *c* into lipid films.

**a) Role of buffers:** Fig. 3.4.1 shows a plot of the QCM mass uptake data of Cyt *c* intercalation into a 250 Å thick AA film during immersion in  $10^{-5}$  M Cyt *c* solutions prepared in different buffers (squares, pH 3; circles, pH 6.8 and triangles, pH 9). The protein solution pH and equilibrium Cyt *c* : AA molar ratios are indicated next to the respective curves. It can be seen that complete incorporation of the protein in this case takes place within 120 minutes of immersion of the AA film in protein solutions. Maximum protein intercalation occurs at pH 6.8 as in the earlier case with 1000 Å thick films. The solid lines are 1-D diffusion fits to the data as

done in the earlier case, with the error bars of 10 % deviation for pH 6.8 case and 5 % deviation for pH=3 and 9.

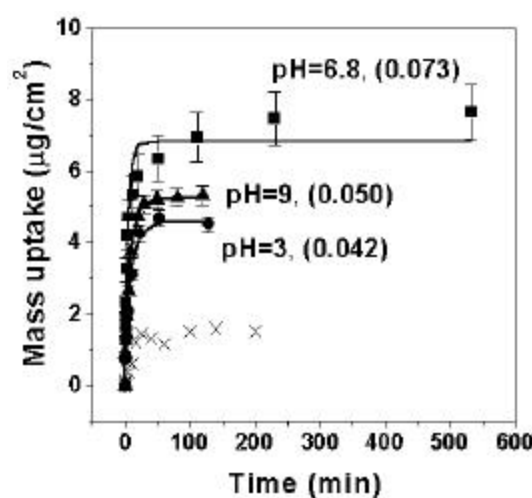


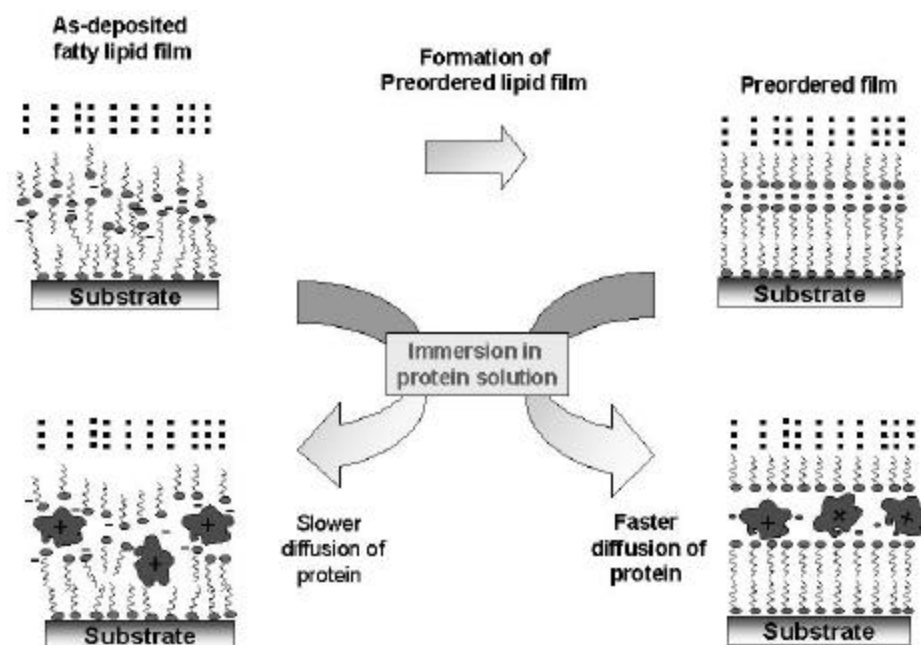
**Figure. 3.4.1:** QCM mass uptake of Cyt *c* with time during immersion of 250 Å thick AA films in  $10^{-5}$  M Cyt *c* at different pH values. The pH values and equilibrium molar ratios of Cyt *c* : AA are indicated in the parenthesis next to the respective curves. The solid lines are fit to the data using 1-D diffusion model (see text for details). The error bars to pH=6.8 are 10 % deviation to the data, and that for other two pH values is 5% deviation to the data (see text for details). A control experiment of mass uptake measured as a function of immersion of 250 Å thick AA film deposited quartz crystal for different time intervals into 0.05 M sodium phosphate, pH=6.8 buffer (crosses; see text for details).

Comparing the two figures (Fig. 3.3.1 and 3.4.1) it is clear that protein loading increases with increase in thickness of the deposited lipid. The diffusion coefficient (as seen from Table 3.3.1) into the film is also increased by two orders of magnitude due to the presence of buffers in the protein solution. This might be due to a competitive diffusion process between the protein and ions from the buffer in the matrix leading to enhanced diffusion rates of the proteins. A control experiment was performed in which the 250 Å thick AA film deposited on QCM crystal was immersed for different time intervals in a buffer (0.05 M, sodium phosphate, pH=6.8). Some amount of mass loading was observed as indicated in Fig. 3.4.1 (crosses) but is negligible as compared to the overall mass uptake due to that of the protein.

#### **b) Preordering the lipid film:**

**1. PbSt-SOM films:** The spontaneous ordering of thermally evaporated AA/StA films by  $Pb^{2+}$  ion incorporation was accomplished by immersion of the 500 Å thick lipid films in  $10^{-4}$  M aqueous solution of  $PbCl_2$  (pH 5.5). The lead ions are electrostatically complexed with the

carboxylate groups of the lipid matrix leading to the formation of a *c*-axis oriented lamellar structure. Intercalation of  $\text{Pb}^{2+}$  ions into the lipid film was followed by QCM, FTIR and XRD measurements. Thereafter these 'preordered' SOM films were immersed into  $10^{-5}$  M Cyt *c* solutions for different time. The methodology has been explained in scheme 3.4.1 below.



**Scheme. 3.4.1:** Diagram showing the intercalation of protein in as-deposited lipid film versus that in the preordered film. The expected microscopic structure of the protein-lipid composite film is also shown.

For comparison, the QCM kinetics of Cyt *c* mass uptake from an as-deposited StA film (500 Å thick), which is not ordered in a lamellar fashion was also performed. The short times required for protein incorporation (30 min for preordered SOMs versus 10 h for 'unordered' as-deposited lipid films) clearly suggests the role of preordering in enhancing the protein diffusivity. This has been clearly shown in the scheme 3.4.1. The diffusion coefficients calculated (Table 3.3.1) clearly shows almost an order of magnitude difference, in protein diffusivities of unordered versus preordered films. The protein loadings are vastly different (3.5 for preordered films vs 8.5  $\mu\text{g}$  for 'unordered' films). This might be due to the presence of the  $\text{Pb}^{2+}$  ions, which limits accessibility of the carboxylate ions to the proteins diffusing in the 'preordered' film.

**2. PbSt-LB films.** Lead stearate LB films of thicknesses corresponding to 5, 9, 15 and 19 monolayers (MLs) were deposited under conditions described in chapter II (section 2.2). QCM, FTIR and XRD were used to characterize the films formed. A 19 ML PbSt-LB film (~ 475 Å thick) deposited on a QCM crystal was immersed into a  $10^{-5}$  M aqueous solution of cyt *c* (pH 6.8) and the protein diffusion was followed by QCM measurements as explained earlier. The inset of Fig. 3.4.3 shows the kinetics of cyt *c* incorporation in the PbSt LB film.

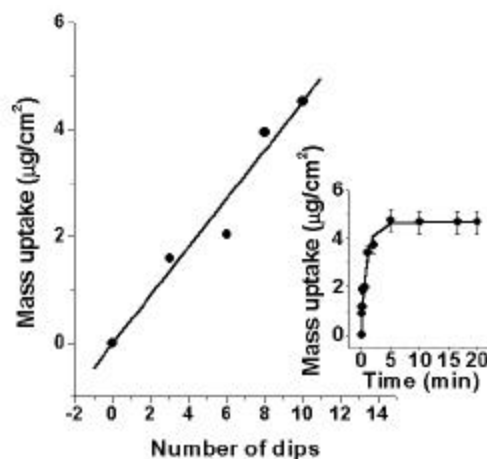


**Figure. 3.4.3:** QCM mass loadings recorded from PbSt LB films of different thickness after immersion in Cyt *c* solution for 20 minutes. The inset shows the QCM mass uptake data recorded from a 19 ML PbSt LB film as a function of time of immersion in Cyt *c* solution. The solid line is based on a 1-D diffusion analysis of the data. The error bars to the data are roughly 10% deviation of the data from the mean values obtained by 3 similar experiments under similar conditions (see text for details).

It can be clearly seen that the time required for complete protein incorporation is ca 5 min as compared to the as-deposited thermally evaporated lipid film (inset of Fig. 3.4.3). Thus, the formation of an ordered, lamellar structure drastically decreases the time of formation of the protein-lipid bioconjugate film. The solid line in the inset is based on a 1-D diffusion analysis of the mass uptake data (diffusion parameters as shown in Table 3.3.1), and the error bars indicate a 10 % standard deviation to the data as measured by 3 separate experiments under similar conditions. The main part of the Fig.3.4.3 shows the equilibrium mass uptakes recorded from PbSt LB films grown on QCM crystals of 5, 9, 15 and 19 ML thickness after immersion in Cyt *c* solution for 20 min each. A linear layer-by-layer (LBL) increase in the protein uptake with

increasing thickness is clearly seen with a non-linear least squares fit yielding  $0.45 \mu\text{g}/\text{dip}$  (per bilayer).

The XRD pattern recorded from the 19 ML PbSt-LB film on Si (111) wafer is shown as curve 1 in Fig. 3.4.4. The (0 0 l) reflections from the lamellar PbSt structure in the LB films can clearly be seen with the distinct odd-even intensity oscillations characteristic of *c*-axis orientation of the film.<sup>12</sup> From the positions of the Bragg reflections, a bilayer thickness value of  $49.5 \text{ \AA}$  was calculated, in excellent agreement with that expected from the dimensions of stearic acid and lead ions.<sup>11</sup> The XRD pattern recorded from the 19 ML PbSt LB film after equilibration of Cyt *c* density in the film is shown in Fig.3.4.4 (curve 2). On comparing the two curves shows it is seen that the intensity of the (0 0 l) Bragg reflections is considerably reduced in intensity subsequent to protein entrapment. The lamellar ordering in the PbSt film is reduced on protein intercalation and is not surprising given the dimensions of the protein (ca.  $35 \text{ \AA}$ ). Accommodation of Cyt *c* in the hydrophilic regions of the bilayers which normally have dimensions of  $3\text{-}5 \text{ \AA}$  with metal ions such as  $\text{Pb}^{2+}$ <sup>12</sup> would lead to distortion of the lamellae as shown in Scheme 3.4.1 and would explain the loss in intensity of the (0 0 l) Bragg reflections in the XRD measurements (curve 2, Fig.3.4.4).

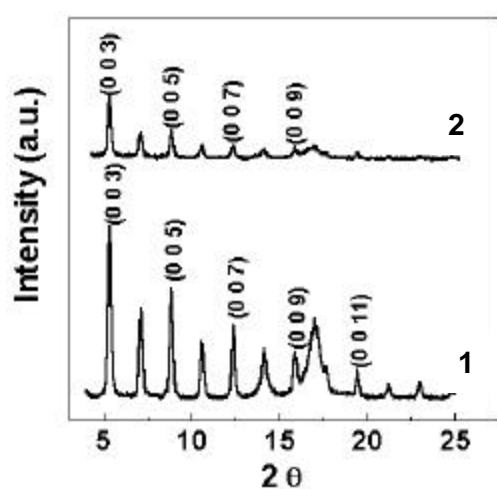


**Figure. 3.4.4.** XRD patterns recorded from a 19 ML thick PbSt-LB film (curve 1) and the LB film shown as curve 1 after further incorporation of Cyt (curve 2; see text for details).

**Table 3.3.1**

Parameters obtained from a 1-D diffusion analysis of QCM mass uptake measurements during incorporation of Cyt c and Hb in fatty lipid matrixes.

**A. Cyt c-AA system:**

Solution pH	Lipid Matrix	Film Thickness/Å	C <sub>0</sub> /molecules cm <sup>-3</sup>	D/Å <sup>2</sup> min <sup>-1</sup>
3	AA	2000	1.3 x 10 <sup>11</sup>	476
6.8	AA	2000	6.3 x 10 <sup>11</sup>	413
9	AA	2000	1.3 x 10 <sup>11</sup>	955
3	AA	500	4.46 x 10 <sup>11</sup>	1.06 x 10 <sup>4</sup>
6.8	AA	500	6.63 x 10 <sup>11</sup>	1.96 x 10 <sup>4</sup>
9	AA	500	5.1 x 10 <sup>11</sup>	1.09 x 10 <sup>4</sup>
6.8	PbSt-SOM	500	3.19 x 10 <sup>11</sup>	1.52 x 10 <sup>4</sup>
6.8	PbSt-LB	500	4.49 x 10 <sup>11</sup>	5.6 x 10 <sup>4</sup>

**B. Hb-ODA system:**

Solution pH	Lipid Matrix	Film Thickness/Å	C <sub>0</sub> /molecules cm <sup>-3</sup>	D/Å <sup>2</sup> min <sup>-1</sup>
3	ODA	1100	1.9 x 10 <sup>10</sup>	4.4 x 10 <sup>5</sup>
6	ODA	1200	4.7 x 10 <sup>10</sup>	1.4 x 10 <sup>5</sup>
9	ODA	1200	8.1 x 10 <sup>11</sup>	9.3 x 10 <sup>4</sup>

### 3.5 DIFFUSION OF PROTEIN INTO FATTY LIPIDS: ROLE OF PROTEIN CHARGE: MASS (e/m), TOTAL PROTEIN CHARGE AND PROTEIN HYDRODYNAMIC RADII:

We have investigated the protein diffusion into fatty lipid matrixes and drawn correlations between different parameters such as the dependence of protein diffusivity and equilibrium mass loadings on protein charge: mass ratio and protein net charge. For this purpose, different proteins such as bovine serum albumin (BSA), pepsin and  $\beta$ -Lactoglobulin, ( $\beta$ -Lac) (all anionic at pH 7) and trypsin, RNase A and lysozyme (all cationic at pH 7) were intercalated into oppositely charged matrixes such as ODA (cationic at pH 7) and StA (anionic at pH 7). The role of other secondary interactions has also been probed by studying the intercalation of these proteins into neutral matrix such as octadecanol (ODOH). The intercalation was studied by

QCM and FTIR measurements as has been explained in the earlier sections. We found the following correlations:

a) The diffusion of proteins into fatty lipid matrixes is to a large extent dependent on electrostatic interactions between the host and the guest molecules. Secondary interactions such as hydrophobic and hydrogen bonding are also responsible for the protein intercalation process. The protein diffusivity ( $D$ ) into the lipid matrix depends on the protein charge: mass ( $e/m$ ) ratio, when electrostatic interactions are the dominating force for protein diffusion. When other secondary interactions dominate the protein diffusion process, the  $e/m$  dependence fails. Fig. 3.5.1 summarizes these observations.

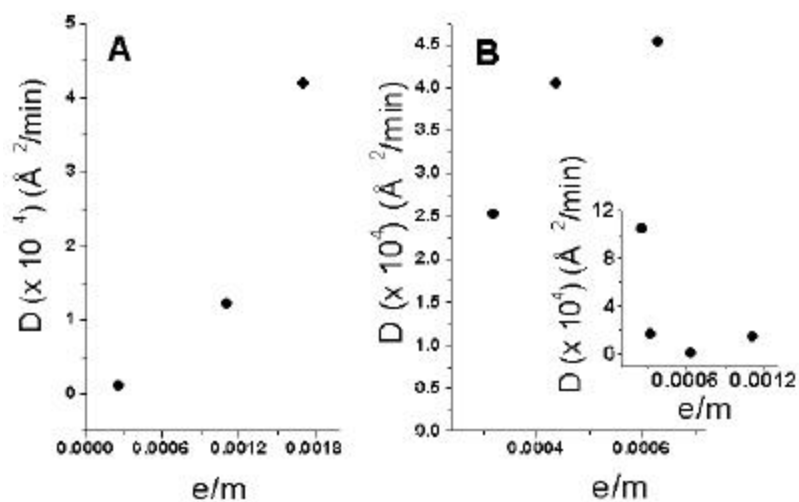


**Figure. 3.5.1:** A) Variation in diffusivity ( $D$ ) calculated for the diffusion of anionic proteins into ODA as a function of changes in  $e/m$  ratio. B) Variation in diffusivity ( $D$ ) calculated for the diffusion of cationic proteins into StA matrix as a function of changes in  $e/m$  ratio. The inset shows the variation in  $D$  values as a function of  $e/m$  variation in a neutral ODOH matrix.

Fig. 3.5.1A and B shows the correlation between the  $e/m$  ratio and the protein diffusivity ( $D$ ) in the case of anionic and cationic proteins respectively. In both the cases a monotonic increase in the  $D$  values as a function of increase in  $e/m$  values is clearly seen. But the rate of increase in the case of anionic protein diffusion is much more rapid than that in the case of cationic proteins. This might possibly be due to the overall variation in the  $e/m$  ratios of anionic proteins ( $e/m$  goes from  $2.6 \times 10^{-4}$  to  $1.1 \times 10^{-3}$ ) than that compared to the cationic proteins ( $e/m$  goes from  $3.21 \times 10^{-4}$  to  $6.28 \times 10^{-4}$ ). The inset of Fig. 3.5.1B shows the variation of  $D$  as a



function of variation in  $e/m$  ratio in the case of protein diffusion into neutral (ODOH) matrix. It can be clearly seen that the diffusivities of the four proteins do not show any trend indicating that the  $e/m$  dependence fails when other secondary interactions are more dominating.

b) The extent of equilibrium protein loadings, as determined by protein: lipid molar ratio depends to a large extent on the degree of charge neutralization, considering the dominance of electrostatic interactions. The protein: lipid ratio is more for proteins with a higher net electronic charge as can be seen from Table 4.5.1 below. The dependence works out well in the case of anionic proteins (BSA, pepsin and  $\beta$ -Lac. In the case of cationic proteins, trypsin bears a larger charge than RNase A, yet the equilibrium protein: StA molar ratio is smaller. This could be due to either experimental uncertainties or due to the differences in the actual size of the proteins. The protein charge: mass ratios in the case of trypsin and RNase A show that even though the charge on trypsin is higher, the  $e/m$  ratio is smaller than that of RNase A (Table 4.5.1). A larger protein mass would mean a larger physical dimension for the protein and indeed, the hydrodynamic radii of trypsin and RNase A are 23.35 and 18.66 Å respectively.

All these co-relations have been tabulated in Table 3.5.1 below.

**Table 3.5.1**

Parameters obtained from a 1-D diffusion analysis of QCM mass uptake measurements during incorporation of proteins in fatty lipid matrixes.

Protein	Lipid Matrix	$e/m$ (units)	$D/\text{Å}^2 \text{ min}^{-1}$	Equilibrium molar ratios of protein:lipid	Charge on protein
BSA	ODA	$2.6 \times 10^{-4}$	$1.05 \times 10^3$	0.019	-17
Pepsin	ODA	$1.1 \times 10^{-3}$	$1.21 \times 10^4$	0.023	-37.5
$\beta$ -Lac	ODA	$1.7 \times 10^{-3}$	$4.18 \times 10^4$	0.017	-11
Trypsin	StA	$3.21 \times 10^{-4}$	$2.53 \times 10^4$	0.018	+7.5
RNase	StA	$4.38 \times 10^{-4}$	$4.05 \times 10^4$	0.040	+6
Lysozyme	StA	$6.28 \times 10^{-4}$	$4.53 \times 10^4$	0.1	+9
Cyt c	AA	$7.73 \times 10^{-4}$	$1.96 \times 10^4$	0.073	+9.5
BSA	ODOH	$2.6 \times 10^{-4}$	$1.04 \times 10^5$	0.0083	-17
Pepsin	ODOH	$1.1 \times 10^{-3}$	$1.43 \times 10^4$	0.010	-37.5
Trypsin	ODOH	$3.21 \times 10^{-4}$	$1.618 \times 10^4$	0.031	+7.5
Lysozyme	ODOH	$6.28 \times 10^{-4}$	$1.14 \times 10^3$	0.065	+9

### 3.6 MONITORING CYT *c* REDOX ACTIVITY.

Cyt *c* is a redox active heme protein and this was followed for the Cyt *c*-AA composite film using UV-vis spectroscopy. The UV-vis spectrum recorded from a 1000 Å thick AA film deposited on a quartz substrate after immersion in Cyt *c* solution (pH 6.8) for 75 hours is shown in the inset of Fig. 3.6.1A. The redox behaviour of the protein in the lipid matrix was confirmed by reaction with ascorbate and ferricyanide solutions and the spectra obtained under both conditions is shown in Fig. 3.6.1 A. The upper spectrum in Fig. 3.6.1A was recorded from the 1000 Å thick Cyt *c* – AA composite film after reduction of the heme center while the lower curve is the spectrum recorded after the oxidation cycle.<sup>12</sup> While the Soret band occurs at 409 nm in both cases, important differences are observed in the Q-band absorption region (500 – 600 nm). In the reduced state, two fairly distinct bands at 520 nm and 550 nm are seen (features a and b respectively, Fig.3.6.1A) and this becomes a broad indistinguishable feature in the oxidized state. This is known to be a signature of the redox activity of the protein<sup>12</sup> and shows that the intercalated protein is accessible to analytes in solution. The inset of Fig.3.6.1A shows the UV-vis spectrum of the as-prepared Cyt *c*-AA composite film and it is observed that the Q-band region (500 nm – 600 nm region) shows two distinct peaks at about 520 nm and at 550 nm in this case as well.

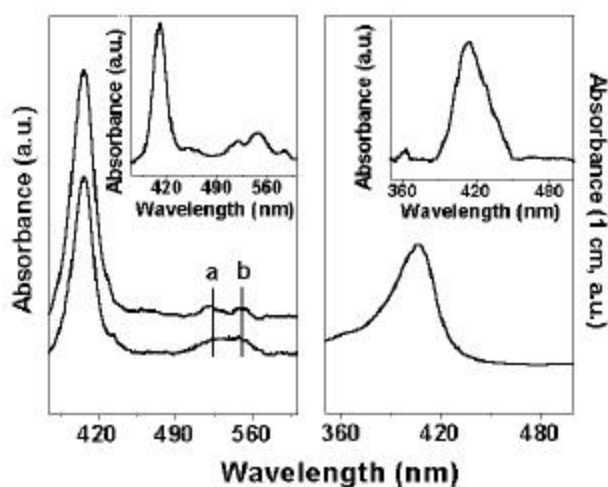


**Figure. 3.6.1:** A) Optical absorption spectra recorded from a 1000 Å thick Cyt *c*-AA composite film after immersion in 1 mM concentrated ascorbate and ferricyanide solutions for 20 minutes (upper and lower curves respectively). The inset shows the as-prepared 1000 Å thick Cyt *c* – AA composite film after immersion in Cyt *c* solution at pH = 6.8 for a period of 70 h (see text for details). B) Optical absorption spectrum recorded from a  $10^{-5}$  M concentrated Hb solution in pH = 9 buffer. The inset shows the optical absorption spectrum recorded from a 1000 Å thick Hb-ODA composite film formed at pH = 9.

This result indicates that the acid matrix behaves like a reducing environment and thus, is not strictly an inert host. The inset of Fig. 3.6.1 B shows the UV-vis spectra of 1000 Å thick Hb-ODA biocomposite film. The appearance of the soret band, comparable with that of the solution form of Hb (main part of Fig. 3.6.1 B) clearly indicates that the protein is present in its native state even in the immobilized form.

### 3.7. PROTEIN NATIVE STRUCTURE STUDIES.

**A. Secondary Structure, FTIR Studies.** The amide linkages between amino acid residues in polypeptides and proteins give well-known signatures in the infrared region of the electromagnetic spectrum. The position of the amide I and II bands in the FTIR spectra of proteins is a sensitive indicator of conformational changes in the protein secondary structure<sup>12,13</sup> and may be used to study the protein molecules in the lipid matrix.

Fig. 3.7.1 A shows the FTIR spectra recorded from a 1000 Å thick as-deposited AA film on Si (111) substrate (curve 1), the 1000 Å thick Cyt *c* – AA composite film (curve 2), a 250 Å thick as-deposited ODA film on Si (111) substrate (curve 3) and the 250 Å thick Hb - ODA composite film (curve 4). A number of vibrational modes can be observed for the four films. The amide I band occurs at ca. 1650 cm<sup>-1</sup> (feature b) for the Cyt *c*-AA and Hb-ODA composite films (curves 2 and 4). This band is clearly absent in the as-deposited AA film (curve 1). The position of this band is close to that reported for the native protein in earlier reports<sup>13</sup> and indicates that the secondary structure of the proteins in the different lipid environments is unperturbed. A small feature can also be seen from the as-deposited ODA film, but the intensity of this band increases in Hb-ODA film (curve 4) clearly indicating its origin from the protein molecules. The amide II band, which occurs at ca. 1545 cm<sup>-1</sup> (feature d), can also be clearly seen for the protein-lipid composite films (curves 2 & 4). This band also indicates that the secondary structure of the protein is maintained in the encapsulated form.<sup>12,13</sup> The band at 1699 cm<sup>-1</sup> (feature a) arises from the carbonyl stretch modes from the carboxylic acid groups in the AA matrix.<sup>14</sup> The band at 1564 cm<sup>-1</sup> (feature c) arises from the ODA host and is tentatively assigned to the N-H deformation vibration from the amine groups in the ODA matrix.

**B. Tertiary Structure, Fluorescence Spectroscopy.** The intactness of the tertiary structure of the heme proteins in the intercalated form was studied by fluorescence spectroscopy measurements of the biocomposite films on quartz substrates. This standard method involves exciting the sample at a particular wavelength and monitoring the fluorescence emission from the tryptophan or tyrosine residues in the protein as has been explained in Chapter II (section 2.6). The encapsulated heme proteins were excited at 295 nm, this wavelength corresponds to excitation of the  $\pi - \pi^*$  transition in the tryptophan residues of the proteins. The wavelength of this transition is known to be a sensitive indicator of the tertiary structure of proteins.<sup>15</sup> Fig. 3.7.1 B shows the fluorescence spectra of cyt *c* solution held at pH 6.8 (curve 1), and that of cyt *c* - AA biocomposite film (curve 2). The nature of the spectra and the similar peak positions clearly indicate that the protein in the biocomposite film is present in its natural conformation without significant distortion to its tertiary structure. Similar spectra were observed for Hb-ODA biocomposite films.

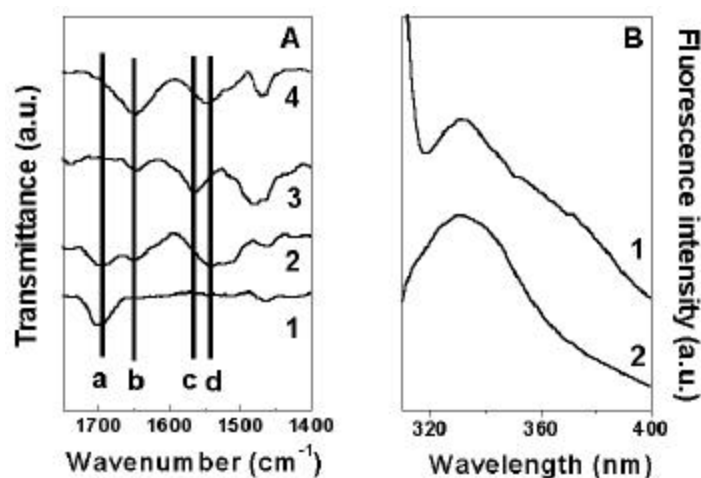


**Figure. 3.7.1:** A) FTIR spectra recorded from a 1000 Å thick as-deposited AA film (curve 1); a 1000 Å thick cyt *c* - AA composite film (curve 2); a 250 Å thick ODA film (curve 3) and a 250 Å thick Hb-ODA composite film (curve 4) (see text for details and assignments). B) Fluorescence spectra recorded from a 10<sup>-5</sup> M concentrated cyt *c* solution at pH 6.8 (curve 1) and a 1000 Å thick cyt *c*-AA composite film (prepared at pH 6.8) on quartz (curve 2, see text for details).

### 3.8. SUMMARY.

In this chapter, the formation of heme-protein-fatty lipid biocomposites has been demonstrated. The proteins are intercalated within the lipid bilayers by simple immersion of the

lipid films into respective protein solutions. The protein diffusion in the lipid matrix is driven to a large extent by electrostatic interactions between the amino acid residues on the protein surface and the ionized lipid molecules. Other secondary interactions such as hydrophobic and hydrogen bonding are also responsible for the protein intercalation. The kinetics of protein incorporation into the lipid matrix has been analyzed in terms of a simple Fickian type one-dimensional (1-D) diffusion model. The rate of diffusion of the protein in the lipid matrix depends to a large extent on the protein charge: mass (e/m) ratio. The e/m dependence on protein diffusion into lipid matrix fails when other secondary interactions are more predominant than electrostatic interactions. The extent of protein loading, which determines the charge neutralization as observed by the protein: lipid molar ratio, depends on the net electronic charge of the protein considering electrostatic interactions to be the major driving force for protein intercalation. The amount of protein loading and time required can be controlled by variation in film thickness, use of buffers and preordering the lipid film. The time required for the protein-lipid biocomposite formation is smaller than other protocols currently in vogue. The redox activity of Cyt *c* into the lipid matrix has been confirmed by immersion of the biocomposite film into ferricyanide and ascorbate solutions, and monitoring the Q band (520-550 nm) in the visible region of the electromagnetic spectrum. The redox activity indicates that the immobilized biomolecules are accessible to external reagents. The secondary and tertiary structure of the immobilized proteins has been studied by FTIR and fluorescence spectroscopy, and the studies indicate no significant changes to the natural conformation of the protein. The flexibility of the lipid bilayers is primarily responsible for this, and indicates that the lipid film is more bio-friendly for intercalating 'soft' biomolecules.

### 3.9. REFERENCES.

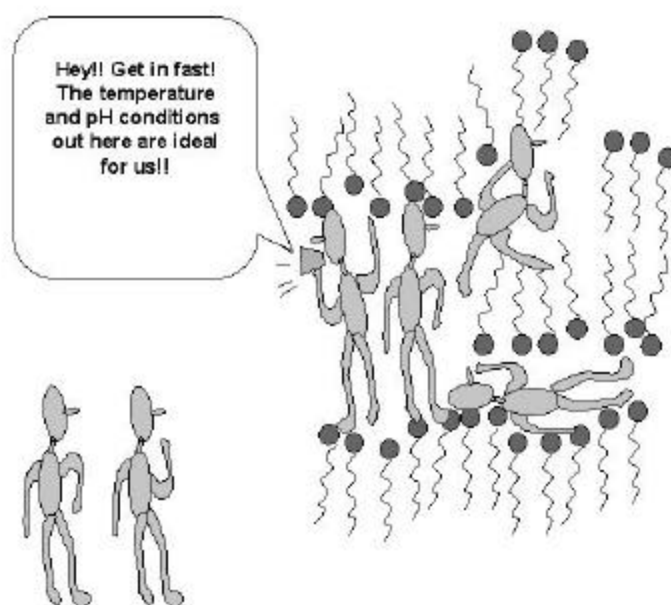
1. a) Ball, P. *Designing the Molecular World : Chemistry at the frontier.*, **1994**, Princeton University Press, New Jersey, USA; b) Fendler, J.H. *Membrane Mimetic Chemistry*, John Wiley & Sons, USA, **1982**; c) May, S.; Ben-Shaul, A. *Biophys. J.*, **1999**, *76*, 751; d) Mouritsen, O.G.; Bloom, M. *Biophys. J.* **1984**, *46*, 141.

2. a) Ray, A.; Reynold, J.A.; Polet, H.; Steinhardt, J. *Biochemistry* **1966**, *5*, 2606; b) Reynolds, J.A.; Herbert, S.; Polet, H.; Steinhardt, J. *Biochemistry* **1967**, *6*, 937; c) Steinhardt, J.; Krijn, J.; Leidy, J.G. *Biochemistry* **1971**, *10*, 4005.
3. a) Himachi, I.; Fujita, A.; Kunitake, T. *J.Am.Chem.Soc.*, **1994**, *116*, 8811; b) f) Chen, X.; Hu, N.; Zeng, Y.; Rusling, J. F.; Yang, J. *Langmuir* **1999**, *15*, 7022; c) Nassar, A-E F.; Zhang, Z.; Hu, N.; Rusling, J. F.; Kumosinski, T. F. *J. Phys. Chem. B.*, **1997**, *101*, 2224; d) Burgess, J. D.; Rhoten, M. C.; Hawkrigde, F. M. *Langmuir* **1998**, *14*, 2467; e) Salamon, Z.; Tollin, G. *Biophys. J.*, **1996**, *71*, 848.
4. a) Ostuni, E.; Chapman, R. G.; Liang, M.N.; Meluleni, G.; Pier, G.; Ingber, D.E.; Whitesides, G. M. *Langmuir* **2001**, *17*, 6336; b) Ostuni, E.; Chapman, R. G.; Holmlin, E.; Takayama, Shuichi.; Whitesides, G.M. *Langmuir* **2001**, *17*, 5605; c) Ostuni, E.; Kane, R. Chen, C.S.; Ingber, D. E. Whitesides, G.M. *Langmuir* **2000**, *16*, 7811; d) Chapman, R.G.; Ostuni, E.; Takayama, S.R.; Holmlin, E.; Yan, L.; Whitesides, G.M. *J. Am. Chem. Soc.*, **2000**, *122*, 8303; e) Roberts, C.; Chen, C. S.; Mrksich, M.; Martichonok, V.; Ingber, D. E.; Whitesides, G.M. *J. Am. Chem. Soc.*, **1998**, *120*, 6548; f) Sigal, G.B. Bamdad, C.; Barberis, A.; Strominger, J.; Whitesides, G.M. *Anal. Chem.* **1996**, *68*, 490.
5. a) Ganguly, P.; Sastry, M.; Pal, S.; Shashikala, M.N. *Langmuir* **1995**, *11*, 1078; b) Pal, C. Ph. D. Thesis, University of Poona, **1996**; c) Gole, A.; Sastry, M. *Inorg. Chem. Commun.*, **2001**, *4*, 568.
6. a) Patil, V.; Mayya, K.S.; Sastry, M. *Langmuir* **1998**, *14*, 2707; b) Sastry, M.; Patil, V.; Mayya, K.S. *Langmuir* **1997**, *13*, 4490; c) Sastry, M.; Patil, V.; Sainkar, S.R. *J.Phys.Chem.B.* **1998**, *102*, 1404; d) Patil, V.; Sastry, M. *Langmuir* **2000**, *16*, 2207; e) Patil, V.; Sastry, M. *Langmuir* **1997**, *13*, 5511; f) Patil, V.; Malvankar, R.B.; Sastry, M. *Langmuir* **1999**, *15*, 8197; g) Patil, V.; Sastry, M. *J.Chem.Soc.,Faraday Trans.* **1997**, *93*, 4347; h) Sastry, M. *Curr.Sci.* **2000**, *72*, 1089.
7. a) Sauerbrey, G. *Z.Phys. (Munich)* **1959**, *155*, 206; b) Buttry, D. A.; Ward, M.D. *Chem. Rev.* **1992**, *92*, 1356; c) Wang, J.; Frostman, L.M.; Ward, M.D. *J.Phys.Chem.* **1992**, *96*, 5224.

8. a) Franchina, J. G.; Lackowski, W. M.; Dermody, D. L.; Crooks, R. M.; Bergbreiter, D. E.; Sirkar, K.; Russell, R. J.; Pishko, M. V. *Anal.Chem.* **1999**, *71*, 3133; b) Rao, M. S.; Dave, B. C. *J.Am.Chem.Soc.* **1998**, *120*, 13270;
9. a) Marshbanks, T.L.; Ahn, D.J.; Frances, E.I. *Langmuir* **1994**, *10*, 276; b) Marshbanks, T.L.; Frances, E.I. *J.Phys.Chem.*, **1994**, *98*, 2166.
10. Carslaw, H.S.; Jaeger, J.C. *Conduction of Heat in Solids*, Clarendon Press, Oxford, **1960**, 101.
11. Cuvillier, N.; Rondelez, F. *Thin Solid Films* **1998**, *327-329*, 19.
12. Kumar, C. V.; McLendon, G. L. *Chem. Mater.* **1997**, *9*, 863.
13. a) Dong, A.; Huang, P.; Caughey, W.S. *Biochemistry* **1992**, *31*, 182; b) Templeton, A.C.; Chen, S.; Gross, S.M.; Murray, R.W. *Langmuir* **1999**, *15*, 66; c) Caruso, F.; Furlong, D. N.; Ariga, Katsuhiko.; Ichinose, I.; Kunitake, T. *Langmuir* **1998**, *14*, 4559.
14. Rabolt, J. F., Burns, F. C., Schlotter, N. E., Swalen, J. D. *J. Chem. Phys.* **1983**, 78.
15. a) Eftink, M. R and Ghiron, C. A. *Anal. Biochem.* **1981**, 199; b) Reynolds, J.A.; Gallagher, J.P.; Steinhardt, J. *Biochemistry* **1970**, *9*, 1232; c) Pace, C.N. *Methods. Enzymol.*, **1975**, *131*, 266.

# CHAPTER IV

## IMMOBILIZED BIOCATALYSTS: STABILITY AND BIOLOGICAL ACTIVITY



---

Immobilization of the enzymes fungal protease (F-prot) and endoglucanase in thermally evaporated fatty lipid films has been demonstrated in this chapter. The kinetics of diffusion has been analyzed by 1-D diffusion model. The retention of secondary and tertiary structure of the enzymes upon immobilization has been confirmed by FTIR, fluorescence and biocatalytic activity measurements. The role of trapped water within the lipid films along with the enzyme has been probed as to the retention of biological activity. The role played by the lipid in stabilizing the enzyme against harsh environmental conditions has been demonstrated.

---

The work presented in this chapter has been published: 1) **Gole, A**; Dash, C.; Mandale, A.B.; Rao, M.; Sastry, M. *Anal. Chem.*, **2000**, *72*, 4301; 2) **Gole, A**; Vyas, S.; Sainkar, S. R.; Lachke, A.; Sastry, M. *Langmuir* 2001, *17*, 5964; 3) Sastry, M.; **Gole, A**; Rao, M.; Ganesh, K.N. *Acc Chem Res.*, in press; d) Sastry, M.; **Gole, A**; Ramakrishnan, V.; Dash, C.; Vyas, S.; Lachke, A.; Rao, M.; Ganesh, K.N. *Trends. Biotechnol.*, in press.



#### 4.1 INTRODUCTION.

Enzymes are biocatalysts that nature has designed in order to perform certain functions *in vivo* in biological systems, which under normal conditions do not take place. Enzymes can be thought of as nature's engineers who often perform very difficult tasks.<sup>1</sup> In general, an enzyme's function will be to cut away a part of a molecule or to stitch its component parts together.<sup>1,2</sup> Some for instance, break down large carbohydrate molecules into the sugar glucose and then further into carbon dioxide and water-the reaction sequence of our principle metabolic pathway. Breaking down large molecules into smaller ones is something that is not so difficult to achieve by nonbiological catalysis, but the trick that enzymes perform is to do this in a controlled manner that allows the energy released by bond breaking to be stored as chemical energy rather than being wasted as heat.<sup>1,2</sup> Other enzymes help to put together protein molecules from their constituent amino acids, or assemble the gene-carrying molecule DNA-tasks that lie well beyond the present capabilities of organic chemists. Enzymes are huge protein molecules, often containing many thousands of atoms, which are structured in a way that makes them very sensitive to the shapes of the molecules on which they perform their catalytic function. Hence they have a 'structure-function' type of a relationship. Enzymes act only on those substrates which have shapes that lock in into the 'substrate binding site' by the so called 'lock and key' type of interaction commonly termed as the 'molecular recognition process'.<sup>1</sup> Just about all of the chemical processes that take place within a living organism rely on enzyme catalysts. There are about 7000 different sorts of enzyme that occur naturally typically measuring up to a tenth of a micrometer across, and many are assemblies of more than one molecular unit, held together by noncovalent bonds. It is therefore unclear whether they should be thought of as homogenous or heterogeneous catalysts-they are certainly bigger than the single molecules that chemists generally recognize as belonging to the homogenous catalysis class.<sup>1</sup> On the other hand, they are much smaller than the 'bulk' particles of metals or other inorganic solids used for heterogeneous catalysis. The truth is that they display aspects of both classes.<sup>1</sup>

Industrial chemists extensively employ these natural catalysts to work to facilitate reactions in the chemicals industry. There are two ways in which enzymes can be used for industrial processes. One way is to employ whole cells or microorganisms which are 'living

factories' that produce enzymes to convert raw materials enzymatically into the desired product.<sup>1,2</sup> It works in many cases, but the disadvantage of such method is that a microorganism may send the reactants down a variety of reaction pathways to yield a mixture that includes unwanted by-products. The second alternative is to separate the enzyme from the cells that produce it, and to use the pure form for catalysis. This method is the widely accepted method and usually employed for industrial processes. Enzymes can be used to a large extent in food, chemical, agriculture industries and pharmaceutical and biomedical processes.<sup>1,2</sup> The main drawback of using free solution based enzymes in industrial processes is that they cannot be reused, making such protocols costly.<sup>2</sup> The utility of the enzymes in these applications may be greatly enhanced if they could be immobilized onto/within suitable solid supports due to the following reasons.<sup>2</sup>

- 1) Convenience in handling.
- 2) Easy separation of the enzyme from the product. This simplifies enzyme applications and supports a reliable and efficient reaction technology.
- 3) Reuse of the enzyme. This provides cost advantages which are often an essential prerequisite for establishing an enzyme-catalyzed process for any industrial application.
- 4) Increased thermal, temporal and pH stability. This is one of a very important point in the case of immobilized biocatalysts. Immobilization in other words is restricting mobility of a substance. Upon immobilization, there is hindered mobility of the enzyme side chains, which resists aggregation of the enzymes even due to significant fluctuations in environmental conditions. This in fact has been observed in many cases.<sup>2</sup>

For all these advantages, there are some factors that need to be considered as to the suitability of the immobilization matrix.<sup>2</sup>

- 1) The matrix should be rugged, stable, biocompatible and inert and should not interfere with the native structure of the protein and thereby compromise its biological activity.
- 2) The matrix should protect the enzyme against microbial degradation, hydrolysis and deamidation and should render the enzyme accessible to cofactors and redox agents.
- 3) The immobilization matrix/process should be relatively quick, inexpensive, protein-friendly, result in high loading factors and should be applicable to a large range of biomolecules.

4) The time required for the substrate to access the immobilized enzyme should be less. This is known as the 'mass transport problem' in which, the yield of the biocatalyst depends on the accessibility of the substrates and co-factors.

Out of the various immobilization protocols discussed in Chapter I, section 1.6, we feel that, biomimetic agents such as lipids in the form of mono/bi-layers, liposomes, polymers, polyelectrolytes are more suitable due to their flexibility and bio-friendliness.<sup>3</sup>

In this chapter, the work on immobilization of fungal protease (F-prot; M.W ~ 37,000; pI ~ 9; cationic at pH 7) and endoglucanase (M.W ~ 50,000; pI ~ 4.1; anionic at pH 7) within stacks of anionic and cationic lipid bilayers has been explained. The native conformation of the immobilized enzymes has been confirmed by FTIR, fluorescence and biocatalytic activity measurements. It was found that drying of the lipid films lead to a loss in biological activity upon aging, possibly due to conformational changes in the enzyme due to dehydration. The immobilized endoglucanase was found to be more stable at higher temperature and pH conditions possibly due to the stabilization offered by the lipid bilayers. The enhanced temporal, temperature and pH stability of the immobilized enzymes makes the protocol based on lipid bilayer entrapment exciting and shows potential for industrial exploitation.

## 4.2 DEPOSITION OF LIPID FILMS.

Amphiphilic molecules such as fatty acids (Arachidic acid, AA,  $\text{CH}_3(\text{CH}_2)_{19}\text{COOH}$ , pKa ~ 3.5, anionic above pKa; Stearic acid, StA,  $\text{CH}_3(\text{CH}_2)_{17}\text{COOH}$ , pKa ~ 3.5) and fatty amines (Octadecylamine, ODA,  $\text{CH}_3(\text{CH}_2)_{17}\text{NH}_2$ , pKb ~ 10.5), were used for this study. As explained in chapter 2 and chapter 3, these lipids were thermally evaporated (using an Edwards E 306A vacuum deposition unit) onto suitable substrates such as gold coated AT-cut quartz crystals (for quartz crystal microgravimetry measurements), Si (111) substrates (for Fourier Transform Infrared Spectroscopy, FTIR, X-ray photoemission spectroscopy, XPS, Scanning electron microscopy, SEM and biocatalytic activity measurements), quartz substrates (for UV-vis and Fluorescence measurements). Deposition was done at a slow rate at a pressure better than  $10^{-7}$  torr. The films formed were checked for degradation using FTIR measurements and found to be intact. The thickness of the films deposited was in the range 250 Å to 1000 Å depending on the type of application.

### 4.3 QUARTZ CRYSTAL MICROGRAVIMETRY.

#### 4.3.1 Fungal protease (f-prot)-Arachidic acid (AA) system.

The entrapment of F-prot into fatty acid films was carried out by immersion of AA coated films in the  $10^{-5}$  M concentrated enzyme solutions held at different pH value buffers. As explained in chapter 2 and 3, 250 Å thick AA films deposited onto quartz crystals, were immersed into the enzyme solutions for different time intervals, and frequency measured *exsitu* after thorough rinsing (in deionized water) and drying (in flowing nitrogen) of the crystals. The frequency changes were converted to mass uptake data by using the standard Sauerbrey formula<sup>4</sup> as has been explained in detail in chapter 2. Fig. 4.3.1A shows a plot of the QCM mass uptake data of F-Prot diffusion into 250 Å thick AA films during immersion in the F-Prot solutions at pH 6 (0.05 M sodium – phosphate; circles), pH 3 (0.05 M, glycine – HCl; squares) and pH 9 (0.05 M Tris – HCl; triangles). The enzyme solution pH is indicated next to the respective curves along with the equilibrium F-Prot-AA molar ratios (numbers within parenthesis). The solid lines are the 1-D diffusion analysis of the QCM data as has been explained in Chapter 3, and the parameters obtained have been displayed in Table 4.3.1.

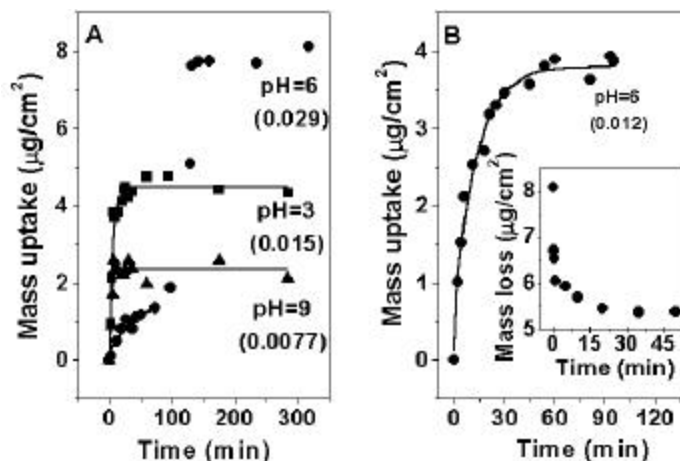


**Figure. 4.3.1:** A) QCM kinetics of incorporation of F-Prot in the AA matrix with time during immersion of 250 Å thick AA films in  $10^{-5}$  M F-Prot solution at different pH values. The pH values are indicated next to the respective mass uptake curves along with the equilibrium F-Prot-AA molar ratio values (within parenthesis). The solid lines are based on fits to the QCM data using a 1-D diffusion model (see text for details). B) QCM kinetics of incorporation of F-Prot in the ODA matrix with time during immersion of 250 Å thick ODA films in  $10^{-5}$  M F-Prot solution at pH 6. The solid line is based on fits to the QCM data using a 1-D diffusion model (see text for details). The inset shows the removal of F-prot molecules from a pre-loaded biocomposite film (at pH 6), during immersion in solution held at pH 3.

It can be seen from the Fig. 4.3.1A that maximum F-Prot encapsulation occurs at pH 6 with the equilibrium F-Prot loading factors being lower at pH 9 and pH 3. The nature of the enzyme diffusion kinetics is quite different for the pH 6 experiment. This difference was observed in three separate experiments carried out at this pH and is clearly a reproducible feature. We do not understand this aspect at this stage. The QCM kinetics data for F-Prot incorporation at pH 6 has therefore not been fit to the one-dimensional diffusion model.

At pH 6, there is maximum electrostatic interaction between the enzyme ( $pI \sim 9$ )<sup>4f,5</sup> and the AA matrix ( $pK_a$  of AA  $\sim 4.5$ ),<sup>6</sup> leading to more loading as compared to the other pH values. At pH 9, the surface charge on the F-Prot molecules is nearly zero while at pH 3, the AA molecules are expected to be completely unionized leading to minimum electrostatic interaction at these pH values. However, the fact that enzyme incorporation does occur under conditions of negligible electrostatic interactions underlines the fact that other interactions such as hydrogen bonding, hydrophobic interactions etc. also contribute to the interaction between the enzyme and AA film.

We also investigated the incorporation of F-Prot from solution at pH 6 into a 250 Å thick thermally evaporated cationic lipid octadecylamine (ODA) film on gold-coated quartz substrates by QCM. Fig. 4.3.1B shows the QCM kinetics of incorporation of F-Prot into a 250 Å thick ODA film (circles). The F-Prot-ODA molar ratio is indicated in the parenthesis in the figure. At pH 6, both the ODA ( $pK_B$  of ODA  $\sim 10.5$ ) and F-Prot molecules ( $pI \sim 9$ ) would be similarly (positively) charged. In spite of the repulsive electrostatic interaction between the host and guest molecules, fairly significant enzyme incorporation (ca. 30 % of the enzyme uptake observed under optimum conditions with AA, Fig.4.3.1A) occurs under these conditions.

The inset of Fig.4.3.1B shows the leaching out QCM kinetics of F-Prot from the biocomposite film (formed under optimum conditions at pH 6) during immersion in water held at pH 3. In the absence of attractive coulombic interaction, the enzyme molecules diffuse out into solution. It is seen that there is a nearly 50 % release of the encapsulated F-Prot molecules in the film and this agrees quantitatively with the enzyme uptake in the AA matrix at pH 3 (Fig. 4.2.1A).

The trends observed in the QCM kinetics study as to the extent in loading are also supported by the parameters obtained by 1-D diffusion model as shown in Table 4.3.1. The concentration at the interface ( $C_0$ ) is more at pH 9 than at pH 3 indicating an enhanced interaction at this pH. Comparing the diffusivities of the enzyme in AA and in ODA, it is seen from the table that the diffusivity in ODA is much less than in AA. This can be understood in terms of the repulsive interaction between the enzyme and the lipid matrix in the case of the F-Prot-ODA system while the interaction is weakly attractive in the other case. What is not understood is the large difference in the diffusivity at pH 3 and 9 in the F-Prot-AA system. It is expected that the strength of the electrostatic interaction in both cases would be roughly the same even though the exact physical situation in both cases is quite different (i.e., uncharged F-Prot-charged lipid at pH 9 and charged F-Prot-uncharged lipid at pH 3). This highlights yet again the role of interactions other than electrostatic in controlling the diffusion of F-Prot into the AA matrix.

**Table 4.3.1**

Parameters obtained from a 1-D diffusion analysis of QCM mass uptake measurements during incorporation of F-Prot in fatty lipid matrixes.

Solution pH	Lipid Matrix	Film Thickness/Å	$C_0$ /molecules $\text{cm}^{-3}$	$D/\text{Å}^2 \text{min}^{-1}$
3	AA	500	$1.46 \times 10^{11}$	15210
9	AA	500	$7.60 \times 10^{11}$	31700
6	ODA	500	$1.2 \times 10^{11}$	7520

#### 4.3.2 Endoglucanase - Octadecylamine (ODA) system.

The role of secondary interactions, other than electrostatic in the intercalation of proteins is much more evident in the endoglucanase-ODA system. Another interesting fact that was seen in this study was the fact that upon immobilization, the enzyme lost its biological activity. We believe that the active site or the substrate-binding site of the enzyme possibly binds/interacts with the lipid host. It is well known that protecting these sites by polyelectrolytes or substrates, could help in circumventing such a loss in biological activity.<sup>18</sup> The details of this study have been elaborated in section 4.7.5 below. What we would like to point out here is the fact that we

have co-immobilized carboxymethyl cellulose (CMC) which is the substrate for endoglucanase enzyme into the fatty amine films.

Three 250 Å thick octadecylamine (ODA) coated quartz crystals were immersed for different time intervals into substrate-protected endoglucanase solutions (1: 2 molar ratio of enzyme: substrate) held at different pH values of 5, 7 and 9 respectively at 4 °C. The substrate protection of the enzyme was achieved by mixing different molar ratios of the enzyme endoglucanase with its substrate, carboxymethyl cellulose (CMC) at 4 °C. Fig. 4.3.2 shows the QCM mass uptake recorded for three different films (triangles, pH 5; circles, pH 7 and squares, pH 9) as a function of time of immersion in the enzyme solutions. The solid lines are an aid to the eye and have no physical significance. The error bars are 5% standard deviation to the QCM data for all the three-pH values are obtained by 5 separate experiments in each case.

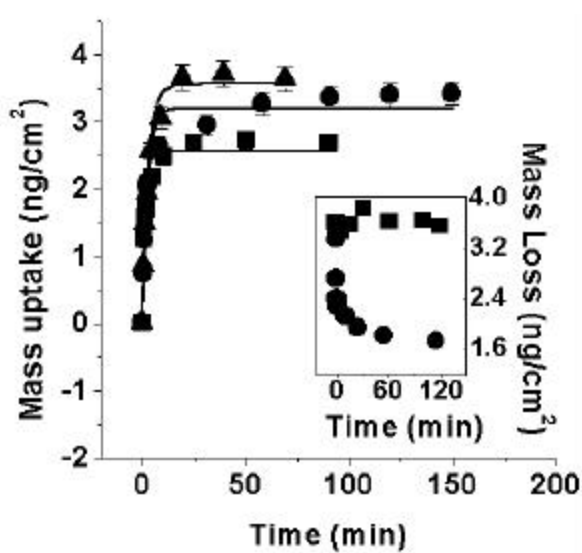


**Figure. 4.3.2:** QCM kinetics of incorporation of substrate protected endoglucanase in the ODA matrix with time during immersion of 250 Å thick ODA films in 2 mg/mL enzyme solution at different pH values (triangles, pH 5; circles, pH 7; squares, pH 9). The solid lines are an aid to the eye and have no physical significance. The inset shows the QCM mass loss recorded during removal of enzyme at pH 2 (circles) and pH 7 (squares) from the 250 Å thick enzyme-ODA composite film formed at pH = 7.

As can be seen from the figure, maximum incorporation of the enzyme takes place at pH 5 instead of at pH 7. This is rather surprising if one considers only electrostatic interactions to control the diffusion process of the enzymes into the ODA matrix ( $pK_b$  of ODA ~ 10.5;  $pI$  of endoglucanase ~ 4.1). However, the incorporation of the substrate-protected enzyme at pH 9 is

less than at both pH 7 and pH 5, indicating that electrostatic interactions do determine to a large extent the entrapment of the enzymes in the lipid matrix. The discrepancies observed could be attributed to the role of secondary interactions such as hydrophobic and hydrogen bonding that would also play a major role in the encapsulation process. The inset of Fig. 4.3.2 shows the release of the substrate-protected endoglucanase molecules by immersion of the fully loaded biocomposite film formed at pH 7 during immersion in the enzyme solution maintained at pH 2 (circles) and at pH 7 (squares). At pH 2, nearly 50 % of the entrapped enzyme molecules are released from the film, the residual molecules within the lipid matrix on complete neutralization of the electrostatic interactions further attesting to the role played by interactions such as hydrophobic, hydrogen bonding etc. in the enzyme immobilization energetics. As can be seen from the inset of Fig.4.3.2 (squares), the release of enzyme molecules at pH 7 is negligible. At this pH, electrostatic interactions dominate and do not allow the removal of the enzyme molecules from the loaded enzyme-ODA composite film. This also supports the fact that biological activity measured (as will be explained subsequently) from the biocomposite film is due to the enzyme *entrapped within the matrix* and not due to enzyme in solution.

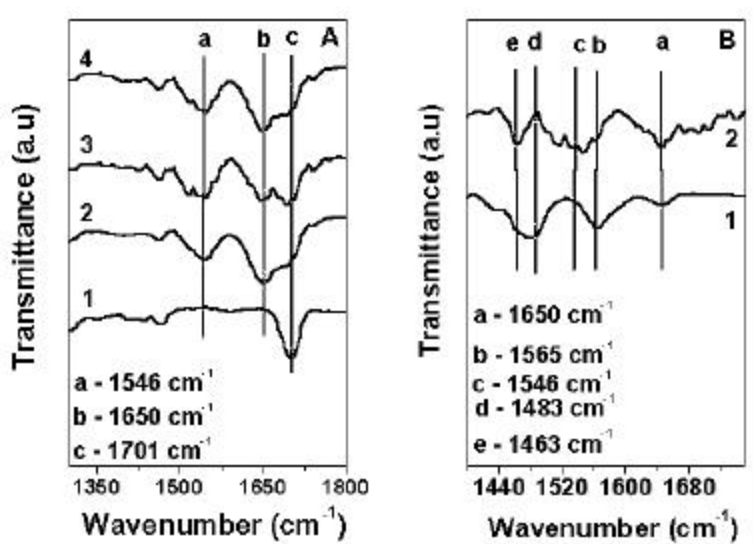
#### 4.4 NATIVE STRUCTURAL STUDIES.

##### 4.4.1 FTIR Analysis.

The amide linkages between amino acid residues in polypeptides and proteins give rise to well-known signatures in the infrared region of the electromagnetic spectrum. The position of the amide I and II bands in the FTIR spectra of proteins is a sensitive indicator of conformational changes in the protein secondary structure<sup>7</sup> as has been discussed in chapter 2 and 3. Fig. 4.4.1A shows the FTIR spectra recorded from a 250 Å thick as-deposited AA film (curve 1), the AA film after immersion in 10<sup>-5</sup> M F-Prot solution kept at pH 6 for 5 hours (curve 2) and F-Prot – AA biocomposite film after reaction with hemoglobin (curve 3). Curve 4 represents the FTIR spectrum recorded from a 250 Å thick F-Prot-AA composite film stored in air at room temperature for a period of 5 days. A number of vibrational modes can be observed for the four films. The amide I band, which is assigned to the stretch mode of the carbonyl group coupled to the amide linkage, occurs at ca.1650 cm<sup>-1</sup> (Fig. 4.4.1A, feature b) for all the three F-Prot-AA composite films. This band is clearly absent in the as-deposited AA film (curve 1). The position



of this band is close to that reported for native proteins in earlier papers, and indicates that the secondary structure of the enzyme in the AA environment is unperturbed.<sup>7</sup> The amide II band, which arises due to the N-H stretching modes of vibration in the amide linkage, occurs at  $1546\text{ cm}^{-1}$  (Fig. 4.4.1 A, feature a) and can also be clearly seen for the F-Prot-AA biocomposite films. The position of this band indicates that the secondary structure of the native enzyme is retained in the encapsulated form. The band at  $1699\text{ cm}^{-1}$  (Fig. 4.4.1A, feature c) arises from the carbonyl stretch modes from the carboxylic acid groups in the AA matrix.<sup>8</sup> There is some variation in the amide bands after reacting the F-Prot-AA film with hemoglobin (for biocatalytic activity measurements) as seen from curve 3, Fig. 4.4.1 A. This may be due to contribution of hemoglobin molecules in the F-Prot-AA composite matrix in the digested/undigested form. It can be seen from curve 4 that the secondary structure of the enzyme is maintained even after 5 days of exposure of the F-Prot-AA composite to air at room temperature indicating increased conformational rigidity of the proteins within the AA matrix as well as inhibition of chemical degradation of sensitive side chains and prevention of aggregation of the enzymes.



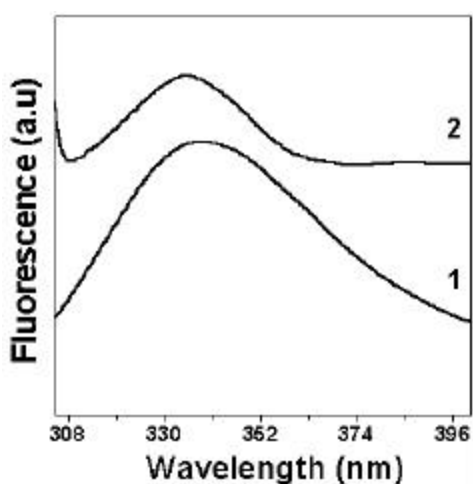
**Figure. 4.4.1:** (A) FTIR spectra recorded from a  $250\text{ \AA}$  thick as-deposited AA film (curve 1); a  $250\text{ \AA}$  thick F-Prot- AA composite film (curve 2, see text for details); a  $250\text{ \AA}$  thick F-Prot - AA composite film after catalytic activity measurements (curve 3, see text for details) and a  $250\text{ \AA}$  thick F-Prot-AA composite film after 5 days of ageing in air at room temperature (curve 4). B) FTIR spectra recorded from a  $250\text{ \AA}$  thick as-deposited ODA film (curve 1) and a  $250\text{ \AA}$  thick endoglucanase-ODA film grown at pH 7 (curve 2). Three bands labeled a-c are identified and discussed in the text.

Fig. 4.4.1B shows the FTIR spectra recorded from a 250 Å thick as-deposited ODA film (curve 1) and the substrate-protected endoglucanase-ODA biocomposite film formed at pH 7. The amide I (C=O stretch at 1650 cm<sup>-1</sup>, feature a) and amide II (the N-H stretch at 1546 cm<sup>-1</sup>, feature c) can be clearly seen in curve 2 (Fig. 4.4.1B). A small feature at ca. 1650 cm<sup>-1</sup> does occur in the as-deposited ODA film (Fig. 4.4.1B, curve 1), the intensity of this band increases in curve 2 clearly showing that it originates from the enzyme molecules in the composite film. A feature at about 1565 cm<sup>-1</sup> is observed in the as-deposited ODA film (feature b, curve 1) and may be possibly due to the N-H deformation vibration mode in the ODA matrix. This feature is yet ill understood. It is well known that peaks typical for carbamates appear in the region of 1560-1570 cm<sup>-1</sup>.<sup>9a</sup> The possibility arises that the band at 1565 cm<sup>-1</sup> could also be due to carbamate formed from a precursor carbamate phase due to the interaction of the amine with atmospheric carbon dioxide. It is well known that upon binding of anions to amine, this band shifts depending on the nature of the interaction.<sup>9b</sup> It is difficult to unambiguously detect the presence of amide bands in the case of enzyme-ODA biocomposite films due to the presence of bands originating from the ODA itself, at roughly similar wavenumbers. The small shifts and broadening in the vibrational frequencies due to enzyme immobilization is the only possible way of monitoring the biocomposite formation. Another feature that can be probed is the broad band at 1483 cm<sup>-1</sup> (feature d, curve 1) in the as-deposited ODA film arising due to NH<sub>3</sub> antisymmetric deformation. It is well known that this band disappears on salt formation.<sup>9b</sup> The disappearance of this band can be clearly seen from curve 2 upon biocomposite formation. A new band that was not previously visible appears at 1460 cm<sup>-1</sup> (feature e, curve 2) is assigned to the methylene scissoring bands. This band along with the amine antisymmetric vibration forms a broad band in the case of as-deposited amine. Fig. 4.4.1A and B indicate that the secondary structures of the enzymes (F-prot and endoglucanase) entrapped within the lipid matrix have intact secondary structures.

#### 4.4.2 Fluorescence studies.

Enzymes are biocatalysts that perform certain specific functions. The performance of these functions or in other words the biological activity of these biocatalysts depends to a large extent on the tertiary structure of the enzyme. The direct way of determining this is to react the

enzyme with its substrate and determine its biological activity under the given conditions. But a more sensitive physical method to determine small changes in the tertiary structure of the enzyme is fluorescence spectroscopy. It is well known that tryptophan emission is sensitive to the local environmental perturbations<sup>10</sup> as also has been explained in chapter 2 and 3. Fig. 4.4.2 shows the fluorescence spectra of F-Prot solution at pH 6 (curve 1) and the F-Prot-AA composite film (curve 2) after 5 hours of immersion of a 1000 Å thick AA film on quartz in the F-Prot solution at pH 6. The F-Prot solution shows a strong emission at 340 nm and arises as a consequence of radiative decay of the  $\pi - \pi^*$  transition from the tryptophan residues in the protein (Excitation wavelength = 295 nm).<sup>11</sup> The fluorescence emission from the F-prot – AA biocomposite film occurs at 335 nm and indicates a small blue shift in the emission line. This shift may be due to electrostatic interaction of F-Prot molecules with the lipid matrix. This fact together with the catalytic activity measurements of the encapsulated enzyme which do not show significantly reduced activity (see section 4.7 below), indicates clearly that the tertiary structure of F-Prot is not affected on encapsulation in the lipid matrix. Furthermore we would like to add that while monitoring emission from the enzyme within the lipid films, one can possibly encounter scattering due to the lipid film, which can further give erroneous results. A proper baseline and its subtraction is therefore crucial.



**Figure. 4.4.2:** Fluorescence spectra of F-Prot in pH = 6 solution (curve 1) and of a 1000 Å thick F-Prot-AA composite film grown on quartz (curve 2, see text for details).

#### 4.5 CHEMICAL ANALYSIS OF ENZYME-LIPID COMPOSITES.

A chemical analysis of the F-prot – AA biocomposite film was performed with X-ray photoelectron spectroscopy (XPS). The measurements were carried out on a VG MicroTech ESCA 3000 spectrometer equipped with a multichanneltron hemispherical electron energy analyser at a pressure less than  $1 \times 10^{-9}$  Torr. The electrons were excited with un-monochromatized Mg  $K_{\alpha}$  X-rays (energy = 1253.6 eV) and the spectra were collected in the constant analyzer energy mode at a pass energy of 50 eV. This leads to an overall resolution of ca. 1 eV for the measurements. Si 2p (substrate), C 1s, N 1s and O 1s core level spectra were recorded from the F-Prot-AA composite film on Si (111) at an electron takeoff angle (ETOA, angle between the surface plane and electron emission direction) of  $60^{\circ}$ . Prior to curve stripping by a non-linear least squares procedure, the inelastic electron background was removed by the Shirley algorithm.<sup>12</sup>

General scan spectra did not reveal the presence of any impurities in the film. Figs.4.5.1 A and B show the C 1s and N 1s core level spectra respectively recorded from a 250 Å thick F-prot-AA biocomposite film. The nitrogen signal arises only from the protein molecules and thus clearly indicates the presence of F-Prot in the film. The C 1s spectrum could be decomposed into three chemically distinct components as shown in Fig. 4.5.1A.

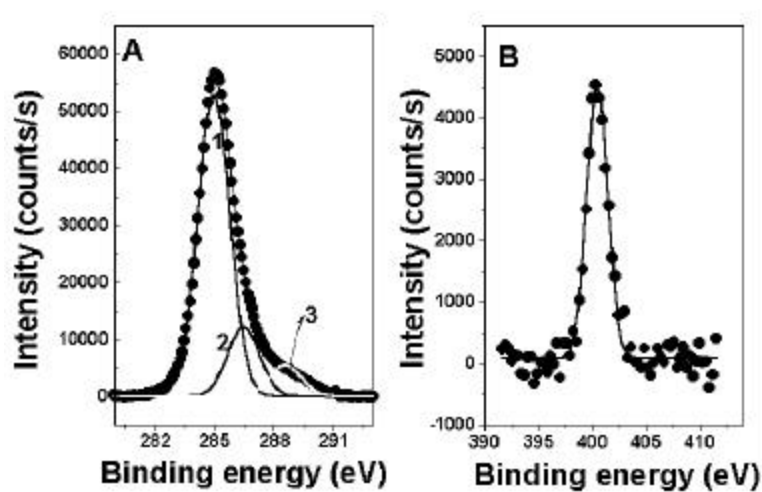


**Figure. 4.5.1:** A) C 1s core level spectrum recorded from a 250 Å thick F-Prot – AA composite film on Si (111) substrate. The three chemically distinct components are shown in the figure and discussed in the text. B) N 1s core level spectrum recorded from a 250 Å thick F-Prot – AA composite film on Si (111) substrate. The spectrum has been fit to a single Gaussian centered at 400.5 eV.

The peak at 285 eV binding energy (BE) arises from carbons in the AA hydrocarbon chains as well as from the various residues of the protein. The component at 288.6 eV BE (curve 3, Fig. 4.5.1A) is assigned to electron emission from carbons in the carboxylate groups of the AA matrix. This value agrees with reported BEs of carboxylate carbons in Langmuir-Blodgett films of fatty acids<sup>13</sup> as well as surface modified polymers.<sup>14</sup> The component at 286.5 eV BE (curve 2, Fig. 4.5.1A) is assigned to carbons co-ordinated to amine groups as well as in the amide linkages of the protein. The smaller chemical shift for this component when compared to the carboxylate carbon (curve 3) is due to the smaller electronegativity of nitrogen when compared to oxygen.<sup>15</sup> The N 1s core level could be satisfactorily fit to a single Gaussian at 400.5 eV BE and is shown in Fig. 4.4.1B.

#### 4.6 BIOCOMPOSITE FORMATION: INTERCALATION OR SURFACE ADSORPTION?:

It is well known that proteins adsorb at interfaces/phase boundaries.<sup>16</sup> In the formation of biocomposite films, the proteins can either intercalate *within the lipid bilayers* or it can be by a purely surface adsorption. We believe that the proteins/enzymes are intercalated/encapsulated *within the lipid bilayers*. To prove this fact, we have performed scanning electron microscopy (SEM) for direct visual evidence and also contact angle measurements. SEM measurements on 250 Å thick ODA films on Si (111) wafers before (data not shown) and after incorporation of substrate protected enzyme (Fig. 4.6.1A) together with films of the substrate protected enzyme drop-dried onto a 250 Å thick ODA film on Si (111; Fig. 4.6.1B) were performed on a Leica Stereoscan-440 scanning electron microscopy (SEM). Contact angle measurements of a sessile water drop (1 µl) on bare Si (111) substrates, 250 Å thick ODA/AA films on Si (111) substrates before and after enzyme intercalation, as well as a drop-dried film of the enzyme on the surface of a 250 Å thick ODA/AA film were carried out on a Rame Hart 100 Goniometer.

Fig. 4.6.1 A and B show SEM images of the enzyme endoglucanase intercalated within the lipid bilayers and that of the drop-dried enzyme on lipid surface respectively. The enzyme aggregates can be clearly seen in the B part of the figure, whereas the intercalated biocomposite film shows no such surface adsorption. Contact angle measurements with a sessile water drop on a 250 Å thick ODA/AA film deposited on Si (111) substrates before and

after immersion in the enzyme solutions (endoglucanase or F-Prot) yielded  $90^\circ$  and  $85^\circ$  respectively. It is clear that the reduction in contact angle after enzyme incorporation is marginal. It is pertinent to mention here that the contact angles measured for the bare Si (111) surface and an enzyme film deposited on the Si (111) substrate by evaporation of a drop of the enzyme solution, and the enzyme solution drop dried on the lipid film yielded values of  $18^\circ$ ,  $15^\circ$  and  $20^\circ$  respectively. These observations along with the SEM images clearly strengthens the conclusion mentioned above that the enzyme molecules are entrapped *within the lipid matrix* and not on the surface.

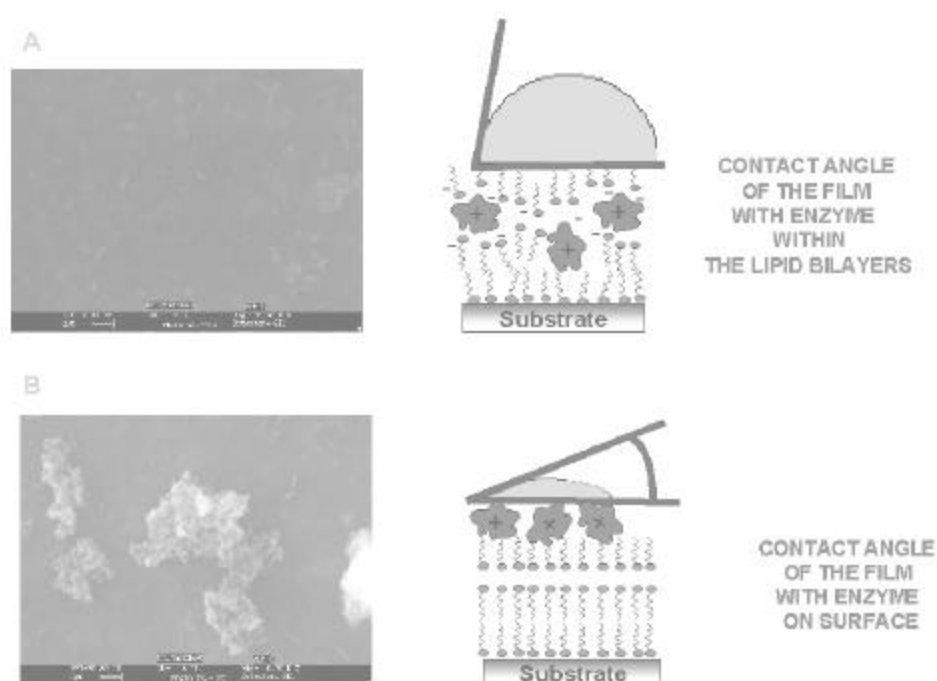


**Figure. 4.6.1:** (A) SEM micrograph recorded from a 250 Å thick *endoglucanase*-ODA composite film formed at pH = 7. The adjacent scheme shows the contact angle measurements of the biocomposite film. The larger contact angle clearly rules out surface adsorption. (B) SEM micrograph recorded from a drop-dried enzyme film deposited on an as-deposited 250 Å thick ODA film. The adjacent scheme shows the contact angle measurements of the enzyme drop dried film. The surface adsorbed enzyme gives a low contact angle.

#### 4.7 BIOCATALYTIC ACTIVITY MEASUREMENTS.

As explained in the earlier section, the biocatalytic activity depends to a large extent on the tertiary structure of the enzyme, which is determined by the tryptophan emission band. But there are other factors, where the tertiary structure is intact (as observed by fluorescence

spectroscopy), yet, the enzyme fails to show any biocatalytic activity. The other factors on which the biological activity will depend are the local environment such as aqueous, polar or nonpolar, accessibility and orientation of active site, presence of cofactors, choice of proper substrate, appropriate temperature and pH conditions etc. In this section we have tried to address some of these issues.

#### 4.7.1. F-prot-AA system.

250 Å thick AA films on Si (111) substrates (4 cm<sup>2</sup> substrate area) were immersed in the F-Prot solution for a period of 5 h and checked for catalytic activity after thorough washing and drying of the biocomposite films in flowing N<sub>2</sub> at room temperature for 5 minutes. The biocatalytic activity of the encapsulated F-Prot molecules in the lipid matrix was determined by reaction with a solution of hemoglobin (5 mg/ml) prepared in sodium – phosphate buffer at pH 6. Since the fungal protease is an enzyme that acts on proteins such as hemoglobin (Hb), they are generally used for biocatalytic activity measurements.<sup>17</sup>

In a typical experiment to estimate the biocatalytic activity of the encapsulated enzyme molecules, an F-Prot – AA composite film of the dimensions mentioned above was carefully immersed in 1 ml of the Hb solution and the reaction mixture was incubated at 37° C for 1 hour. After the incubation time, the film was removed and 1.7 M perchloric acid was added to the reaction solution to precipitate the remaining Hb. After 1 hour, the precipitate was removed by centrifugation and the optical absorbance of the filtrate measured at 280 nm. F-Prot digests hemoglobin and yields acid soluble products (tryptophan and tyrosine residues) which are readily detected by their strong UV signatures at 280 nm.<sup>17b</sup> The activity of the enzyme in the AA matrix was quantified in terms of a "specific activity". One unit of the specific enzymatic activity produces an increase in the absorbance of 0.001 unit at 280 nm per minute per microgram of the enzyme. For comparison, the biocatalytic activity of F-Prot in solution at pH 6 was also estimated in the manner above. The knowledge of exact amount of enzyme in the biocomposite film is crucial in determining the "specific activity" of the enzyme and comparing it with free solution form of the enzyme. In this regard, QCM plays a very important role, as one can quantify in exact amounts the entrapped enzyme. In order to check the reproducibility of the enzyme activity, 10 F-Prot-AA composite films were reacted with Hb as described above. Table

4.6.1 lists the specific activities of an F-Prot solution at pH 6 along with the activities determined for a 250 Å thick F-Prot – AA composite film for which the F-Prot loading factor was determined from QCM measurements. To check the reproducibility of enzyme activity, 10 F-Prot-AA composite films were studied. It can be seen from Table 4.7.1 that the specific activity in the films is about  $62 \pm 5$  Units/mg which shows that the activity is highly reproducible with little deviation from the mean. We would like to point out here that the specific activity of the encapsulated F-Prot molecules is comparable to that of the enzyme molecules in solution (Table 4.7.1). This provides unequivocal evidence that the tertiary structure of the enzyme remains intact upon immobilization into AA matrix. The biocatalytic activity of a single F-Prot – AA composite film was tested during three reaction cycles with Hb and the values obtained are given in the table. The specific activity of the encapsulated enzyme diminishes steadily with each immersion cycle. This appears to be a consequence of replacement of the enzyme molecules by Hb molecules during successive immersion cycles. That this is a likely mechanism is borne out by UV-vis measurements as will be explained subsequently (Fig.4.7.3, inset) which clearly shows the presence of a small amount of Hb in the films after reaction. The replacement of F-prot by Hb molecules would also lead to blockage of the diffusion pathways of solution based Hb molecules and thus contributes further to a reduction in catalytic activity.

**Table 4.7.1**

Comparison of enzymatic activity of Fungal Protease in solution and that in encapsulated form using hemoglobin as the substrate.

System	Specific Activity <sup>#</sup> (Units / mg)
F-Prot solution	65
F-Prot-AA*	$61.83 \pm 4.9$
F-Prot-AA (run 1)	64
F-Prot-AA (run 2)	30
F-Prot-AA (run 3)	10
F-Prot-AA (t=45 min) <sup>§</sup>	68
F-Prot-AA (t=24 hrs) <sup>§</sup>	42
AA Film (blank)	0

<sup>#</sup> One unit of enzyme will produce a change in absorbance at 280 nm of 0.001 per minute at pH=6.0 and 37°C measured as acid soluble products using hemoglobin as the substrate.\*10 F-Prot-AA films were studied for catalytic activity and a statistical average with standard deviation is given in the table.

<sup>§</sup> F-Prot-AA films were dried in flowing nitrogen at room temperature and the catalytic activity determined as a function of time of storage in air.



#### 4.7.2 Endoglucanase-ODA system.

250 Å thick substrate protected endoglucanase-ODA composite films were formed by encapsulation of a mixture of different molar ratios of endoglucanase: carboxymethyl cellulose (CMC) at the three different pH values (pH 5, 0.05 M sodium citrate buffer; pH 7, 0.05 M sodium phosphate buffer; pH 9, 0.05 M glycine-NaOH buffer, film dimensions 4 cm<sup>2</sup>). The biocatalytic activity of these films was checked by reaction with an aqueous solution of CMC (10 mg/ml; sodium-phosphate buffer, pH = 7) and incubating the mixture at 60 °C for 1 h. The reducing sugar released was determined by the Nelson-Somogyi method.<sup>18</sup> For comparison, the biocatalytic activity of an identical amount of different molar ratios of endoglucanase: CMC molecules (held at the three different pH values mentioned) in solution was determined as described above. As shown subsequently, the molar ratio of 1: 2 (enzyme: CMC) yielded optimum biological activity in the film and was chosen for all further experimentation. Five 250 Å thick similarly loaded endoglucanase-CMC (1:2 molar ratio) films (film dimensions = 4 cm<sup>2</sup>) were formed at the three different pH values and were tested for biological activity, to determine the standard deviation to the data.

A control experiment was performed to estimate the biocatalytic activity of an as-deposited 250 Å thick ODA film under similar assay conditions (film dimensions = 4 cm<sup>2</sup>). Another control experiment was performed in which a 250 Å thick substrate protected enzyme-ODA composite film (4cm<sup>2</sup> film dimensions) was assayed at a temperature of 40°C, pH=7 (0.05 M sodium phosphate buffer). This was done in order to estimate the amount of glucose released, if any, during the "protection phase".

**Table 4.7.2**

Comparison of enzymatic activity of endoglucanase molecules in solution and after encapsulation in ODA films using carboxymethyl cellulose (CMC) as the substrate.

System	Activity <sup>#</sup> (Units / mg)	*Relative activity
Endoglucanase in solution	2.00 ± 0.10	100 %
Endoglucanase-ODA composite film	0.84 ± 0.20	42 %
Substrate protected endoglucanase-ODA composite film, enzyme pre-complexed with CMC in the ratio 1 : 2.	1.82 ± 0.10	91 %
ODA film (blank)	0	0
Substrate protected endoglucanase-ODA composite film, assayed at 4°C in pH=7 buffer	0	0

<sup>#</sup> One unit of enzyme activity is defined as the amount of enzyme that produces 1  $\mu$ mol of glucose equivalent per minute from CMC in sodium-phosphate buffer at pH = 7 after incubating the reaction mixture at 60 °C for 1 h.

\*Relative activity (percent) is the bio-catalytic activity of the enzyme in the encapsulated form relative to that of the free enzyme in solution under ambient assay conditions. The maximum enzyme activity in solution at pH = 5 is taken to be 100 %.

In order to check the reproducibility of the biocatalytic activity measurements, 5 similarly loaded films of the substrate-protected enzyme molecules were tested under identical assay conditions and yielded an activity of  $1.81 \pm 0.10$  units (Table 4.7.2). The small variance in the biocatalytic activity clearly shows that the protocol for the growth of the enzyme-lipid composite films is highly reproducible. The activity of the substrate-protected enzyme (1.81) compares favorably with the activity of the free enzyme in solution (2.0) indicating little compromise with the biological activity of the enzyme on entrapment in the lipid matrix.

**4.7.3 Mechanism of biocatalytic activity.** There are two possible mechanisms for biological activity of the biocomposite films. Either the entrapped enzyme diffuses out of the film during the reaction process, or the substrate diffuses inside the matrix to be acted upon by the enzyme within the matrix, and the products released out of the matrix. The latter seems to be a more

probable mechanism due to two evidences. The first evidence comes from the QCM leaching result of endoglucanase presented in section 4.3.2 inset of Fig. 4.3.2 (circles). The endoglucanase-ODA biocomposite film formed at pH 7, was immersed into water held at pH 7 to check the leaching of the enzyme at this pH. As can be clearly seen there is no leaching out of the enzyme, electrostatic interactions between the matrix and the enzyme prevents the leach. This indicates that the enzyme would not leach out during activity process at pH 7. The second evidence is seen from the UV-vis analysis (inset of Fig. 4.7.3) of F-prot-AA biocomposite films upon successive cycles of reaction with Hb. A 4 cm<sup>2</sup> F-prot-AA biocomposite film was formed on quartz substrate and subjected to two cycles of biological activity. After each reaction, UV-vis spectra of the film was recorded, as shown in the inset of Fig. 4.7.3, indicating the increase in sorlet band due to the heme protein. The intensity of this band is marginally increased on the second cycle (curve 2), indicating the increased presence of Hb in the film. The main part of the figure shows yet another way of characterizing the biocomposite films by monitoring the  $\pi-\pi^*$  transition at ~280 nm characteristic of any protein. (curve 1 = enzyme in solution; curve 2 = enzyme in film). The intensity of this band is also used to estimate the biological activity of the enzyme after it releases tryptophan and tyrosine from the cleaved protein.

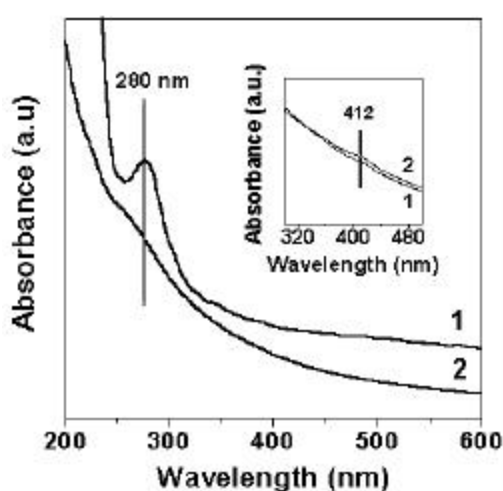


**Figure. 4.7.3:** UV-vis spectra recorded from a 10<sup>-5</sup> M F-Prot solution at pH 6 (curve 1) and a 1000 Å thick F-Prot – AA biocomposite film deposited on quartz (curve 2, see text for details). The inset shows the UV-vis spectra of the F-Prot-AA composite film after two cycles of catalytic activity measurement, the cycle indicated next to the respective curve.

#### 4.7.4 Biocatalytic activity: Role of entrapped water.

It was found that water entrapped along with the enzyme molecules plays a crucial role in maintaining the biological activity of the enzyme. It was found that endoglucanase-ODA composite films completely lost their biological activity upon drying. This effect was less pronounced in the case of F-prot-AA films. To investigate in detail the role of entrapped water in the films, one film each was dried in flowing  $N_2$  at room temperature for 45 minutes and 24 h and reacted with Hb. FTIR spectra were recorded for the F-prot-AA biocomposite films on Si (111) substrates for similar periods of drying in order to ascertain the presence of entrapped water as shown in Fig. 4.7.4.

The biocatalytic activity of the F-prot-AA biocomposite films did not lead to a detectable fall in catalytic activity after 45 minutes of drying but showed a 38 % loss in specific activity on drying for 24 h. This indicates that prolonged exposure to air leads to deterioration in the performance of the composite film. Even though the FTIR measurements shown above indicates complete dehydration of the composite films within 60 minutes of drying in air, it is clear that immersion of the F-prot films in the Hb solution leads to rehydration of the enzyme molecules and thereby, a restoration of the catalytic activity of the film. On the other hand, drying of the endoglucanase-ODA biocomposite film for 5 minutes in flowing nitrogen, resulted in a complete loss in the activity. We do not understand this fact currently as to why F-prot-AA composite retains activity for ca. 24-48 h on drying whereas endoglucanase-ODA composite loses its activity immediately upon drying.

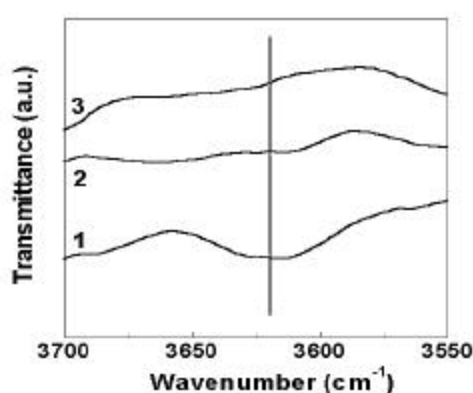


**Figure 4.7.4:** FTIR spectra recorded from a 250 Å thick F-Prot-AA composite film as a function of time of drying of the composite film. Curve 1, time  $t = 0$ ; curve 2 –  $t = 60$  min and curve 3 –  $t = 120$  min.

#### 4.7.5 Accessibility of active site: Substrate protection.

The main problem in the case of immobilized biocatalysts is the accessibility of catalytic or substrate binding sites to the substrates. If the immobilized enzyme or the amino acid residues surrounding the catalytic/substrate-binding site were oriented in such a way so as to hinder its accessibility to substrates or cofactors, one would not get any biological activity. In our studies on F-prot-AA,<sup>3f</sup> and pepsin-ODA biocomposites,<sup>3i</sup> the enzymes gave a fairly good biocatalytic activity in comparison with solution form of the enzyme. This might be possibly due to favorable access of the catalytic/substrate-binding sites to the external reagents. We observed a completely different picture in the case of endoglucanase-ODA composites. This has been clearly illustrated in Table 4.7.5 below. Initial experiments indicated that endoglucanase molecules encapsulated in the ODA matrix showed a 58% loss in the biocatalytic activity relative to that of the free enzyme in solution (Table 4.7.2; row 2). This result clearly indicated inaccessibility of the active site of the entrapped enzyme molecules to substrate molecules in solution possibly due to blockage of the active sites by electrostatic complexation with the lipid molecules. This necessitated substrate protection of the enzyme active site by carboxymethyl cellulose (CMC). Studies on protection of the enzyme active site by precomplexing the enzyme with CMC in different ratios before immobilization into 250 Å thick ODA films was carried out at pH 7. Table 4.7.5 shows that complete protection of enzyme active site was accomplished at an enzyme: substrate molar ratio of 1: 2, which yields optimum catalytic activity. At this ratio of enzyme: substrate, the biological activity of the encapsulated enzyme relative to that of the free enzyme in solution is close to 91 % (Tables 4.7.2 and 4.7.5). Hence, all further experiments were carried out by pre-complexing the substrate, CMC, with endoglucanase prior to immobilization of the enzyme in the thermally evaporated ODA films.

**Table 4.7.5**

Substrate protection of endoglucanase at pH 7 by addition of different concentrations of the substrate carboxymethyl cellulose (CMC).

Enzyme : Substrate (CMC) molar ratios	Activity <sup>#</sup> (units/mg)	Relative Activity <sup>*</sup>
1:1	1.40	71%
1:2	1.82	91 %
1:4	1.26	63 %

As discussed above, substrate protection is important in the case of endoglucanase molecules entrapped in ODA films and a possible explanation is as follows. It is expected that the enzyme molecules are encapsulated in the hydrophilic regions of the lipid bilayers as shown in the scheme of Fig. 4.5.1. The location of the negatively charged acid sites on the enzyme surface would determine the electrostatic coordination of the enzyme with the protonated amine groups in the film and hence, the orientation of the enzyme molecules within the ODA bilayers. It is conceivable that if these negatively charged sites are located close to the active site of the enzyme, then the orientation of the enzyme in the lipid bilayers would not favor easy access of substrate molecules from solution to the "blocked" active sites of the enzyme. Heller *et al* have observed that complexing flexible polycations with lactate and glycolate oxidases before immobilization into silicate sol gels dramatically stabilizes the enzyme by reducing the electrostatic interaction of the silica anions and the cationic arginine groups in the active sites.<sup>19</sup> A similar protection mechanism might be possible in our case as well but in the absence of crystallographic information on the endoglucanase-CMC system, we are unable to make a definite statement on this aspect. Experimentally, however, an enzyme : substrate ratio of 1: 2 was determined to be ideal in optimising the biocatalytic activity of the encapsulated enzyme in the lipid matrix and is an important result of this investigation.

**4.7.6. Enhanced thermal and pH stability of the immobilized biocatalysts.** It is well known that immobilized enzyme molecules have restricted mobility preventing structural changes and 'locking' the enzyme in certain preferred orientation. This would give it enhanced stability against harsh environmental conditions. The immobilized biocatalyst would then be able to retain biological activity under conditions when the free solution form of the enzyme would fail. We have studied this feature with the endoglucanase-ODA biocomposite films.

***Shift in optimum temperature of operation of the endoglucanase-ODA composite.*** The temperature dependence of the biocatalytic activity of substrate-protected endoglucanase molecules in solution at pH 7 (Fig. 4.7.6, circles) was compared with same amount of the substrate-protected 250 Å thick endoglucanase-ODA biocomposite films at pH 7 (Fig. 4.7.6, squares).

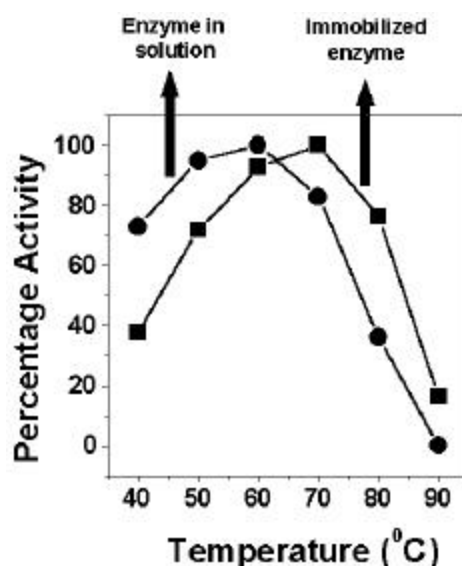


**Figure. 4.7.6:** Variation in the percentage bio-catalytic activity from substrate-protected *endoglucanase* molecules in solution (circles) and substrate-protected *endoglucanase* molecules entrapped in 250 Å thick ODA films grown at pH = 7 (squares) as a function of temperature.

While the free enzyme in solution shows maximum activity at 60 °C, the biocomposite film shows optimum biocatalytic activity at 70 °C. This 10 °C shift in the optimum operating temperature was found reproducible for 5 separate biocomposite films. Furthermore, the fact that the entrapped enzymes still show significant activity even above 70 °C under conditions where the free enzyme molecules in solution are almost inactive (Fig. 4.7.6) shows significant stabilization of the enzyme molecules by the lipid matrix. The reduced degrees of freedom brought about by the entrapment of the enzyme in the lipid matrix is expected to be responsible for this increased temperature stability of the composite material and is well known in immobilized protein systems.<sup>2</sup>

***Biocatalytic activity as a function of pH.*** The pH dependence of the biocatalytic activity of the substrate-protected *endoglucanase* molecules in solution as well as in the encapsulated form have been measured and the data obtained is shown in Table 4.7.6. While in both cases the optimum biological activity of the enzyme occurs at pH 5, the decay in biocatalytic activity of the free substrate-protected enzyme molecules with increasing pH of the solution is much more rapid than that observed for the encapsulated *endoglucanase* molecules (Table 4.7.6).

**Table 4.7.6**

pH dependence of the enzymatic activity of endoglucanase in solution and entrapped in the ODA matrix.

pH	Activity (units/mg) <sup>#</sup>		Relative activity <sup>*</sup>	
	Solution form	Immobilized form	Solution form	Immobilized form
5	2.52	2.32	100%	100%
7	2.02	2.00	80%	86%
9	0.757	1.67	30%	72%

At pH 9, the biocatalytic activity of free substrate-protected enzyme in solution drops to 30 % of its original activity (at pH 5), while the encapsulated enzyme retains most of its original activity. This significant stabilization of the enzyme at high pH again points to the role of the ODA matrix in stabilizing the enzyme at higher pH values.

The stability of the substrate protected encapsulated enzyme at high pH values as compared to that of substrate protected enzyme in solution indicates the role of local pH experienced by the enzyme in the lipid matrix. It has been observed that the surface acidity of a carboxylic acid functional group on a 2-D self assembled monolayer (SAM) and 3-D SAM is different than that for the free monomeric functional group in solution.<sup>20</sup> Lee *et al*<sup>20</sup> observe that the titration curves for ionization of carboxylic acid terminated SAMs not only show a shift in the actual pKa values but also that the width of these titration curves is found to increase. Such a behavior is expected to be true for the amine functional groups in the ODA matrix as well. The combined effect of broadening of the titration curves of both the ODA molecules in the lipid matrix and carboxylic acid groups on the enzyme surface would lead to considerable insensitivity of the local pH within the micro-environment of the lipid bilayers to variations in the bulk solution pH. This would satisfactorily explain the constancy in the biocatalytic activity of the entrapped endoglucanase molecules with varying solution pH as observed in this study. The high temperature-high pH stability of the entrapped enzyme molecules in ODA matrixes highlights the utility of our technique in paper and pulp as well as detergent and biopolishing industries where such conditions are normally encountered.



#### 4.8 SUMMARY.

This chapter demonstrates the formation of enzyme-lipid biocomposite films, which act as immobilized biocatalysts. The diffusion of the enzymes into the lipid matrix is governed to a large extent by electrostatic interactions. Other secondary interactions such as hydrophobic and hydrogen bonding are also responsible for the intercalation. The diffusion of enzymes into the lipid matrix was analyzed in terms of 1-D diffusion model. QCM data is useful to obtain the exact amount (in  $\mu\text{g}$ ) of immobilized enzymes. This is a very useful in order to compare the biological activity of free versus immobilized enzyme in terms of 'specific biological activity'. Hence, one can estimate the enhancement/reduction if any in the biological activity of the immobilized enzyme. FTIR, fluorescence and biological activity confirmed the intactness of the secondary and tertiary enzyme structures. The enzyme molecules are immobilized *within the lipid bilayers* as evidenced by SEM and contact angle measurements. The enzyme-lipid biocomposite films were reusable over a few cycles of biocatalysis. It was found that the biological activity of the biocomposite films depends on the entrapped water and falls due to dehydration of the films. The active site of immobilized F-prot was oriented in such a way so as to give optimum biological activity. On the other hand, 'unprotected' immobilized endoglucanase failed to give biological activity probably due to the binding of the amino acid residues around the substrate-binding site to the lipid molecules. This was circumvented by protection of this enzyme active site by co-immobilizing its substrate (carboxymethyl cellulose; CMC) along with the enzyme. The lipid molecules play a crucial role in protecting the enzyme endoglucanase against harsh environmental conditions such as high temperature and pH. The shift in the optimum temperature and pH conditions at which enzyme gives biological activity, enhanced thermal and pH stability are important feature of our protocol which can be exploited for industrial use.

#### 4.9. REFERENCES.

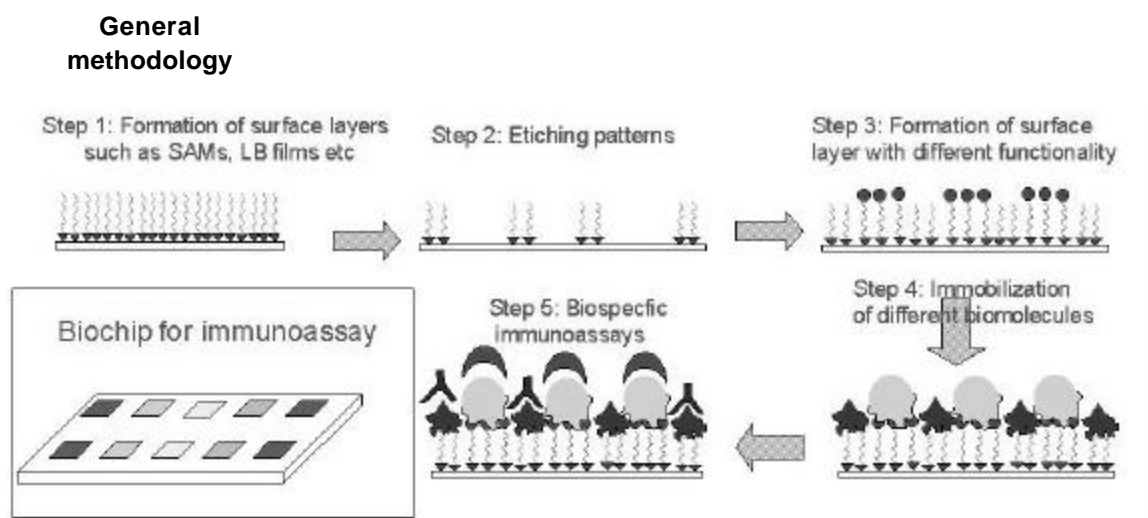
1. Ball, P. *Designing the Molecular World : Chemistry at the frontier.*, **1994**, Princeton University Press, New Jersey, USA.
2. a) Tischer, W.; Wedekind, F. **2000**, *Top. Curr. Chem.*, *200*, 95-126; b) Tischer, W.; Kasche, V. *Trends. Biotechnol.*, **1999**, *17*, 326; c) Avnir, D.; Braun, S. *Biochemical Aspects of Sol-*

- Gel Science and Technology*; Kluwer : Hingham, MA, **1996**; d) Shabat, D.; Grynszpan, F.; Saphier, S.; Turniansky, A.; Avnir, D.; Keinan, E. *Chem. Mater.*, **1997**, *9*, 2258.
3. a) Fendler, J. H. *Membrane mimetic chemistry*, **1982**, Wiley-Interscience, USA; b) Mouritsen, O. G.; Bloom, M. *Biophys. J.*, **1984**, *46*, 141; c) Tanford, C. *The hydrophobic effect: Formation of micelles and biological membranes*, **1980**, Wiley Interscience, USA; d) Whitesides, G. M. *Sci. Am.*, **1995**, *Sept*, 114.
4. a) Sauerbrey, G. *Z. Phys., (Munich)* **1959**, *155*, 206; b) Buttry, D. A.; Ward, M.D. *Chem. Rev.* **1992**, *92*, 1356; c) Caruso, F.; Rodda, E.; Furlong, N.D.; Niikura, K.; Okahata, Y. *Anal. Chem.*, **1997**, *69*, 2043; d) Gole, A.; Sainkar, S. R.; Sastry, M. *Chem. Mater.*, **2000**, *12*, 1234; e) Sastry, M.; Patil, V.; Sainkar, S. R. *J. Phys. Chem. B.*, **1998**, *102*, 1404; f) Gole, A.; Dash, C.; Mandale, A. B.; Rao, M.; Sastry, M. *Anal. Chem.*, **2000**, *72*, 4301; g) Gole, A.; Chaudhari, P.; Kaur, J.; Sastry, M. *Langmuir* **2001**, *17*, 5646; h) Gole, A.; Vyas, S.; Sainkar, S.R.; Lachke, A. L.; Sastry, M. *Langmuir* **2001**, *17*, 5964; i) Gole, A.; Dash, C.; Rao, M.; Sastry, M. *J.Chem.Soc., Chem. Commun.*, **2000**, 297.
5. The pI value of the enzyme was determined by using an isoelectric focusing unit built in-house. The pertinent references are: a) Sathivel, C.; Lachke, A.; Radhakrishnan, S. *J. Chromat. A.*, **1995**, *705*, 400; b) Gole, A.; Sathivel, C.; Lachke, A.; Sastry, M. *J. Chromat. A.*, **1999**, *848*, 485.
6. Roser, S.J.; Lovell, M.R. *J.Chem.Soc., Faraday Trans.*, **1995**, *91*, 1783.
7. a) Dong, A.; Huang, P.; Caughey, W.S. *Biochemistry* **1992**, *31*, 182; b) Templeton, A.C.; Chen, S.; Gross, S.M.; Murray, R.W. *Langmuir* **1999**, *15*, 66; c) Kumar, C. V.; McLendon, G. L. *Chem. Mater.*, **1997**, *9*, 863; d) Caruso, F.; Furlong, D. N.; Ariga, Katsuhiko.; Ichinose, I.; Kunitake, T. *Langmuir* **1998**, *14*, 4559.
8. Rabolt, J. F., Burns, F. C., Schlotter, N. E., Swalen, J. D. *J. Chem. Phys.*, **1983**, 78.
9. a) Bardosova, M.; Tredgold, R.H.; Ali-Adib, Z. *Langmuir* **1995**, *11*, 1273; b) Pal, S. *Ph.D thesis*, University of Pune, **1996**.
10. a) Eftink, M. R and Ghiron, C. A. *Anal. Biochem.*, **1981**, 199; b) Reynolds, J.A.; Gallagher, J.P.; Steinhardt, J. *Biochemistry* **1970**, *9*, 1232; c) Pace, C.N. *Methods. Enzymol.*, **1960**, *131*, 266.

11. Eftink, M.R and Ghiron, C. A. *Anal. Biochem.* **1981**, 199.
12. Shirley, D.A. *Phys. Rev. B.*, **1972**, 5, 4709.
13. Ganguly, P.; Paranjape, D.V.; Sastry, M.; Chaudhary, S.K.; Patil, K.R. *Langmuir* **1993**, 9, 487.
14. Davies, M.C.; Lynn, R.A.P.; Davis, S.S.; Hearn, J.; Watts, J.F.; Vickerman, J.C.; Johnson, D. *Langmuir* **1994**, 10, 1399.
15. Sastry, M.; Ganguly, P. *J. Phys. Chem. A.*, **1998**, 102, 697.
16. Razumovsky, L.; Damodaran, S. *Langmuir* **1999**, 15, 1392.
17. a) *Sigma Catalogue*, **1999**, 888; b) Anson, M. *J. Gen. Physiol.*, **1938**, 22, 79.
18. a) Nelson, N. *J. Biol. Chem.*, **1944**, 153, 376. b) Somogyi, M. *J. Biol. Chem.*, **1952**, 195, 19.
19. Heller, J.; Heller, A. *J. Am. Chem. Soc.*, **1998**, 120, 4586.
20. Lee, T. R.; Carey, R. I.; Biebuyck, H. A.; Whitesides, G. M. *Langmuir* **1994**, 10, 741.

# CHAPTER V

## FORMATION OF PATTERNED ASSEMBLIES OF NANOBIOCOMPOSITES



In this chapter we demonstrate the formation of patterned assemblies of nano/biocomposites. Four different proteins have been immobilized into a patterned 2 x 2 array of oppositely charged lipid films by appropriate masking of lipid regions and sequential immersion in the protein solutions. FTIR spectroscopy was used as a tool to monitor the protein immobilization process, check for possible protein intermixing into different regions of the lipid patterns, and also to confirm the intactness of the secondary structure of the immobilized protein. The technique has been used to realize patterned assemblies of silver, gold and cadmium sulfide nanoparticles. This protocol can be extended towards patterned assemblies of biological cells and DNA with exciting implications.

The work presented in this chapter has been published: 1) **Gole, A**; Sastry, M. *Biotech. Bioeng.*, **2001**, *74*, 172; 2) Sastry, M.; **Gole, A**; Sainkar, S. R. *Langmuir* **2000**, *16*, 3553; 3) Sastry, M.; **Gole, A**; Rao, M.; Ganesh, K.N. *Acc Chem Res.*, Communicated.

## 5.1. INTRODUCTION.

Immobilization of entities such as atoms, molecules, particles or biomolecules onto specific regions of a material is a topical area of interest and challenge.<sup>1</sup> This interest has largely been motivated by the silicon chip industry wherein different components such as transistors, capacitors etc are etched or grown by suitable lithographic and ion-implantation techniques on a single chip. This is the so called "top-down" (or "engineering down") approach.<sup>2</sup> If one extrapolates into the future using the current rate of miniaturization in silicon memory technology as a bench-mark<sup>2</sup>, very soon the physical limits of device dimensions realizable by ultraviolet, electron/ion beam and soft X-ray lithographic techniques will be reached. It is thus clear that an alternative approach based on possibly completely different principles would be required to overcome this barrier towards further miniaturization. The famous talk by Prof. Feynman at Caltech "*There's plenty of room at the bottom*",<sup>3</sup> motivated a number of researchers into completely new area of "bottom up" approach for the organization of nanoscale entities. This approach has made tremendous breakthroughs in the field of nanotechnology. In a broad sense, nanotechnology is the synthesis and organization of objects having nano-dimensions such as molecules and other nanoscale matter such as quantum dots, buckyballs (also known as fullerenes) and nanotubes.<sup>4</sup> Apart from the silicon chip industry, specific arrangement of biologically important structures and biomolecules (such as proteins, DNA, cells) is important, the motivation to a large extent being the development of biosensors<sup>5</sup> and high throughput multianalyte arrays.<sup>6</sup> Recently there has been much interest in the patterning of biomolecules mainly due to their potential application in patterned cell growth<sup>7</sup> and patterned antibodies for immunoassays.<sup>8</sup>

## 5.2 DIFFERENT STRATEGIES USED FOR PATTERNING.

Strategies for fabricating patterned nanostructures include a host of techniques such as lithography by photons, particles and scanning probes, moulds or physical contacts, self assembly, templated deposition and size reduction.<sup>9</sup> Photolithographic methods all share the same operational principle of exposure of an appropriate material and region to electromagnetic radiation (UV, Xray, e-beam etc) and then developing the latent image through etching.<sup>10</sup> Exposure is usually patterned either by interposing a mask between the source of radiation (or

particles) and the material or by scanning a focused spot of the source across the surface of the material.<sup>9,10</sup> Most of the fabrication in the integrated circuit (IC) industry uses projection-mode photolithography resulting in feature sizes of 250 nm with 248 nm UV light. The resolution of photolithography increases as the wavelength of the light used for exposure decreases. A reliable and economical solution to patterning features as small as ~ 150 nm can be achieved by the use of 193 nm ArF laser with calcium fluoride lenses. One of the several technical challenges to extending photolithographic methods into the sub-100-nm range is the development of reflection optics or stencil masks that can be used with very short wavelengths (~ 0.2-0.4 nm). Energetic particles such as electrons, ions and electrically neutral metastable atoms can also be used to form patterns with nanometer resolution in appropriate resist films. This approach is attractive because the de-Broglie wavelengths of these particles are sufficiently short (<0.1 nm) that they minimize the defects of diffraction that currently limit many photolithographic approaches. A resolution as good as ~ 10nm can be achieved with e-beam lithography,<sup>11a</sup> but it is a time consuming and serial process.<sup>11b</sup>

Scanning probe lithography (SPL) is one of the very powerful tools used for patterning atoms, molecules, biomolecules and nanoparticles with resolution in the nanometer regime. SPL uses the principle of "ploughing" a resist material on the surface to generate patterns using < 50 nm tips in the configuration of scanning tunneling microscopes (STMs),<sup>12a</sup> atomic force microscopes (AFMs),<sup>12b</sup> scanning electrochemical microscopes (SECM),<sup>12c</sup> or near-field scanning optical microscopes (NSOMs).<sup>12d</sup> Although scanning probes were originally designed to provide high-resolution images of surfaces, their lithographic capability was demonstrated in a set of experiments with an STM, just five years after the first STM images were recorded. In that work, a large electrical bias applied between a tungsten tip and a germanium surface caused transfer of a single atom from the tip to the surface.<sup>13a</sup> There is yet another pioneering example of the writing of the IBM logo by placing individual atoms on a surface using an STM tip.<sup>13b</sup> In this elegant work, Eigler and Schweizer showed that xenon atoms could be picked up using an STM tip and placed at specific sites on a Ni (110) surface<sup>13b</sup> and thus to "write" atomic-resolution patterns on surfaces. Since then, STMs, AFMs, SFMs etc have been used in many different ways to perform sophisticated lithography.<sup>14</sup> Mirkin and co-workers have developed the

dip pen nanolithography technique (DPN) to 'write' structures using molecular 'inks' such as alkanethiols, using an AFM tip as a 'nib' and the gold surface as 'paper'.<sup>15</sup> DPN works on the principle of transfer of molecules from an AFM tip to a surface via capillary forces, through a water meniscus which naturally forms in the ambient atmosphere, via capillary forces.<sup>15</sup> Recently, they have used the DPN-based strategy for generating charged chemical templates to study the assembly of single polystyrene (PS) particles into two-dimensional square lattices.<sup>15d</sup> Furthermore, they have demonstrated the use of DPN to create nanostructures of DNA on a surface, which can be used subsequently to guide the assembly of discrete nanoparticle building blocks with complementary DNA in an orthogonal manner.<sup>15e</sup> This strategy, they believe could lead to a new and general way for preparing multicomponent nanostructures for a wide-range of applications ranging from biological diagnostics to nano-electronics, to the preparation of colloidal crystals for use in catalysis and photonics.

One of the most popular types of lithographies currently in use is soft lithography.<sup>9,16</sup> It is the collective name for a set of lithographic techniques comprising replica molding (REM), microcontact printing (**mCP**), micromolding in capillaries (MIMIC), microtransfer molding (**mTM**), solvent-assisted micromolding (SAMIM), and near field conformal photolithography using an elastomeric phase-shifting mask. These techniques use a patterned elastomer (usually PDMS) as the mold, stamp, or mask to generate or transfer the pattern. Soft lithography has advantages over other lithographic techniques for applications in which patterning of nonplanar substrates, unusual materials or large patterning area are the major concerns.<sup>1,9,16</sup> Whitesides and co-workers have extensively used **mCP** for patterning surfaces with required functionality, and thereafter forming nanostructures and immobilizing biomolecules such as proteins and biological cells.<sup>17</sup> In **mCP**, an elastomeric PDMS stamp, inked with an appropriate solution of alkanethiol, is brought into contact with the surface of a substrate to transfer the ink molecules to those regions of the substrate that contact the stamp.<sup>17</sup> **mCP** is a rapid process with minimal waste of starting materials.<sup>17</sup> It is a parallel process wherein patterned SAMs can be formed over relatively large areas (~50 cm<sup>2</sup>) in a single impression.<sup>17</sup> It is also applicable to curved substrates and hence is useful in some kinds of 3-D fabrication.<sup>17</sup>

### 5.3 PATTERNED PROTEIN-LIPID BIOCOMPOSITES.

Patterning biomolecules such as proteins, enzymes, DNA, and biological cells have tremendous applications in biomedical industries towards realization of biochips for efficient immunoassays.<sup>5-8</sup> A host of techniques are used for immobilization of biomolecules into specific regions and prevent adsorption into 'unwanted' regions. In this direction, Whitesides and co-workers have studied in detail the nature of surface functionality of a SAM to assist/resist biomolecular immobilization.<sup>18</sup> Patterned surfaces for immobilization of biologicals have been obtained using microcontact printing ( $\mu$ -CP) on reactive, mixed self-assembled monolayers (SAMs).<sup>18</sup> They characterize the immobilization process by surface plasmon resonance (SPR) spectroscopy and lateral force microscopy measurements.<sup>18</sup> Crooks *et al* have used the same technique of  $\mu$ CP to selectively immobilize biological cells.<sup>19</sup> The assembly of macrophage cells within hydrophobic "corrals" of dimensions 63  $\mu$ m (depth = 54 nm) surrounded by hydrophilic walls, wherein the patterned corral structures were obtained by a three-step lithographic procedure consisting of  $\mu$ -CP, polymer grafting and polymer functionalization.<sup>19</sup> Sol-gel technique<sup>20a</sup> and elastomeric membranes<sup>20b</sup> have also been used for patterned immobilization of biomolecules. In one of the methods, UV radiation was used to oxidize the terminal thiol group of a (3-mercaptopropyl) trimethoxysilane (MTS)-coated surface leading to a surface resistant to protein adsorption. Thereafter selective attachment of the fluorescent protein phycoerythrin to the un-irradiated areas was demonstrated by Bhatia *et al*.<sup>21a</sup> The biotin-avidin interaction has been successfully utilized in targeted assembly of antibodies by a few researchers<sup>21b-d</sup> and also DNA by Niemeyer *et al*.<sup>21e-g</sup> Micropatterned lipid membranes with varying compositions and charge densities have been used for selective cell assembly and growth by Groves *et al*.<sup>21h</sup> They observed that all the membrane cultures except phosphatidylserine (PS) blocked cell adhesion. This fact was utilized for directed cell-immobilization on membrane microarrays displaying alternating corrals of PS-containing and PS-free lipids.<sup>21h</sup>

Most of the techniques mentioned above have dealt with the immobilization of single-component biologicals and exhibit little scope for extension to patterned, multicomponent protein structures. In this laboratory, we have developed a completely new technique for

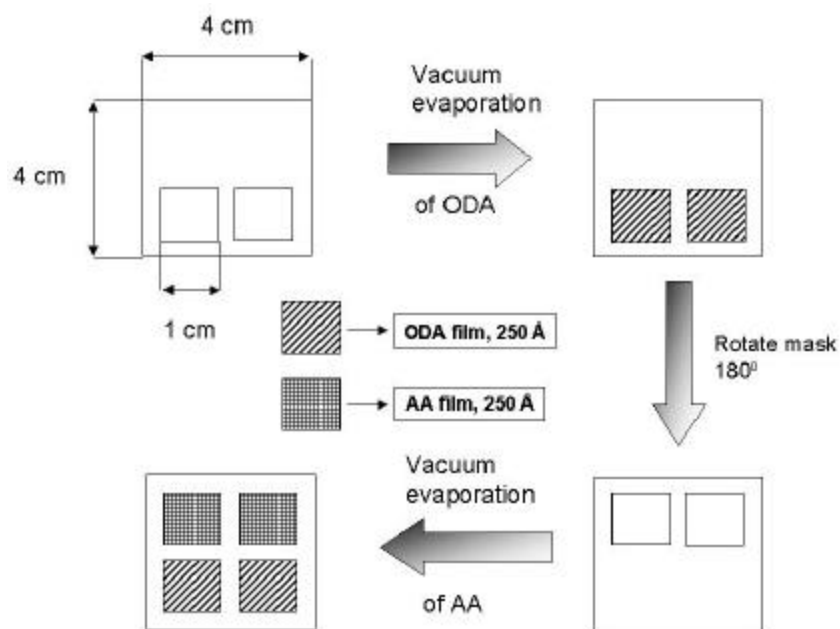


patterning nanoparticles, biomolecules and biological cells.<sup>22</sup> The main principle in our patterning procedure is the use of electrostatic interactions between the host (lipids) and guest molecules, appropriate masking of the lipids (hosts) using hydrophobic masks, and sequential immersion into guest molecule solutions. The guest molecules could be proteins/enzymes,<sup>22a,b</sup> DNA,<sup>22e</sup> biological cells,<sup>22c</sup> surface modified nanoparticles.<sup>22d</sup> This simple technique can be extended towards the realization of efficient DNA chips for sequence specific mismatch detection and is currently being pursued in this laboratory.

In this section we demonstrate the selective immobilization of four different proteins into four different regions of a 2 x 2 lipid array matrix by selective masking procedure. We chose two cationic proteins Cytochrome *c* (Cyt *c*), and fungal protease (F-prot), and two anionic proteins bovine hemoglobin (Hb), and pepsin. The pI values for all the four proteins were determined using a mini-scale iso-electric focusing unit built in-house.<sup>23</sup> The pI values are: Cyt *c* ~ 9; F-prot ~ 9.5 (these two proteins are cationic below their pI values), pepsin ~ 1; Hb ~ 7 (these two proteins are anionic above their pI values). To facilitate electrostatic interactions between the host (lipid) and the guest (protein), the choice of lipid was: anionic lipid (AA; pKa ~ 4.5<sup>24</sup>; anionic above pH 4.5) for cationic proteins (Cyt *c* and F-prot; cationic below their pI values) and cationic lipid (ODA; pKb ~ 10.5; cationic below pH 10.5) for anionic proteins (pepsin and Hb; anionic above their pI). In case of enzymes (F-prot and pepsin), the pH at which the enzyme displayed optimum biological activity was chosen as the pH for its intercalation. The entire process is described below.

**Patterned lipid deposition:** 250 Å thick lipid films were deposited by thermal evaporation in an Edwards vacuum coating unit as explained in Chapter 2, onto different substrates such as Si (111) for FTIR measurements and onto quartz substrates for UV-vis studies. The deposition of the lipid arrays was carried out as indicated in the scheme 5.3.1. Initially upper half of the substrates [Si (111) and quartz] were masked and placed in the coating unit. 250 Å thick ODA film was deposited on the unmasked region of the lower half of the substrates to get 2 ODA elements. This procedure was repeated for the deposition of the 2 AA elements on the top half of the substrates. This finally yields a 2 x 2 array of lipid films. FTIR spectra were recorded from

all the four regions of the 2 x 2 array after thermal evaporation onto a Si (111) substrate to ascertain whether any intermixing in the lipid films had occurred during the deposition stage.



**Scheme 5.3.1:** Diagram showing the various steps involved in the deposition of 2 x 2 array of AA and ODA lipid films by sequential masking of the substrate. The type of mask used for the experiments and its dimensions is also shown.

**Formation of patterned protein-lipid composites:** The formation of the patterned biocomposite film has been demonstrated in Scheme 5.3.2 below. An 'L' shaped teflon mask of the dimensions of the substrate was prepared. The mask was tied to the substrate using a teflon thread in such a way (scheme 5.3.2) that one of the lipid arrays is exposed and the remaining three are masked. Appropriate masking and sequential immersion of the lipid substrate in different protein solutions could lead to the formation of patterned 2 x 2 array of proteins. It was observed that hydrophobic masking material, such as teflon, is better for 'sealing' the unexposed regions of the substrate rather than a hydrophillic mask such as glass. A hydrophobic material forms a 'water-tight' mask thus preventing the seepage of water/protein solutions in the unexposed areas. The incorporation of the proteins into the individual array elements was characterized by the presence of the amide I and II bands in the infrared spectra, which also confirms the intactness of the protein conformation, and in the case of the heme-protein Hb, the Soret band in the UV-vis absorption spectra.

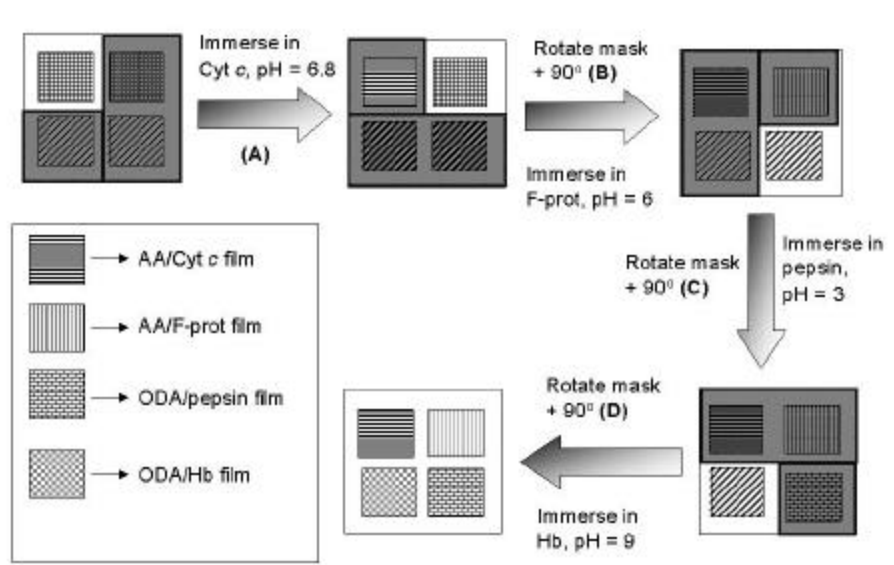
**1. Cyt *c* – AA composite film.**  $10^{-5}$  M solutions of Cyt *c* were prepared in aqueous solution close to physiological pH (pH 6.8). The 'L' shaped teflon sheet was fixed to the Si (111) substrate in such a way as to expose one of the two AA film elements and mask the remaining one AA and two ODA elements [Scheme 5.3.2, step A]. The film was immersed into the Cyt *c* solution for a period of 5 h. The time of immersion of the AA film in the protein solution was obtained from our earlier studies on Cyt *c*-AA biocomposite film formation.<sup>25a</sup> FTIR measurements of the cyt *c* - AA element were made after thorough washing and drying of the biocomposite film and the intensity of the amide I and II bands were used to monitor the protein incorporation process as well as to confirm the intactness of the secondary structure of the entrapped Cyt *c* molecules.

**2. F-prot-AA composite.** A  $10^{-5}$  M Fungal protease (F-prot) solution was prepared in a sodium – phosphate buffer (0.05 M, pH = 6). After rotating the mask by 90 degrees relative to the Cyt *c* immersion cycle, another AA element of the 2 x 2 array was exposed and the Si(111) substrate was immersed in the enzyme solution at pH 6 for 5 hours [Scheme 5.3.2, step B] and FTIR measurements of the F-prot-AA composite element were made after thorough washing and drying of the films. The time required for biocomposite formation was obtained from our previous studies on F-prot-AA biocomposites.<sup>25b</sup>

**3. Pepsin-ODA composite.** A  $10^{-5}$  M concentrated solution of pepsin was prepared in glycine-HCL buffer (0.05 M, pH 3), close to the pH value at which pepsin exhibits maximum catalytic activity.<sup>25c</sup> The mask on the Si (111) substrate was rotated by an angle of 90 degrees relative to the previous immersion cycle to expose one of the ODA elements [Scheme 5.3.2, step C] and the film was immersed for a period of 30 minutes in the protein solution. FTIR measurements were performed on the pepsin/ODA composite element as mentioned earlier. Pepsin intercalates within the ODA matrix within a period of 30 minutes as studied by us earlier.<sup>25c</sup>

**4. Hb-ODA composite.** A  $10^{-5}$  M concentrated solution of Hb was prepared in Tris – HCl buffer (0.05 M, pH = 9). After appropriate masking, [Scheme 5.3.2, step D] the Si (111) film was immersed in the hemoglobin solution for a period of 1 h. FTIR measurements confirmed the presence of the Hb molecules in the ODA matrix. Our earlier studies on Hb intercalation into ODA matrix indicates that complete incorporation of Hb molecules within the matrix is attained

within 1h.<sup>25a</sup> Hence this time was used for immersion of the ODA segment of the 2 x 2 array into the Hb solution. It can be clearly seen from the scheme 5.3.2 below that the procedure would yield a 2 x 2 array of different proteins immobilized into different array elements.



**Scheme. 5.3.2:** Diagram showing different stages of formation of protein-lipid composites: A) Immersion of one of the AA element of the array into cyt *c* solution at pH 6.8 after masking the other three regions with a teflon mask. B) Immersion of 2<sup>nd</sup> AA array element into F-prot solution held at pH=6 after rotation of the mask by 90°. C) Immersion of one of the ODA array elements into pepsin solution at pH=3 after further rotation of the mask by 90°. D) Immersion of the remaining ODA element into hemoglobin solution at pH=9 after further rotation of the mask by 90°.

As mentioned earlier, FTIR spectroscopy was used as a tool to monitor the protein incorporation process, check possible intermixing of the proteins into different array elements and to confirm the intactness of the protein secondary structure. FTIR was performed onto the 2 x 2 lipid arrays before and after protein incorporation, after thorough washing (in deionized water) and drying (in flowing nitrogen) of the films on a Shimadzu 8201 PC instrument at a resolution of 4 cm<sup>-1</sup>. 256 scans of the films were recorded in order to obtain a good signal to noise ratio. Fig. 5.3.1A shows the FTIR spectra of the as-deposited AA film (curve 1), the Cyt *c* /AA composite film recorded after immersion of the masked AA film in cyt *c* solution (pH 6.8) for a period of 5 h [curve 2; Scheme 5.3.2, step A] and the cyt *c* /AA element after completion of the immersion cycles in F-prot, pepsin and Hb [curve 3; Scheme 5.3.1, step B-D]. At physiological pH, the AA matrix is negatively charged (pKa ~ 4.5)<sup>24</sup> while Cyt *c* (pI 9)<sup>23</sup> is positively charged. This leads to maximum attractive electrostatic interaction between the protein and the lipid

element and thus drives the diffusion of the Cyt *c* molecules from solution. It is expected, considering the normal trajectory of the protein molecule, that it be immobilized into the unmasked region of the substrate. Lateral diffusion of the protein into other areas was ruled out by FTIR measurements of the lipid patterns as detailed below. Furthermore, as the hydrophobic L-shaped mask is 'water-tight' and hence would prevent such an intermixing.

A number of vibrational modes can be observed in the 3 curves shown in Fig.5.3.1A. The amide I band assigned to the characteristic carbonyl (C=O) stretch frequency in the amide bond of the polypeptide chains, occurs at ca.  $1650\text{ cm}^{-1}$  (feature b in Fig.5.3.1A) in the Cyt *c*/AA composite films (curves 2 and 3). This band is clearly absent in the as-deposited AA film (curve 1). The position of this band is close to that reported for the native protein in earlier reports<sup>26</sup> and indicates that the secondary structure of the proteins in the lipid environments is relatively unperturbed. The amide II band, assigned to the characteristic N-H stretch mode of vibration in the amide bond of the polypeptide chains, occurs at  $1544\text{ cm}^{-1}$  (feature d, Fig. 5.3.1A) can also be clearly seen for the Cyt *c*-AA composite films. This band also indicates that the secondary structure of the protein is maintained in the encapsulated form.<sup>26</sup> The band at  $1700\text{ cm}^{-1}$  (feature a, Fig. 5.3.1A) arises from the carbonyl stretch modes from the carboxylic acid groups in the AA matrix.<sup>27</sup> On electrostatic complexation of the AA matrix with the cyt *c* molecules, this band shifts to ca.  $1570\text{ cm}^{-1}$  (feature c, Fig. 5.3.1A) and is indicative of the fairly strong interaction of the AA 'host' with the protein 'guest'. Fig 5.3.1B shows the FTIR spectra of the other 3 array elements on the Si (111) substrate (curves 1 and 2 – ODA elements and curve 3 – AA element) recorded after the first immersion cycle. These regions were masked with hydrophobic teflon during the incorporation of Cyt *c*. It can be seen that the amide I and II bands (features b and d, Fig.5.3.1B) arising from Cyt *c* are clearly absent in the unexposed AA element (curve 3) while the amide II band is absent in the spectra recorded from the ODA elements thus indicating that the Cyt *c* diffuses only into the exposed AA element. The ODA film exhibits a feature close to where the amide I band occurs and is assigned to the N-H band in the amine matrix.

The FTIR spectrum of the Cyt *c* - AA matrix after the completion of all the four immersion cycles is shown as curve 3 (Fig 5.3.1A). The  $1700\text{ cm}^{-1}$  peak (carboxylic asymmetric stretch) and the amide I band at  $1650\text{ cm}^{-1}$ , are markedly different from the bands of curve 2 (fig

5.3.1A). Also the intensities of amide II band at  $1544\text{ cm}^{-1}$  and the  $1570\text{ cm}^{-1}$  band have increased. All this indicates that there might be small intermixing of the proteins in the cyt-*c*-AA matrix. This might be due to the surface roughness of the teflon mask used in the experiments leading to improper sealing of the matrix element. This is assigned to experimental errors and in principle there would not be any intermixing under ideal conditions.

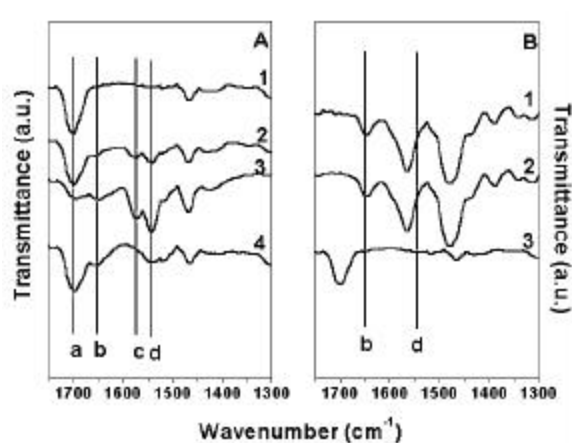


**Figure. 5.3.1:** A) FTIR spectra recorded from the various elements of the  $2 \times 2$  array at different stages of formation of protein-lipid composites. Curve 1 - the  $250\text{ \AA}$  thick as-deposited AA element; curve 2 -  $250\text{ \AA}$  thick cyt-*c*- AA composite element (see text for details); curve 3 - the  $250\text{ \AA}$  thick cyt-*c* - AA composite element after completion of all the four immersion cycles (see text for details) and curve 4 - the  $250\text{ \AA}$  thick F-prot-AA composite element (see text for details). B) FTIR spectra recorded after the first immersion cycle in cyt-*c* from one  $250\text{ \AA}$  thick as-deposited unexposed ODA element (curve 1), from the second  $250\text{ \AA}$  thick unexposed ODA element (curve 2) and the  $250\text{ \AA}$  thick unexposed AA element (curve 3).

The FTIR spectrum obtained from the F-prot/AA element after the second immersion cycle [Scheme 5.3.2, step B] is shown as curve 4 in Fig.5.3.1A. The amide I and II bands occur at wavenumbers close to that observed for the Cyt *c*/AA composite indicating encapsulation of F-prot with little distortion to the protein secondary structure. As in the case of the Cyt *c* immersion cycle, immersion in F-prot solution did not lead to incorporation of the protein in the unexposed ODA elements.

Fig. 5.3.2A shows the FTIR spectra of the as-deposited ODA film (curve 1), the pepsin/ODA composite film recorded after immersion of the masked ODA film in pepsin solution (pH 3) for a period of 30 min [curve 2; Scheme 5.3.2, step C] and the pepsin/ODA element after completion of the immersion cycle in Hb [curve 3; Scheme 5.3.2, step D]. As mentioned earlier, the as-deposited ODA (curve 1, Fig. 5.3.2A) film exhibits a feature at  $1646\text{ cm}^{-1}$  (close to the amide I band in native proteins, feature a, Fig. 5.3.2A). We assign this band to the N-H and C-N

torsional motions in the ODA molecules.<sup>25</sup> On immersion in pepsin solution, it is observed that a new band grows at roughly this energy and leads to a clearly discernible composite peak centred at ca.  $1640\text{ cm}^{-1}$ . The increase in intensity of this feature is attributed to the amide I band from the pepsin molecules encapsulated in the ODA matrix (Fig. 5.3.2A, feature a, curves 2 and 3) and is within the range expected for the native protein.<sup>26</sup>

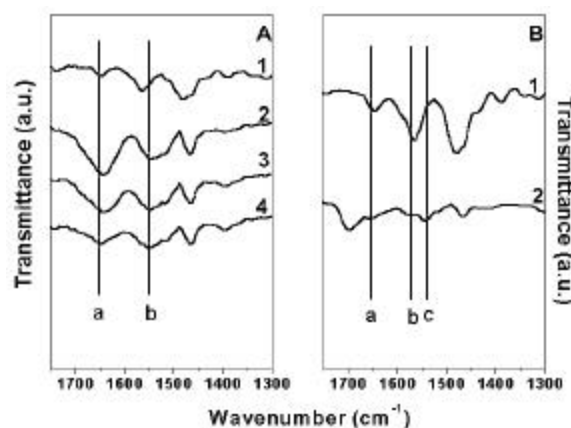


**Figure 5.3.2** A) FTIR spectra recorded from the different elements of the  $2 \times 2$  lipid array after various stages of protein-lipid composite formation. Curve 1 – the as-deposited unexposed  $250\text{ \AA}$  thick ODA element 2 (cycle 2); curve 2 – the  $250\text{ \AA}$  thick pepsin-ODA composite element; curve 3 – the  $250\text{ \AA}$  thick pepsin-ODA composite element after completion of all the four cycles and curve 4 – the  $250\text{ \AA}$  thick Hb-ODA element (see text for details). B) FTIR spectra recorded after the third immersion cycle in pepsin from one  $250\text{ \AA}$  as-deposited unexposed ODA element (curve 1) and the unexposed cyt-c-AA composite element (curve 2).

The amide II band is seen to grow at  $1544\text{ cm}^{-1}$  on encapsulation of the protein (Fig. 5.3.2A, feature b, curves 2 and 3) thus clearly establishing the presence of pepsin in the ODA element. Fig. 5.3.2B shows the FTIR spectra recorded from the unexposed ODA element (curve 1) as well as the Cyt c /AA element (curve 2). It can clearly be seen that there is little indication of the presence of pepsin in the unexposed ODA element and corroborates the finding mentioned earlier that this masking procedure does indeed lead to insignificant seepage of the protein solution between the mask and the surface of the lipid film elements. The FTIR spectrum recorded from the final ODA element after immersion in Hb solution for 1 h [Schematic 5.3.2, step D] is shown as curve 4 in Fig. 5.3.2A. The amide I and II bands are clearly observed as in the case of the pepsin/ODA composite element indicating the encapsulation of Hb in the lipid matrix.

Further characterization of patterned protein immobilization was carried out by UV-vis spectroscopy. The heme-proteins such as Cyt *c* and Hb have a characteristic absorption at ~ 410 nm which is known as the Soret band.<sup>28</sup> The nature of this band is known to give information about the intactness of the protein conformation.<sup>28</sup> The other two proteins (pepsin and F-prot) do not show Soret bands and are not colored. So we have used this signature (at 410 nm) of the protein to check whether any intermixing of the proteins has occurred. The absence of Soret bands in the other two protein-lipid arrays (pepsin and F-prot) would rule out any intermixing. Fig. 5.3.3A shows the UV-vis spectrum of a  $10^{-6}$  M concentrated Hb solution held at pH 9 (0.05 M Tris – HCl buffer). An intense absorption is clearly seen at 410 nm and is responsible for the characteristic red color of this heme protein. Fig. 5.3.3B shows the spectrum of Hb/ODA composite film (curve 1) obtained by immersion of the 1000 Å thick ODA element deposited on quartz under conditions identical to that reported for the FTIR measurements [Scheme 5.3.2, step D; Fig. 5.3.3, curve 1] and the ODA film which is unexposed to the hemoglobin solution (the pepsin/ODA element, curve 2). The Soret band is clearly seen at 410 nm in the Hb/ODA composite film and is absent in the pepsin-ODA array element (curve 2).

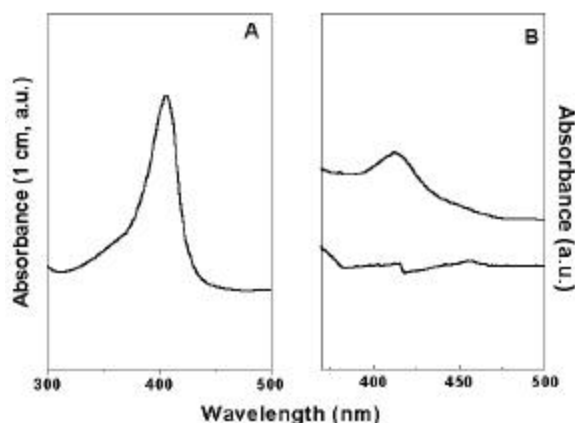


**Figure. 5.3.3** A) UV-vis spectrum showing the Soret band at 410 nm of hemoglobin solution in Tris - HCl buffer (pH=9). B) UV-vis spectra of 1000 Å thick Hb-ODA composite film after immersion of the ODA array element in Hb solution at pH=9 (curve 1, see text for details) and curve 2- the 1000 Å thick unexposed ODA array element (see text for details).

We have successfully extended the protocol of patterning entities on single substrates by patterning different surface modified nanoparticles via immobilization onto ODA patterns. Furthermore, recently we have shown the patterned immobilization of *Yarrowia lipolitica* yeast



cells onto 40  $\mu\text{m}$  x 40  $\mu\text{m}$  lipid patterns, the immobilization driven by specific interactions between the hydrocarbon degrading enzymes present in the yeast cell walls and the lipid matrix.

#### 5.4 FORMATION OF PATTERNED NANOPARTICLE THIN FILMS.

We demonstrate the formation of thin, patterned, *hetero-colloidal* nanoparticle assemblies of gold, silver and Q-state CdS. This simple technique is illustrated in Scheme 5.3.1 below. The synthesis of individual gold (size:  $35 \pm 6 \text{ \AA}$ ), silver (size:  $70 \pm 13 \text{ \AA}$ ) and Q-state Cadmium sulfide (CdS; size:  $45 \pm 10 \text{ \AA}$ ) colloidal particles nanoparticles is done as follows:

a) Gold and silver colloidal particles: The borohydride reduction of  $\text{Ag}_2\text{SO}_4$  salt has been done by the method of Vukovic and Nedeljkovic.<sup>29</sup> The gold salt (chloroauric acid;  $\text{HauCl}_4$ ) was also reduced to form gold colloids by the similar method of borohydride reduction. Typically, a 100 ml of  $10^{-4}$  M concentrated aqueous solutions of silver sulfate/ chloroauric acid is reacted with 0.01 g of sodium borohydride at room temperature with rigorous stirring. The standard characterization of the silver and gold sols have been done in earlier work by Sastry *et al.*<sup>30</sup> The UV-vis spectra of silver sol gives a peak at 388 nm, which is characteristic of silver colloidal particles arising due to the surface plasmon resonance, and is well documented by the Mie theory.<sup>31</sup> Colloidal gold on the other hand is ruby red in color and gives a surface plasmon resonance peak at ca 514 nm.<sup>30b,32</sup> The Transmission electron microscopy (TEM) analysis of the silver and gold colloidal particles was performed in the previous studies.<sup>30</sup> The analysis gave a mean cluster diameter (for silver colloids) of 73  $\text{\AA}$  with a standard deviation of 13  $\text{\AA}$ .<sup>30a</sup> The gold colloidal particles had a mean particle diameter of 34  $\text{\AA}$  with a deviation of 7  $\text{\AA}$ .<sup>30b</sup>

The particles in a colloidal solution are highly reactive due to the very high surface to volume ratio and they tend to flocculate. In order to achieve long term stability of these particles, their surface is modified using suitable surfactants such as alkane thiols,<sup>33</sup> fatty acids,<sup>34</sup> amines<sup>35</sup> and polymers.<sup>36</sup> Our application requires the terminal functional group of the chemisorbed surfactant to be ionizable in order to use its functionality for organization into lipid films via electrostatic interactions. Hence we have used a bi-functional molecule such as 4-carboxythiophenol (4-CTP). This molecule anchors to the colloidal surface via the thiol bond,<sup>30</sup> and the terminal functional group-the carboxylic acid group can be ionized and used for

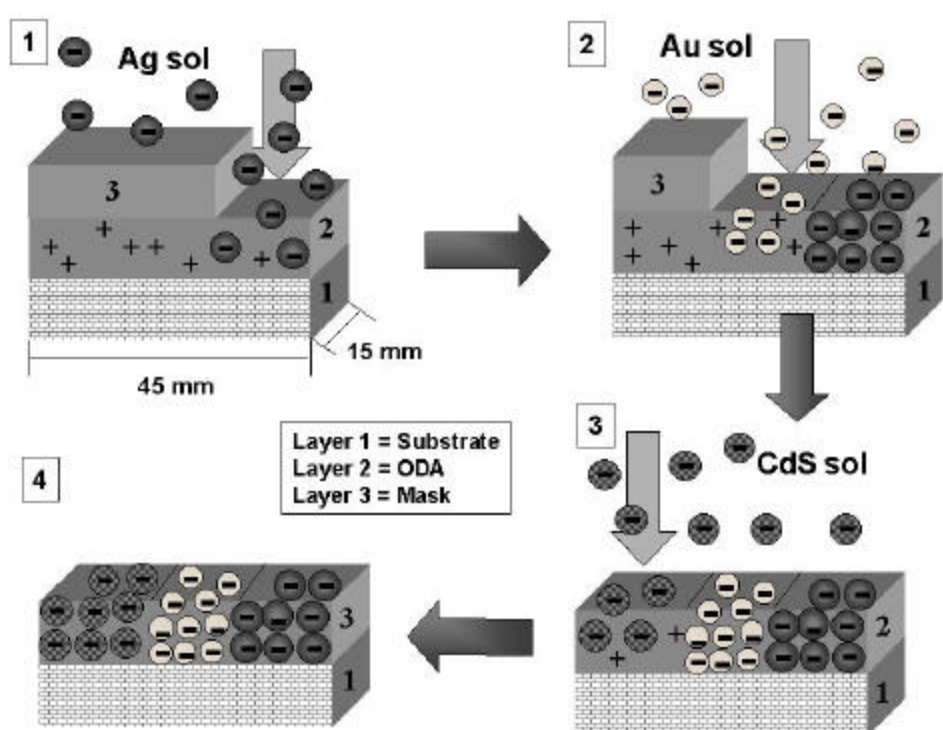
electrostatic complexation into cationic matrix (ODA). This has been successfully demonstrated by Sastry *et al* in the earlier studies on Langmuir-Blodgett films<sup>37</sup> and by diffusion technique<sup>38</sup>

b) Synthesis of CdS colloidal particles: The CdS hydrosol was prepared by reacting a  $10^{-4}$  M concentrated aqueous solution of cadmium sulfate ( $\text{CdSO}_4$ ) with stoichiometric amounts of sodium sulfide ( $\text{Na}_2\text{S}$ ) [Cd: S ratio of 1:1], in the presence of the capping molecule, 4-CTP (capping concentration  $\sim 10^{-5}$  M). The reaction was carried out under continuous stirring for 30 min after which argon was bubbled in the hydrosol for ca. 40 min to remove excess  $\text{H}_2\text{S}$ . The formation and stability of CdS colloidal particles stabilized by 4-CTP, was followed using UV-vis spectroscopy. The absorption edge was found to occur at  $\sim 480$  nm, which from the particle size-band edge data of Henglein<sup>39</sup> indicates a particle diameter of  $\sim 6$  nm and therefore, CdS particles are in the Q-state regime.

Thin films of octadecylamine (ODA, 500 Å thickness) were thermally vacuum deposited (as has been explained in chapter II, section 2.2) onto gold coated AT-cut quartz crystals for quartz crystal microgravimetry measurements (QCM) as well as quartz substrates for UV-vis spectroscopy studies. Before immersion of the ODA films in the different colloidal particle solutions, regions of the film surface were masked using teflon sheets. The teflon sheets were held in contact with the film surface by binding with teflon tape. After suitable masking of the ODA coated substrates, they were immersed sequentially in 4-CTP capped silver, gold and CdS solutions whose pH was adjusted to 9. At this pH, the carboxylic acid group of the 4-CTP molecule on the colloidal particle surface is completely ionized ( $\text{pK}_a \sim 4.5$ ).<sup>24</sup> The amine molecules in the ODA matrix are also protonated at this pH ( $\text{pK}_b \sim 10.5$ ). So at this pH, maximum electrostatic interactions between the surface modified colloidal particles and the ODA matrix exists and leads to rapid and complete immobilization of the colloidal particles into the matrix. This has been observed earlier by Sastry *et al*.<sup>38</sup> The time required for complete incorporation of the colloidal nanoparticles was obtained from QCM measurements.

The entire procedure has been clearly depicted in scheme 5.4.1 below. Initially 33 % of the lipid was exposed to 4-CTP capped colloidal silver particles (pH 9) for 5h (time obtained by QCM studies). The remaining 66 % of the lipid was masked by the teflon mask. After complete incorporation of the silver particles, a further 33 % of the lipid was exposed to colloidal gold

solution. Hence, the lipid containing the silver nanoparticles (33 % of total lipid area) and another 33 % of the lipid surface was now immersed in gold solution. The remaining 33 % of the lipid area was masked as in the earlier case. After complete incorporation of the gold nanoparticles, the entire substrate (33 % silver particle covered lipid, 33 % gold particle covered lipid and a further 33 % of the previously unexposed lipid area) was immersed into aqueous solution of CdS nanoparticles. Thus by judicious masking of the fatty lipid surface and sequential immersion in different colloidal nanoparticle solutions, an *in-plane* spatially separated assembly of hetero-colloidal particles was obtained.



**Scheme. 5.3.1:** Diagram showing the masking process used for the generation of spatially separate, patterned colloidal particle films by an electrostatically controlled diffusion mechanism into ODA films.

Visibly it would seem that the colloidal particles are immobilized into their respective regions without any intermixing. To check this fact, spot profile energy dispersive analysis of X-rays (EDAX) measurements were carried out in the different colloidal particle regions of the film. EDAX measurements on the silver portion of the nanoparticle film yielded 9.87 weight percent silver and 90.13 weight percent Si (from quartz). The gold region of the film yielded 4.04 weight percent gold and 95.96 percent Si while the CdS region of the film yielded corresponding weight

percentages of 11.41 for Cd, 4.08 for S and 84.51 for Si. Thus, it can be seen from the EDAX measurements that there is no evidence for the presence of colloidal particles other than those incorporated by design into the respective regions of the film. This result shows that once bound, it is difficult to exchange the colloidal particles with another colloidal particle species. In this sense, colloidal nanoparticle composites with fatty lipid films behave differently from salts of fatty acids where for example,  $\text{Cd}^{2+}$  ions could be readily replaced with  $\text{Pb}^{2+}$  ions by immersion in  $\text{PbCl}_2$  solution.<sup>40</sup> We also checked the boundary regions of the Ag-Au and the Au-CdS regions by spot profile EDAX measurements. This essentially consisted of mapping the weight percent concentration ratio of, for example, Au and Cd as a function of distance from the Au-CdS "edge". The "edge" was chosen to be the visual edge as seen by SEM imaging of the film surface and was the origin for the distance measurement. It was observed that the individual ratios reach saturation values well within the respective regions as in to be expected. What is surprising is the extent of the interfacial region where the density of *both* colloidal CdS and gold particles is very small. This interfacial region is ca. 200 nm wide. A similar interfacial region was observed at the Au-Ag colloidal particle film edge. This interfacial region of intermixing might be due to the roughness of the mask edge. This result exposes the limitations of conventional microscopy and highlights the importance of chemical profile analysis of the edge. The colloidal particles do not intermix into the inner regions of the lipid, as they do not 'laterally diffuse'. So the time-averaged trajectory of the colloidal particles as they diffuse into the ODA matrix is essentially normal to the film surface. This result also supports the use of a 1-D diffusion model used by us for the analysis of nanoparticles and proteins into thin lipid films.<sup>38,41</sup>

## 5.5. SUMMARY

This chapter demonstrates the formation of patterned assemblies of proteins onto a single substrate by masking (using a teflon sheet) and sequential immersion in the protein solutions. Four different proteins (Cyt c, Hb, F-prot and pepsin) have been immobilized into different regions of a 2 x 2 array of lipid elements (2 cationic lipids and 2 anionic lipids). Electrostatic interactions between the protein guest and the lipid host drives the immobilization process. The choice of the lipid and pH for immobilization was selected depending on the pl of

the enzyme (which reflects to the total charge on the protein) and the optimum conditions for biological activity (in case of enzymes). FTIR spectroscopy was used as a tool to monitor the protein immobilization process, check for possible intermixing of the proteins into other regions of the lipid patterns, and to confirm the intactness of the protein secondary structure. As a secondary check to confirm the faithfulness of the templated protein immobilization, UV-vis spectroscopy was used to monitor the 410 nm solet band arising from the heme-protein Hb. The absence of this band in other regions of the array element rules out any possibility of intermixing. It was found that the use of a hydrophobic mask such as teflon was much more efficient in blocking the intermixing of proteins into different regions as compared to hydrophilic masks such as glass. The technique is shown to be extended towards the realization of patterned nanoparticle thin films. The colloidal nanoparticles (silver, gold and CdS) were immobilized onto a single substrate to obtain a hetero-colloidal patterned films. There is a small amount of intermixing of the nanoparticles at the interface, as observed by spot profile EDAX analysis, which might be possibly due to roughness of the mask used. There is no intermixing of the particles in the inner part of the template indicating that there is no lateral diffusion of the nanoparticles and the time-averaged trajectory of the particle diffusion is normal to the surface. Recently we have shown the patterned assembly of yeast cells, the assembly driven by specific interactions between the hydrocarbon degrading enzymes on the cell surface and the lipids. This simple yet powerful technique can be extended towards the realization of patterned oligonucleotide assemblies for possible DNA mismatch detection.

## 5.6. REFERENCES

1. Xia, Y.; Whitesides, G.M. *Angew. Chem. Int. Ed.*, **1998**, *37*, 551.
2. a) Sastry, M. *Nanoparticle thin films: An approach based on self assembly*, Handbook of surfaces and interfaces of materials, Vol. 3, 2001, Academic Press, San Diego, USA; b) In 1965, Gordon Moore (co-founder of Intel Corp.) predicted that transistor density (memory storage capacity) on an integrated circuit would double every 18 months. This has come to be known as "Moore's law" and the silicon industry has been following this trend till date.
3. The classic talk by Richard Feynman entitled "There's plenty of room at the bottom" delivered at an annual meeting of the American Physical Society at the California Institute

of Technology in 1959 is possibly the first serious exposition on the problem of manipulating nanoscale objects (the talk is available on <http://www.zyvex.com/nanotech/feynman.html>).

4. Dresselhaus, M.S.; Dresselhaus, G.; Eklund, P.C. *"Science of fullerenes and nanotubes"*, Academic Press, San Diego, **1996**.
5. Guschin, D.; Yershov, G.; Zaslavsky, A.; Gemmell, A.; Shick, V.; Proudnikov, D.; Arenkov, P.; Mirzabekov, A. *Anal. Biochem.*, **1997**, *250*, 203.
6. Byfield, M. P.; Abuknesha, R.A. *Biosens. Bioelectron.*, **1994**, *9*, 373.
7. a) Stenger, D. A.; Georger, J. H.; Dulcey, C. S.; Hickman, J. J.; Rudolph, A. S.; Nielson, T. B.; McCort, S. M.; Calvert, J. M. *J. Am. Chem. Soc.*, **1992**, *114*, 8435; b) Singhvi, R.; Kumar, A.; Lopez, G. P.; Stephanopoulos, G.N.; Wang, D.I.C.; Whitesides, G. M.; Ingber, D.E. *Science* **1994**, *264*, 696; c) Ghosh, P.; Amirpour, M.L.; Lackowski, W.M.; Pishko, M.V.; Crooks, R.M. *Angew.Chem.Int.Ed.*, **1999**, *38*, 1592.
8. Pritchard, D.J.; Morgan, H.; Cooper, J. M. *Anal Chem.*, **1995**, *67*, 3605.
9. Xia, Y.; Rogers, J.A.; Paul, K.E.; Whitesides, G.M. *Chem. Rev.*, **1999**, *99*, 1823.
10. a) Moreau, W.M. *Semiconductor lithography: Principles and materials*, Plenum: New York, **1988**; b) Tani, T.; *Phys. Today.*, **1989**, 36.
11. a) Broers, A.N.; Molzen, W.; Cuomo, J.; Wittels, M. *Appl. Phys. Lett*, **1976**, *29*, 596; b) Gibson, J.M. *Phys. Today.*, **1997**, 56.
12. a) Kramer, N.; Birk, H.; Jorritsma, J.; Schonenberger, C. *Appl. Phys. Lett.*, **1995**, *66*, 1325; b) Dagata, J.A. *Science* **1995**, *270*, 1625; c) Bard, A.; Denault, G.; Lee, C.; Mandler, D.; Wipf, D.O. *Acc. Chem. Res.*, **1990**, *23*, 357; d) Betzig, E.; Trautman, K. *Science* **1992**, *257*, 189.
13. a) Becker, R.S.; Golovchenko, J.A.; Swartzentruber, B.S. *Nature* **1987**, *325*, 419; b) Eigler, D.M.; Schweizer, E.K. *Nature* **1990**, *344*, 524.
14. a) Lyo, L-W. Avouris, Ph. *Science* **1991**, *253*, 173; b) Eigler, D.M.; Lutz C.P.; Rudge, W.E. *Nature* **1991**, *352*, 600; c) Resch, R.; Baur, C.; Bucacov, A.; Koel, B.E.; Echternach, P.M.; Madhukar, A.; Montoya, N.; Requicha A.A.G.; Will, P. *J. Phys. Chem. B.*, **1999**, *103*, 3647; d) Baur, C.; Gazen, B.C.; Koel, B.; Ramachandran, T.R.; Requicha A.A.G.; Zini, L. *J. Vacuum Sci. Technol. B.*, **1997**, *15*, 1577; e) Resch, R.; Baur, C.; Bugacov, A.; Koel, B.E.;

- Madhukar, A.; Requicha, A.A.G.; Will, P. *Langmuir* **1998**, *14*, 6613; f) Kim, Y. Lieber, C.M. *Science* **1992**, *257*, 375.
15. a) Piner, R.D.; Zhu, J.; Xu, F.; Hong, S.; Mirkin, C.A. *Science* **1999**, *283*, 661; b) Piner, R.D.; Mirkin, C.A. *Langmuir* **1997**, *13*, 6864; c) Hong, S.; Zhu, J.; Mirkin, C.A. *Science* **1999**, *286*, 523; d) Demers, L.M.; Mirkin, C.A. *Angew. Chem. Int. Ed.*, **2001**, *40*, 3069; e) Demers, L.M.; Park, S.-J.; Taton, T.A.; Li, Z.; Mirkin, C.A. *Angew. Chem. Int. Ed.*, **2001**, *40*, 3071.
16. Xia, Y.; Whitesides, G.M. *Annu. Rev. Mater. Sci.*, **1998**, *28*, 153.
17. a) Xia, Y.; Kim, E.; Whitesides, G.M. *J. Electrochem. Soc.*, **1996**, *143*, 1070; b) Biebuyck, H.A.; Whitesides, G.M. *Langmuir* **1994**, *10*, 4581; c) Xia, Y.; Venkateswaran, N.; Qin, D.; Tien, J.; Whitesides, G.M. *Langmuir* **1998**, *14*, 363; d) Rogers, J.A.; Jackman, R.J.; Whitesides, G.M. *Adv. Mater.*, **1997**, *9*, 475; e) Jackman, R.J.; Wilbur, J.L.; Whitesides, G.M. *Science* **1995**, *269*, 664; f) Kumar, A.; Biebuyck, H.; Whitesides, G.M. *Langmuir* **1994**, *10*, 1498; g) Xia, Y.; Kim, E.; Mrksich, M.; Whitesides, G.M. *Chem. Mater.*, **1996**, *8*, 601; h) Xia, Y.; Mrksich, M.; Kim, E.; Whitesides, G.M. *J. Am. Chem. Soc.*, **1995**, *117*, 9576; i) Wang, D.; Thomas, S.G.; Wang, K.L.; Xia, Y.; Whitesides, G.M. *Appl. Phys. Lett.*, **1997**, *70*, 1593.
18. a) Ostuni, E.; Chen, C.S.; Ingber, D.E.; Whitesides, G.M. *Langmuir* **2001**, *17*, 2828; b) Whitesides, G.M.; Ostuni, E.; Takayama, S.; Jiang, Xi.; Ingber, D.E. *Annu. Rev. Biomed. Eng.*, **2001**, *3*, 335; c) Holmlin, R. E.; Schiavoni, M.; Chen, C.Y.; Smith, S. P; Prentiss, M.G.; Whitesides, G.M. *Angew. Chem., Int. Ed.*, **2000**, *39*, 3503; d) Ostuni, E.; Kane, R.; Chen, C.S. Ingber, D.E.; Whitesides, G.M. *Langmuir* **2000**. *16*, 7811; e) Kane, R.S.; Takayama, S.; Ostuni, E.; Ingber, D.E.; Whitesides, G.M. *Biomaterials* **1999**, *20*, 2363; f) Zhang, S.; Yan, L.; Altman, M.; Lasse, M.; Nugent, H.; Frankel, F.; Lauffenburger, D.A.; Whitesides, G.M.; Rich, A. *Biomaterials* **1999**, *20*, 1213.
19. a) Ghosh, P.; Amirpour, M. L.; Lackowski, W. M.; Pishko, M. V.; Crooks, R. M. *Angew. Chem. Int. Ed.*, **1999**, *38*, 1592; b) Ghosh, P.; Crooks, R.M. *J. Am. Chem. Soc.*, **1999**, *121*, 8395; c) Aoki, A; Ghosh, P; Crooks, R.M. *Langmuir* **1999**, *15*, 7418; d) Amirpour, M.L.; Ghosh, P.; Lackowski, W.M.; Crooks, R.M.; Pishko, M.V. *Anal. Chem.*, **2001**, *73*, 1560.

20. a) Chia, S.; Urano, J.; Tamanoi, F.; Dunn, B.; Zinc, J.I. *J. Am. Chem. Soc.*, **2000**, *122*, 6488; b) Ostuni, E.; Kane, R.; Chen, C. S.; Ingber, D. E.; Whitesides, G. M. *Langmuir* **2000**, *16*, 7811.
21. a) Bhatia S K.; Hickman, J.J.; Ligler, F. S. *J. Am. Chem. Soc.*, **1992**, *114*, 4432; b) Blawas, A.S, Oliver, T.F, Pirrung, M.C.; Reichert, W.M. *Langmuir* **1998**, *14*, 4243; c) Spinke, J.; Liley, M.; Guder, H.J.; Angermaier, L.; Knoll, W. *Langmuir* **1993**, *9*, 1821; d) Ahlers, M.; Muller, W.; Reichert, A.; Ringsdorf, H.; Venzmer, J. *Angew. Chem. Int. Ed. Engl.*, **1990**, *29*, 1269; e) Niemeyer, C.M.; Ceyhan, B.; Blohm, D. *Bioconjugate Chem.*, **1999**, *10*, 708; f) Niemeyer, C.M.; Boldt, L.; Ceyhan, B.; Blohm, D. *Anal. Biochem.*, **1999**, *268*, 54; g) Niemeyer, C.M.; Adler, M.; Pignataro, B.; Lenhert, S.; Gao, S.; Chi, L.; Fuchs, H.; Blohm, D. *Nucleic Acids Res.*, **1999**, *27*, 4553; h) Groves, J.T.; Mahal, L.K.; Bertozzi, C.R. *Langmuir* **2001**, *17*, 5129.
22. a) Sastry, M.; Gole, A.; Sainkar, S. R. *Langmuir* **2000**, *16*, 3553; b) Gole, A.; Sastry, M. *Biotech. Bioeng.*, **2001**, *74*, 172; c) Gole, A.; Dixit, V.; Lala, N.; Pant, A.; Sastry, M. *Coll. Surf. B*, in press; d) Sastry, M.; Gole, A.; Rao, M.; Ganesh, K.N. *Acc Chem Res.*, in press; e) Sastry, M.; Gole, A.; Ramakrishnan, V.; Dash, C.; Vyas, S.; Rao, M.; Lachke, A. Ganesh, K. N. *Trends. Biotechnol.*, in press.
23. a) Sathivel, C.; Lachke, A.; Radhakrishnan, S. *J. Chromat. A*, **1995**, 705; b) Gole, A.; Sathivel, C.; Lachke, A.; Sastry, M. *J. Chromat. A*, **1999**, *848*, 485.
24. Roser, S.J.; Lovell, M.R. *J.Chem.Soc., Faraday Trans.*, **1995**, *91*, 1783.
25. a) Gole, A.; Chaudhari, P.; Kaur, J.; Sastry, M. *Langmuir* **2001**, *17*, 5646; b) Gole, A.; Dash, C.; Mandale, A. B.; Rao, M.; Sastry, M. *Anal. Chem.*, **2000**, *72*, 4301; c) Gole, A.; Dash, C.; Rao, M.; Sastry, M. *Chem. Commun.*, **2000**, 297.
26. a) Dong, A.; Huang, P.; Caughey, W.S. *Biochemistry* **1992**, *31*, 182; b) Templeton, A.C.; Chen, S.; Gross, S.M.; Murray, R.W. *Langmuir* **1999**, *15*, 66; c) Kumar, C. V.; McLendon, G. L. *Chem. Mater.*, **1997**, *9*, 863; d) Caruso, F.; Furlong, D. N.; Ariga, Katsuhiko.; Ichinose, I.; Kunitake, T. *Langmuir* **1998**, *14*, 4559.
27. Rabolt, J. F.; Burns, F. C.; Schlotter, N. E.; Swalen, J. D. *J. Chem. Phys.*, **1983**, *78*, 946.

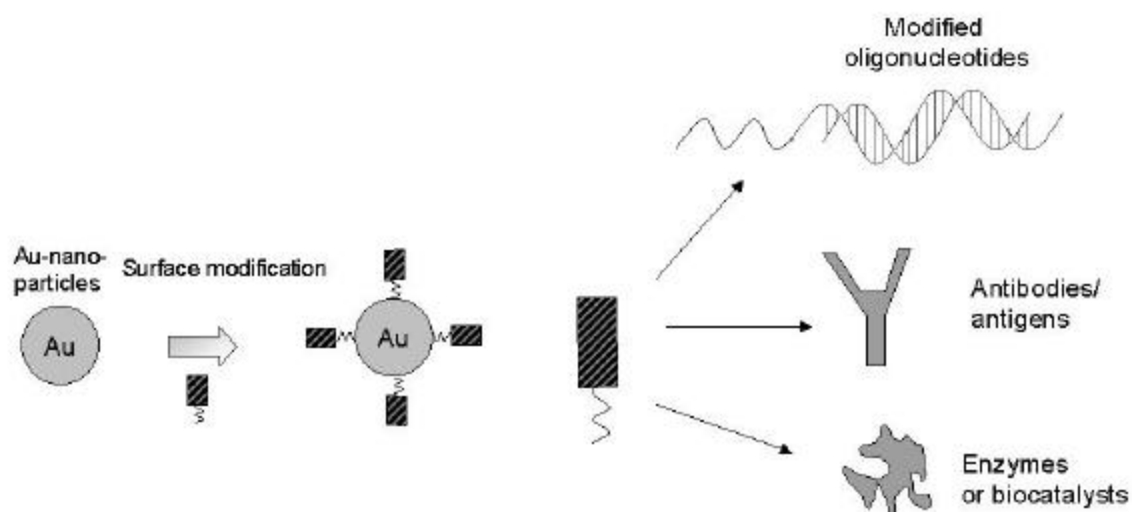


28. a) Margoliash, E.; Frohwirt, N. *Biochem. J.*, **1993**, *241*, 1473; b) Kumar, C. V.; McLendon, G. L. *Chem. Mater.*, **1997**, *9*, 863; c) Himachi, I.; Noda, S.; Kunitake, T. *J. Am. Chem. Soc.*, **1990**, *112*, 6744; c) Hamachi, I.; Honda, T.; Noda, S.; Kunitake, T. *Chem. Lett.*, **1991**, 1121.
29. Vukovic, V.V.; Nedeljkovic, J.M. *Langmuir* **1993**, *9*, 980.
30. a) Sastry, M.; Patil, V.J.; Sainkar, S.R. *J. Phys. Chem. B.*, **1998**, *102*, 1404; b) Patil, V.; Malvankar, R. B.; Sastry, M. *Langmuir* **1999**, *15*, 8197.
31. a) Mie. G. *Ann. Phys.* **1908**, *25*, 377; b) Creighton, J.A.; Eadon, D.G.; *J. Chem. Soc., Faraday Tras.* , **1991**, *87*, 3881; c) Henglein, A. *J. Phys. Chem.*, **1993**, *97*, 5764; d) Henglein, A. *Top. Curr. Chem.*, **1988**, *143*, 113.
32. Alvarez, M. M.; Khoury, J. T.; Schaaf, T. G.; Shafiqullin, M. N.; Vezmar, I.; Whetten, R. L. *J. Phys. Chem B.*, **1997**, *101*, 3706.
33. a) Brust, M.; Walker, M.; Bethell, D.; Schiffrin D.J.; Whyman, R.; *J.Chem.Soc., Chem. Commun.*, **1994**, 801; b) Templeton, A.C.; Wuelfing, W.P.; Murray, R.W. *Acc. Chem. Res.*, **2000**, *33*, 27; c) Sarathy, K. V.; Raina, G.; Yadav, R. T.; Kulkarni, G. U.; Rao, C. N. R. *J. Phys. Chem. B.*, **1997**, *101*, 9876; d) Badia, A.; Cuccia, L.; Demers, L.; Morin, F.; Lennox, R. B. *J. Am. Chem. Soc.*, **1997**, *119*, 2682; e) Whetten, R.L.; Khoury, J.T.; Alvarez, M.M.; Murthy, S.; Vezmar, I.; Wang, Z.L.; Stephens, P.W.; Cleveland, C.L.; Luedtke W.D.; Landman, U. *Adv. Mater.*, **1996**, *8*, 428; f) Sastry, M.; Mayya, K. S.; Patil, V. *Langmuir* **1998**, *14*, 5921; g) Gole, A.; Sainkar, S.R. Sastry, M. *Chem. Mater.*, **2000**, *12*, 1234.
34. a) Erokhin, V.; Facci, P.; Carrara, S.; Nicolini, C. *Biosens. Bioelectron.*, **1997**, *12*, 601; b) Patil, V.; Mayya, K.S.; Pradhan S.D.; Sastry, M. *J. Am. Chem. Soc.*, **1997**, *119*, 9281; c) Erokhin, V.; Facci, P.; Gobbi, L.; Dante, S.; Rustichelli, F.; Nicolini, C. *Thin Solid Films*, **1998**, *327-329*, 503; d) Sastry, M.; Mayya, K. S.; Patil, V. *Langmuir* **1998**, *14*, 5921; e) Damle, C.; Gole, A.; Sastry, M. *J. Mater. Chem.*, **2000**, *10*, 1389.
35. a) Leff, D.V.; Brandt, L.; Heath, J.R. *Langmuir* **1996**, *12*, 4723; b) Kumar, A.; Mukherjee, P.; Guha, A.; Adyantaya, S. D.; Mandale, A. B.; Kumar, R.; Sastry, M. *Langmuir* **2000**, *16*, 9775.
36. a) Pan, C.; Pelzer, K.; Philippot, K.; Chaudret, B.; Dassenoy, F.; Lecante, P.; Casanove, M-J. *J. Am. Chem. Soc.*, **2001**, *123*, 7584; b) Lim, M. H.; Ast, D. G. *Adv. Mater.*, **2001**, *13*,

- 718; c) Akamatsu, K.; Tsuboi, N.; Hatakenaka, Y.; Deki, S. *J. Phys. Chem. B*, **2000**, *104*, 10168; d) Gonsalves, K. E.; Carlson, G.; Benaissa, M.; Jose-Yacaman, M.; Kim, D. Y.; Kumar, J. *J. Mater. Chem.*, **1997**, *7*, 703.
37. Langmuir-Blodgett films: a) Mayya, K.S.; Patil, V.; Sastry, M. *Langmuir* **1997**, *13*, 2575; b) Sastry, M.; Mayya, K.S.; Patil, V.; Paranjape, D.V.; Hegde, S.G. *J.Phys.Chem.B*. **1997**, *101*, 4954; d) Mayya, K.S.; Sastry, M. *J. Phys. Chem. B*, **1997**, *101*, 9790; e) Mayya, K.S.; Patil, V.; Sastry, M. *J.Chem.Soc., Faraday Trans.*, **1997**, *93*, 3377; f) Mayya, K.S.; Sastry, M. *Langmuir* **1998**, *14*, 74; g) Mayya, K.S.; Patil, V.; Kumar, M.; Sastry, M. *Thin Solid Films* **1998**, *312*, 300; h) Sastry, M.; Mayya, K.S.; Patil, V. *Langmuir* **1998**, *14*, 5921.
38. Diffusion into lipid films: a) Sastry, M.; Patil, V.; Mayya, K.S. *Langmuir* **1997**, *13*, 4490; b) Patil, V.; Sastry, M. *J.Chem.Soc.Faraday Trans.* **1997**, *93*, 4347; c) Patil, V.; Sastry, M. *Langmuir* **1997**, *13*, 5511; d) Sastry, M.; Patil, V.; Sainkar, S.R. *J.Phys.Chem.B*. **1998**, *102*, 1404; e) Patil, V.; Sastry, M. *Langmuir* **1998**, *14*, 2707; f) Patil, V.; Malvankar, R.B.; Sastry, M. *Langmuir* **1999**, *15*, 8197.
39. Henglein, A. *Chem. Rev.*, **1989**, *89*, 1861.
40. Ganguly, P.; Paranjape, D.V.; Pal, S.; Sastry, M. *Langmuir* **1994**, *10*, 1670.
41. a) Gole, A.; Chaudhari, P.; Kaur, J.; Sastry, M. *Langmuir* **2001**, *17*, 5646; b) Gole, A.; Dash, C.; Mandale, A. B.; Rao, M.; Sastry, M. *Anal. Chem.*, **2000**, *72*, 4301; c) Gole, A.; Kaur, J.; Pavaskar, N.; Sastry, M. *Langmuir* **2001**, *17*, 8249; d) Gole, A.; Thakar, J.; Sastry, M. *Langmuir* communicated.

# CHAPTER VI

## FORMATION OF PROTEIN- GOLD COLLOID BIOCONJUGATES



This chapter demonstrates the formation of bioconjugates of enzymes with colloidal gold particles. The bioconjugates were formed by simple mixing of enzymes F-prot and endoglucanase with colloidal gold solution, centrifuged to remove uncoordinated enzyme molecules, and resuspended into appropriate buffers. The bioconjugates so formed were characterized by UV-Vis, TEM, SEM and XRD. The intactness of the natural conformation of the enzyme in the bioconjugates was confirmed by FTIR, fluorescence and biological activity measurements. The stability of the endoglucanase-colloidal gold was found to be enhanced relative to free enzyme in solution. The colloidal gold particles were stabilized against aggregation by enzyme molecules and in turn colloidal gold particles stabilize the enzyme molecules against denaturation.

The work presented in this chapter has been published: 1) Gole, A.; Dash, C.; Soman, C.; Sainkar, S. R.; Rao, M.; Sastry, M. *Bioconjugate Chemistry*, **2001**, *12*, 684; 2) Gole, A.; Vyas, S.; Phadtare, S.; Lachke, A.; Sastry, M. *Coll.Surf.B.*, In press.

## 6.1 INTRODUCTION.

The previous chapters (chapter III, IV and V) discussed the formation of biocomposites of proteins/enzymes with lipid films via immobilization onto 2-D surfaces. In this chapter, we discuss the formation of bioconjugates with colloidal gold nanoparticles, wherein the immobilization of enzymes such as fungal protease (F-prot) and endoglucanase onto 3-D curved surfaces (colloidal gold particles) has been demonstrated.

The utility of nanoscale curved surfaces such as those provided by colloidal particles in immobilizing biomolecules for immunoassays has been recognized in the early 1980's.<sup>1</sup> Rembaum, *et al*<sup>1</sup> demonstrated the formation of immunospheres which they defined as specially designed microscopic particles that have antibodies or similar molecules chemically bound to their surfaces. The antibody-coated microspheres react in a highly specific way with target cells, viruses, or other antigenic agents. The use of colloidal particles as templates for biomolecule immobilization has a unique advantage that the individual and combined properties of the biomolecules and the template can be exploited for technological and biomedical applications. Furthermore, the high surface-to-volume ratio offered by colloidal particles result in the concentration of the immobilized entity being considerably higher than that afforded by protocols based on immobilization on planar, 2-D surfaces, resulting in enhanced detection signals. Antibodies bound to highly fluorescent microspheres can serve as fluorescent markers to detect specific cells when bound to antigens on the cell surfaces and examined with a fluorescent microscope. The variation in mobility of cells tagged to microspheres as opposed to free cells could be used for electrophoretic cell separation procedures.

The two main types of colloidal particles that can be used for biomolecule immobilization are polymer and inorganic particles, each template having its own advantage.

## 6.2. IMMOBILIZATION OF BIOMOLECULES ONTO POLYMER MICROSPHERES.

One of the main advantage of using polymer microspheres is the ability to produce monodisperse particles (as good as  $\pm 1.5\%$  standard deviation to the average particle diameter) with variable sizes (mean diameter of a few nanometers to a few microns). Furthermore the surface functionality (hydrophobicity/ hydrophilicity/ addition of different functional groups on the surface) can also be easily varied depending on the synthetic conditions used.<sup>1</sup> This also helps

in varying the nature of interaction of the immobilizing biomolecule and the colloidal template. Rembaum *et al*,<sup>1</sup> first gave a complete report on use of polymer microspheres for different applications and found that hydrophilic surface character is one of the essential parameter for successful immobilization of biomolecules. Since then, a number of groups have worked on single and multiple protein/enzyme/DNA immobilization onto colloidal particles. Schmitt *et al*.<sup>2a</sup> reported on the formation of a monomolecular layer of bovine serum albumin (BSA) on the surface of polystyrene (PS) latex particles while Elgersma *et al* have demonstrated the adsorption of BSA on positively and negatively charged polystyrene lattices.<sup>2b</sup> Kamyshny *et al*<sup>2c</sup> studied the adsorption of native and hydrophobically modified IgGs on hydrophobic PS latex beads. They reported that under conditions where both the latex particles and IgG molecules are negatively charged, the IgG had a high affinity for the particle surface. This affinity increased with increasing hydrophobicity of the IgG molecules, leading to the conclusion that the main driving force for IgG adsorption on PS beads is hydrophobic binding.<sup>2c</sup> Peula *et al*<sup>2d</sup> have studied the adsorption of monomeric BSA (m-BSA) on sulfonated PS model colloids as a function of pH and ionic strength. Maximum protein loading occurs near the protein isoelectric point, the protein loading depending on surface charge density of the colloids. They also observe the significance of hydrophobic interactions with contributions from electrostatic interactions. One of the major requirements of bioconjugates is its stability against aggregation at physiological pH. Peula, *et al*<sup>2e</sup> have studied the colloidal stability of sulfonated PS latex particles covered by monomeric (m-BSA) and oligomeric BSA (o-BSA) as a function of pH and solution ionic strength. Zeta potential measurements of the protein coated particles of m-BSA showed high stability at pH 7 (protein is highly negatively charged) as opposed to pH 5 (zero charge on the protein). In spite of the fact that o-BSA is unionized at pH 5, steric stabilization prevented colloidal aggregation. Derjaguin-Landau-Verwey-Overbeek (DLVO) theory predicts a loss in colloidal stability as a function of increase in salt concentration. On the contrary, an anomalous stability of protein stabilized colloidal particles is found with increased salt concentrations.<sup>2f</sup> Molina-Bolivar *et al*<sup>2f</sup> attribute this "non-DLVO" stability to hydration forces responsible between hydrophilic systems. They demonstrate this with the help of different proteins (IgG, fibrinogen, myoglobin and serum albumin) adsorbed onto chloromethylstyrene

(CMS) latex particles. They also studied the orientation of adsorbed proteins onto colloidal particle surface as a function of pH.<sup>2f</sup>

A new method for immobilization of biomolecules onto polymer colloids has been demonstrated by Caruso and coworkers using the layer-by-layer (LBL) protocol. After the introduction of the LBL protocol by Decher<sup>3a</sup> in 1991, it has been successfully extended towards the assembly of polyelectrolytes,<sup>3a,b</sup> inorganic particles<sup>3c,d</sup> and biomolecules<sup>3e,f</sup> onto 2-D planar surfaces. Caruso and coworkers have successfully extended the L-B-L technique to the assembly of protein/enzyme layers on polystyrene (PS) latex particles (3-D surfaces).<sup>3g-k</sup> They also showed the immobilization of multiple enzymes by alternating layers of polyelectrolytes for sequential catalysis. A decrease of biological activity with insertion of spacer polyelectrolytes was found which they attribute to the obstruction of active site of the biocatalyst. Colloids precoated with Fe<sub>3</sub>O<sub>4</sub> nanoparticles and polyelectrolyte layers along with enzyme layer was useful in separation of the biocolloids after reaction using a magnet.

### 6.3 IMMOBILIZATION OF BIOMOLECULES ONTO INORGANIC PARTICLES

Colloidal metal particles such as nanosized gold have been a topic of interest dating back to the Roman times.<sup>4</sup> Their unusual optoelectronic properties were utilized to create complex optical effects to impart colors in glasses. This prompted Faraday to investigate into the colors of colloidal gold in the mid-nineteenth century. He found that these lyophobic (liquid hating) sols if stabilized kinetically can exist for many years. In fact, some of the colloidal systems Faraday prepared are still on display in the British Museum in London.<sup>4</sup> Since then, a number of scientists working in this area have studied in great detail various properties of metal and semiconductor colloidal nanoparticles. The study led to the observation that when the size of crystallite approaches (or becomes less than) the bulk exciton diameter (in the case of semiconductors) or the electron mean free path (in case of noble metals), novel size dependent properties become prominent.<sup>5</sup> These novel properties led to an explosion in research for possible applications of these nanoparticles in various areas such as optoelectronics and magnetic devices,<sup>6</sup> catalysis<sup>7</sup> and sensors.<sup>6</sup> These unusual properties and surface sensitivity of inorganic particles make them efficient templates for the immobilization of biomolecules such as proteins, enzymes, antigen/antibody and DNA. Any modification to the nanoparticle surface is

manifested in the change in its optical properties and hence forms an efficient and simple methodology for antibody/antigen or DNA mismatch detection. Recently Niemeyer has given a detailed report and advances in the area of nanobiotechnology (the combined area of nano and biotechnology).<sup>8</sup>

The conjugation of biomolecules to nanoparticles can be achieved by a number of ways.<sup>8</sup> Typically, wet-chemical preparation of the nanoparticles is carried out in the presence of stabilizing agents (often citrate, phosphanes, or thiols) which bind to the surface atoms of the nanoparticles, and stabilize them against aggregation. Biomolecules can be linked directly with the metal particles by exchange reactions with stronger binding ligands. This method is usually applied in coating colloidal gold with thiol-containing proteins such as IgG, serum albumins or proteins with cysteine residues on the surface. Colloidal gold labeled antibody has been used for the detection of antigens in solution by electrochemical metalloimmunoassay system<sup>9a</sup> and also by surface plasmon resonance (SPR) immunosensing<sup>9b</sup> wherein covalent interactions between the antibody and the colloidal gold particles is used for immobilization. From a fundamental point of view, studies on protein-nanoparticle interactions also throw light on the orientation of the protein and the involvement of amino acid residue in its binding to nanoparticles. In this direction, Natan and co-workers have studied in a great detail the binding of Cytochrome *c* to colloidal gold particles which they show to occur via lysine rich pockets of the protein.<sup>9c</sup> From a spectroscopy point of view, roughened gold or silver surfaces exhibit vibrational spectral intensities that are enhanced 1,00,000 fold. This fact is known as surface-enhanced Raman scattering (SERS). Natan *et al* demonstrate that cytochrome *c* sandwiched between colloidal gold and silver leads to SERS of these metal particles.<sup>9d</sup> In an interesting recent report, single molecule spectroscopy (SMS) of hemoglobin molecules adsorbed on 100 nm sized citrate-reduced silver colloidal particles using SERS has been reported.<sup>9e</sup> In the area of metal nanoparticle-enzyme conjugate materials, Crumbliss, Stonehuerner and co-workers have studied the formation and enzymatic activity of gold nanoparticles complexed with horseradish peroxidase,<sup>9f</sup> xanthine oxidase<sup>9g</sup> as well as glucose oxidase and carbonic anhydrase molecules.<sup>9h</sup> A salient feature of their work is the demonstration that enzyme molecules are bound tightly to gold colloidal particles and retain significant biocatalytic activity in

the conjugated form while the enzyme molecules denature on adsorption to planar surfaces of gold.<sup>9h</sup> In this direction, we have reported the conjugation of pepsin, fungal protease and endoglucanase enzymes with colloidal gold particles, with excellent stability and biological activity of the immobilized enzymes.<sup>10</sup>

Bio labeling is another key area where metal/semiconductor nanoparticle-biomolecule bioconjugates have been used for a long time. They are used as markers in electron microscopic studies via biospecific or site specific labeling of distinguished regions of tissue samples or biomolecules.<sup>11a,b</sup> These labels have advantages of better resolution, stability, uniformity, better penetration and a more quantitative labeling of antigenic sites.<sup>11a,b</sup> Semiconductor nanoparticles are also powerful fluorescent probes, which can be used for the labeling of biological components.<sup>11c-f</sup> The quantum dots have several advantages over conventional fluorescent dyes. Their fluorescence absorption and emission are conveniently tunable by their size and material composition, and the emission peaks have a narrow spectral linewidth (~ 20-30 nm). Quantum dots are about 100 times more stable against photobleaching and reveal a long fluorescence lifetime of several hundred nanoseconds, thus allowing time-delayed fluorescence measurements.<sup>11c-f</sup>

The conjugation of DNA with gold nanoparticles has been recently introduced by the groups of Alivisatos<sup>12a</sup> and Mirkin<sup>12b,c</sup> who demonstrated that superstructures of these bioconjugates could be formed by hybridization of complementary base sequences in the gold surface-bound DNA molecules. From a fundamental point of view, Mirkin *et al* have used this strategy to critically study the role of inter-particle separation and aggregate size on the optical properties of DNA-modified colloidal gold solution.<sup>12d</sup> This strategy can be used for simple and economically viable sensors in biomedical diagnostics, for example, for the detection of nucleic acids from pathogenic organisms. In fact, several analytical applications that allow the detection of nucleic acids in homogenous solutions have already been reported.<sup>12e-i</sup> Sastry *et al* have used electrostatic interactions between the negatively charged phosphate backbone of the DNA and positively charged lysine modified colloidal gold particles to form bioconjugates. Nanowire like structures were shown to form by the simple mixing or drop drying protocol used.<sup>12j,k</sup> Recently Willner *et al* reported the use of DNA-functionalized CdS nanoparticles for



photoelectrochemical detection of nucleic acid hybridization.<sup>12l</sup> In a very recent report, *insitu* reduction of chloroauric acid by silk fibroin protein to yield efficient gold colloid-protein bioconjugates has been demonstrated.<sup>12m</sup>

The enormous activity in this area clearly indicates the immense potential towards fundamental, biomedical and industrial applications of these biomolecule coated inorganic particles. As mentioned earlier, we have focussed our work in the formation, characterization and biological activity of enzyme coated colloidal gold particles.<sup>10</sup> Simple mixing of the colloidal gold and enzyme solutions under protein friendly conditions (pH 3) followed by centrifugation (to remove un-coordinated gold nanoparticles and protein molecules) results in the formation of the enzyme: gold colloid bioconjugates. The advantages of our protocol are the ease of bioconjugate synthesis avoiding enzyme modification and presence of enzyme-friendly conditions. This chapter discusses the formation of bioconjugates with colloidal gold particles (synthesized by borohydride reduction of chloroauric acid) using two industrially important enzymes such as fungal protease (F-prot) and endoglucanase.

#### 6.4 SYNTHESIS OF BIOCONJUGATES

**Colloidal gold synthesis.** The gold salt (chloroauric acid;  $\text{HauCl}_4$ ) was reduced to form gold colloids by the method of Vukovic and Nedeljkovic<sup>13a,b</sup> used for synthesis of silver colloids. Typically, a 100 ml of  $10^{-4}$  M concentrated aqueous solutions of chloroauric acid was reacted with 0.01 g of sodium borohydride at room temperature with vigorous stirring. The standard characterization of the gold sols has been done in earlier work by Sastry *et al.*<sup>13b</sup> The ruby red colored gold sol gives a peak at 514 nm in the visible region of the electromagnetic spectrum, which is a characteristic of gold colloidal particles arising due to the surface plasmon resonance, and is well documented by the Mie theory.<sup>13c-f</sup> The Transmission electron microscopy (TEM) analysis of the gold colloidal particles has been performed in the previous studies.<sup>13b</sup> The analysis gave a mean cluster diameter of 34 Å with a standard deviation of 7 Å.<sup>13b</sup>

**Formation of bioconjugates.** A  $10^{-6}$  M standard solution of the enzyme, F-prot (M.W ~ 37000, pI ~9.5) and endoglucanase (M.W ~ 50,000, pI ~ 4.1) was prepared in buffer solutions. The choice of the pH of the enzyme solutions and bioconjugates was adjusted keeping in mind the optimum conditions required for the enzymes where it would be stable and would give maximum

biological activity. Hence, F-prot was prepared at pH 3 (0.05 M, glycine – HCl buffer) and endoglucanase at pH 5 (0.05 M citrate buffer).<sup>10a-c</sup> Different amounts of these standard solutions were added to colloidal gold to yield an enzyme concentration of  $10^{-7}$ ,  $10^{-8}$  and  $10^{-9}$  M in the conjugate solution. The solutions were stored for a period of 12-18 h at 4 °C and then centrifuged to remove uncoordinated enzyme molecules in solution. Centrifugation was done on a Du Pont Sorvali RC-5B superspeed centrifuge instrument with a cooling facility at 6000 r.p.m, 4°C. The pellet so obtained was rinsed several times with buffer solutions, centrifuged once again to remove free uncoordinated enzyme molecules (if any) and then re-suspended in appropriate buffer solutions (pH 3 for F-prot-Au and pH 5 for endoglucanase-Au bioconjugates) and stored at 4 °C for further experimentation. In the case of endoglucanase-Au bioconjugates, initial experiments indicated a considerable loss in the amount of bioconjugate material during centrifugation. In order to overcome this loss, 0.07 % NaCl was added to the colloidal gold along with the enzyme. This improves the quality and quantity of the enzyme pellet formed upon centrifugation and the losses are considerably reduced.

### 6.5 UV-Vis SPECTROSCOPY STUDIES.

UV-vis spectroscopy is a powerful tool to analyze the formation of bioconjugates due to the presence of distinct features of colloidal gold (visible region) and the enzyme (UV region). The absorbance band above 500 nm arising from excitation of the surface plasmon resonance in the gold particles<sup>13b-f</sup> and the resonance at 280 nm due to the  $\pi$ - $\pi^*$  transition in the tryptophan and tyrosine residues of the enzyme<sup>14</sup> were monitored immediately after addition of enzyme molecules to gold solution as well as after centrifugation/re-suspension. Three separate sets of solutions were prepared and tested for UV-Vis signatures in order to check the reproducibility of the data. The spectrophotometer used was a Shimadzu dual-beam spectrophotometer (model UV-1601 PC) operated at a resolution of 1 nm.

Fig.6.5.1A shows the UV-vis spectra recorded from the gold colloidal solution before (curve 1) and after (curve 2) addition of the F-prot solution (overall F-prot concentration in the solution =  $10^{-7}$  M). The spectra have been displaced vertically for clarity. The surface plasmon resonance due to gold can be clearly seen at about 514 nm<sup>13b-f</sup> for the as-prepared gold solution (curve 1, Fig. 6.5.1A). On addition of F-prot, a broadening and red shift of the plasmon

resonance is seen (curve 2, Fig. 6.5.1A) and clearly indicates surface coordination of F-prot with the gold particles. The broadening of the plasmon resonance is also indicative of some degree of aggregation of the gold particles mediated by the enzyme molecules. The absorbance at about 280 nm seen prominently in the F-prot : Au solution (curve 2, Fig. 6.5.1A) is due to the  $\pi$ - $\pi^*$  transitions arising from the tryptophan and tyrosine residues on the enzyme surface.<sup>14</sup> UV-Vis spectra corresponding to F-Prot-colloidal gold bioconjugates after centrifugation/resuspension for the three different concentrations of F-prot in the solution are shown in Fig. 6.5.1B. It is observed that both the surface plasmon resonance intensity from the gold particles as well as the concentration of F-prot molecules in the resuspended solution (as evidenced by the intensity of the absorption at 280 nm) scale with the concentration of F-prot molecules in the starting solution (i.e., the solution prepared prior to centrifugation). Thus, a larger number of gold particles are required to stabilize a greater concentration of F-prot molecules in solution and provides a simple recipe for increasing the loading factor of the enzyme molecules in the bioconjugate material. The magnitude of absorbance, for example, in the case of  $10^{-7}$  M F-prot concentration in colloidal gold bio-conjugate material, at 280 nm before centrifugation reduces considerably after centrifugation and resuspension. This is also true for other concentrations and the large decrease in intensity of this band indicates removal of un-coordinated F-prot from the respective solutions. Fig. 6.5.1 C shows the UV-vis spectra of as-prepared colloidal gold solution (curve 1), endoglucanase : colloidal gold bioconjugate immediately after addition of the enzyme and 0.07 % NaCl at pH 5 (curve 2) and after centrifugation and resuspension of the bioconjugate in pH 5 buffer solution (curve 3). The surface plasmon band due to colloidal gold, and the  $\pi$ - $\pi^*$  transition band due to the enzyme can be clearly seen. After centrifugation-resuspension of the bioconjugate solution, the intensity of the plasmon band decreases due to some loss in the gold colloids (curve 3). The intensity of  $\pi$ - $\pi^*$  band at 280 nm diminishes indicating removal of excess uncoordinated enzyme molecules in solution (curve 3).

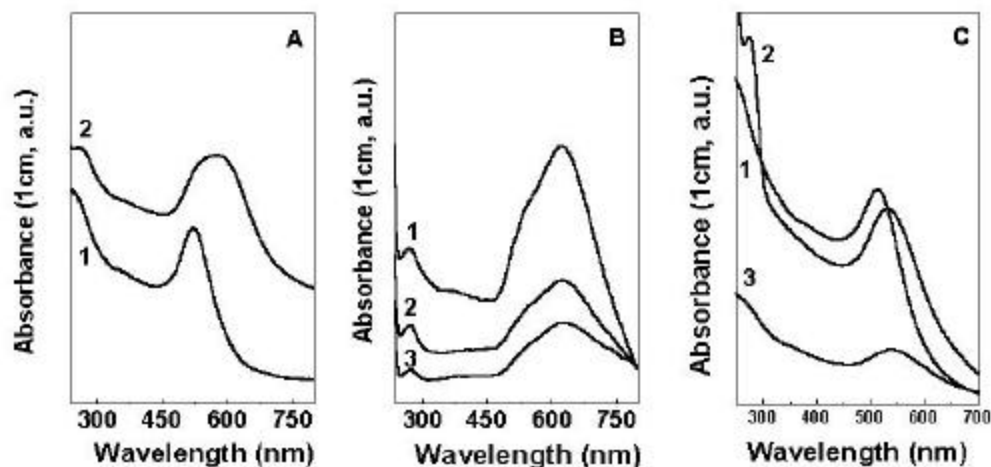


**Figure. 6.5.1:** A) UV-vis spectra of the F-prot-colloidal gold bioconjugate solution immediately after addition of  $10^{-6}$  M F-prot in the colloidal gold solution at pH = 3 to give equilibrium concentration of  $10^{-7}$  M of F-prot (curve 2) and the gold solution before addition of F-prot. B) UV-vis spectra of F-prot-colloidal gold bioconjugate solution after centrifugation, rinsing and re-suspension in pH = 3 buffer. The spectra corresponding to concentrations of F-prot in the starting bioconjugate solutions are : curve 1 -  $10^{-7}$  M; curve 2 -  $10^{-8}$  M and curve 3 -  $10^{-9}$  M. C) UV-vis spectra of the as-prepared colloidal gold solution (curve 1), *endoglucanase* : colloidal Au bioconjugate solutions immediately after addition of *endoglucanase* to colloidal gold at pH 5 (curve 2) and the bioconjugate in buffer solution after centrifugation and re-suspension (curve 3, see text for details) .

## 6.6 MORPHOLOGY OF THE BIOCONJUGATES

To study the overall nature and morphology of the bioconjugates, a drop of F-prot-colloidal gold bioconjugate on Si (111) substrate was dried and studied by Scanning electron microscopy (SEM) measurements as shown in Figs. 6.6.1 A and B. The instrument used was a Leica Stereoscan-440 scanning electron microscope equipped with a Phoenix EDAX attachment. A number of agglomerates can be seen in the images and may be due to enzyme induced cross-linking of the colloidal gold particles. Fig. 6.6.1 B gives a magnified view of one of the aggregates. On careful observation, it is seen that the aggregate is made up of dark and bright spots. EDAX spot measurements were performed and the dark regions were found deficient in gold particles (but enhanced in protein concentration as evidenced by a large nitrogen signal) while the bright regions were rich in gold particles. Thus, the SEM images indicate aggregates within the F-prot : gold colloid conjugate material with spatially separated regions of gold particles and the protein molecules. We would like to add here that a similar surface morphology was observed by Caruso *et al* in multilayer films of polymer-anti-IgG composite material.<sup>15</sup>

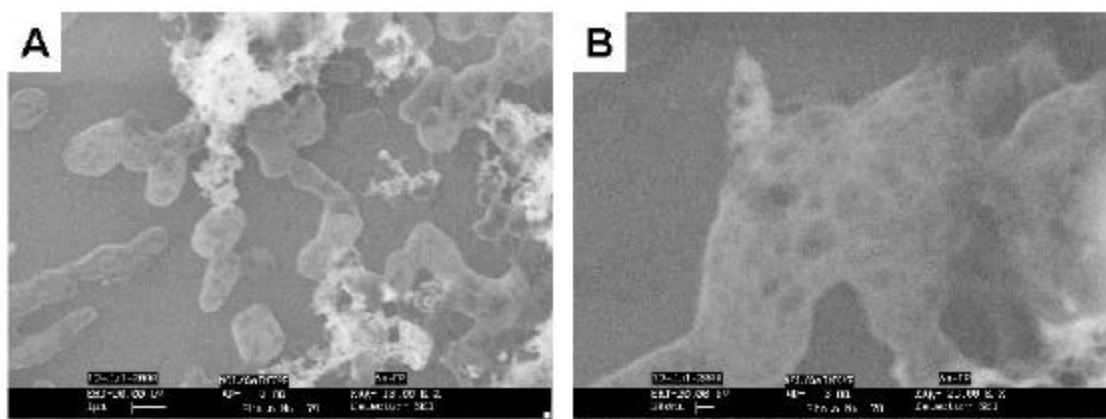


**Figure. 6.6.1:** A) SEM image of a film of the F-prot : colloidal gold bioconjugate material drop-dried on a Si (111) substrate (see text for details). B) SEM image of a magnified aggregate of bio-conjugate material (see text for details).

### 6.7 DETERMINATION OF SIZE OF COLLOIDAL GOLD IN THE BIOCONJUGATE SYSTEM

The size of colloidal gold in the bioconjugate system was determined by Transmission electron microscopy (TEM) for the endoglucanase-colloidal gold system and by X-ray diffraction (XRD) for the F-prot-colloidal gold system. TEM measurements were performed on a JEOL Model 1200EX instrument operated at an accelerating voltage of 120 kV. Samples for TEM were prepared by placing a drop of centrifuged/resuspended endoglucanase : colloidal gold solution on a carbon-coated TEM copper grid. The film was allowed to dry for 1 min and the extra solution was removed using a blotting paper. TEM measurements of F-prot: colloidal gold system was tried, but the particles aggregate due to electron beam heating. This indicates that endoglucanase: colloidal gold is a much stable system than F-prot: colloidal gold. This might be possible due to the pH conditions used (pH ~ 3 for F-prot and pH ~ 5 for endoglucanase), which is responsible for a better stability of colloidal gold. This led us to use an indirect method, such as XRD, for particle size estimation for F-prot:colloidal gold system. A few drops of the centrifuged/re-suspended F-prot-colloidal gold bioconjugate solution were placed on 2 x 2 cm Si (111) substrates and dried in air. XRD measurements of these films were made on a Philips PW 1830 instrument operating at 40 kV voltage and a current of 30 mA with Cu  $K_{\alpha}$  radiation. The size of the colloidal gold was estimated using the peak width of the (111) gold peak using the Debye-Scherrer formula.<sup>16</sup>

Fig. 6.7.1A shows the TEM micrograph of endoglucanase : colloidal gold bioconjugate system formed on a carbon-coated copper grid. At higher magnification, the film was observed to melt under the electron beam, due to possible electron-induced degradation of the enzyme molecules in the film. It is observed from Fig.6.7.1A that the gold particles are ordered without the particles being in direct contact as is normally observed in TEM images of un-protected gold colloids. Furthermore, the separation between the particles appears to be fairly uniform indicating the presence of stabilizing endoglucanase molecules between the gold particles.

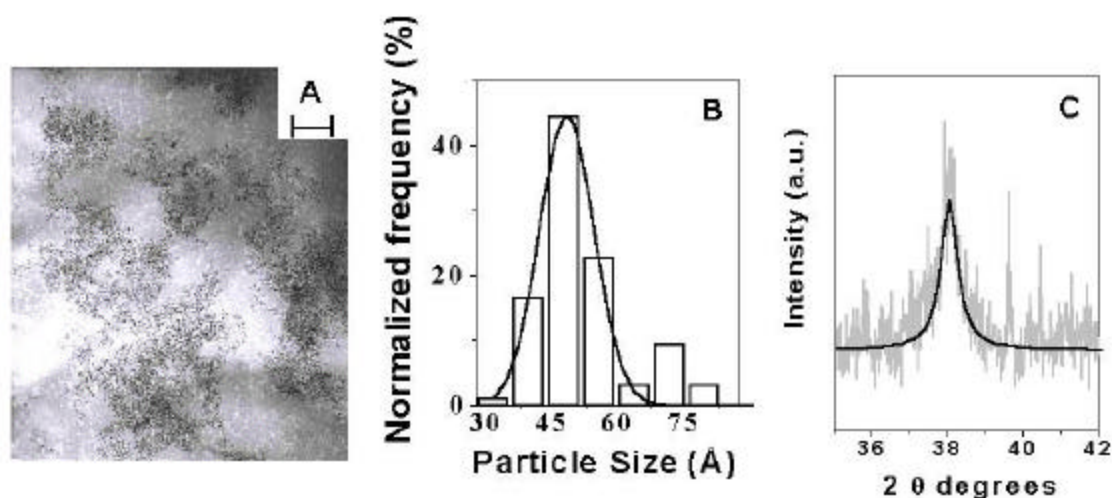


**Figure. 6.7.1:** A) TEM micrograph of a drop-dried *endoglucanase* : colloidal Au bioconjugate film on a carbon-coated copper TEM grid (see text for details). The scale bar corresponds to 100 nm. B) Particle size distribution histogram estimated from the micrograph shown in Fig.1B. The solid line is a Gaussian fit to the data and yields a gold particle size of  $49 \text{ \AA} \pm 6 \text{ \AA}$ . C) XRD pattern of a film of the F-prot : colloidal gold solution on a Si (111) wafer prepared by a simple drop-drying method (see text for details). The solid line is a Lorentzian fit to the spectra. The size of the gold particles has been determined from the line-broadening to be  $250 \text{ \AA}$ .

Thus, the gold particles stabilize the ensemble of enzyme molecules while preventing their aggregation. This is important in retaining the biological activity of the enzymes and is of concern in enzyme immobilization protocols. Fig. 6.7.1B is a plot of the particle size distribution of the TEM image shown in Fig. 6.7.1A and shows a mean particle diameter of  $49 \text{ \AA}$  with a standard deviation of  $6 \text{ \AA}$ . This result is in fairly good agreement with the expected size of the as-prepared colloidal gold of  $35 \pm 7 \text{ \AA}$ .<sup>13b</sup>

Fig. 6.7.1C shows the XRD pattern of a film of F-prot: colloidal bioconjugate formed by drop drying on a Si (111) substrate. As can be seen, the Au (111) peak occurs at a  $2\theta$  value of  $38.2$  degrees. After fitting the curve to a Lorentzian, the size of the colloidal gold was calculated

from the line-broadening<sup>16</sup> to be 250 Å. The size of as-prepared colloidal gold particles is about 35 Å but on forming a bioconjugate with F-prot molecules, the size increases indicating a small amount of aggregation of the particles. But since the bioconjugates are well dispersed in solution for a long period and furthermore, the fact that the enzyme on the surface of the colloidal gold particles is active (as explained subsequently by the biocatalytic activity measurements), enzyme aggregation may be ruled out.

## 6.8 NATIVE CONFORMATION OF THE ENZYME IN BIOCONJUGATE SYSTEMS.

**Secondary structure studies.** Fourier transform infrared spectroscopy (FTIR) was used to study the secondary structure of the enzyme in the bioconjugate. The instrument used was a Shimadzu FTIR-8201 PC instrument operated in the diffuse reflectance mode at a resolution of 4 cm<sup>-1</sup> with 256 scans. Figs. 6.8.1A and B show the FTIR spectra of the drop dried [on Si (111) substrate] pure endoglucanase film (curve 1) and that of the endoglucanase: colloidal gold bioconjugate system (curve 2) in the spectral window 3500 – 2200 cm<sup>-1</sup> and 1750 – 1200 cm<sup>-1</sup> respectively. A number of features can be seen in both the curves. The feature at ca 3216 cm<sup>-1</sup> in curve 1 (feature a, Fig. 6.8.1A) arises from the free amine groups (N-H stretching vibration mode) in the endoglucanase molecules. This band shifts and appears as a broad shoulder at ca 3000 cm<sup>-1</sup> in the endoglucanase: colloidal gold system (curve 2, Fig. 6.8.1A). This shift in the band can be attributed to the binding of amine groups on the enzyme surface to colloidal gold. The methylene antisymmetric and symmetric vibrations at 2916 cm<sup>-1</sup> and 2850 cm<sup>-1</sup> arising in the enzyme molecules can be seen in curve 1 (Fig. 6.8.1A). These bands cannot be clearly seen in the bioconjugate system (curve 2, Fig. 6.8.1A) due to the broad shoulder at 3000 cm<sup>-1</sup>. Another feature at about 2520 cm<sup>-1</sup> can be clearly seen in the bioconjugate system (feature b, curve 2, Fig. 6.8.1A) and is tentatively assigned to the –SH stretch vibration bands in the cysteine residues in the enzyme.<sup>17</sup> The point to be noted is the fact that this band is absent in the pure enzyme. This can be explained as follows. As mentioned earlier, endoglucanase has 18 cysteine residues which all form disulfide linkages to stabilize the substrate binding site.<sup>18</sup> It is well known that under reducing conditions the S-S bond breaks to form –SH bonds.<sup>19</sup> We believe that in our case the excess borohydride present in the colloidal gold solution may reduce the S-S bond to form –SH bonds. This would result in changes to the natural conformation of

the enzyme. However (as will be discussed subsequently), the enzyme in the bioconjugate shows biological activity comparable to that of the free enzyme in solution and indicates the intactness of the tertiary structure of the enzyme.

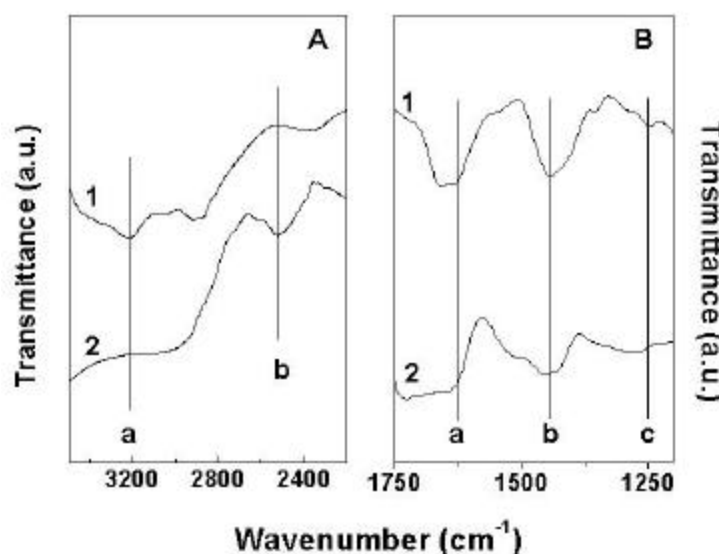


**Figure 6.8.1:** A) FTIR spectra recorded from a drop-dried *endoglucanase* film (curve 1) and *endoglucanase* : colloidal Au bioconjugate film on a Si (111) substrate (curve 2) in the 3500 to 2200  $\text{cm}^{-1}$  spectral region (see text for assignments). B) FTIR spectra recorded from a drop-dried *endoglucanase* film (curve 1) and *endoglucanase* : colloidal Au bioconjugate film on Si (111) substrate (curve 2) in the range 1750  $\text{cm}^{-1}$  to 1200  $\text{cm}^{-1}$ . (See text for details and assignments).

The spectral window 1750 - 1200  $\text{cm}^{-1}$  (Fig. 6.8.1B) provides information about the amide bands, which are sensitive to the secondary structure of the enzyme. The bands at 1650  $\text{cm}^{-1}$  and 1240  $\text{cm}^{-1}$  in the drop-dried enzyme film (curve 1, Fig. 6.8.1B) are assigned to the amide I and III bands respectively. The amide I band originates from the C=O stretching vibrations of the peptide bonds<sup>20</sup> and amide III band arises from the C-N stretching modes of the polypeptide chains.<sup>20b</sup> The amide I band in the bioconjugate system (feature a, curve 2, Fig. 6.8.1B) shows some amount of broadening indicating structural changes in the enzyme due to bioconjugate formation. The amide III band in the bioconjugate system (feature c, curve 2, Fig. 6.8.1B) shows a small shift to lower wavenumbers along with some amount of broadening. This also might be due to coordination of enzyme molecules with gold particles. A broad feature at about 1440  $\text{cm}^{-1}$  in the enzyme (feature b, curves 1 and 2, Fig. 6.8.1B), is assigned to a combination of symmetric stretching modes of carboxylate groups and the methylene scissoring



band. This band coincides with that observed by Caruso *et al* for immobilization of IgG<sup>21a</sup> on PSD spheres and Roddick-Lanzilotta *et al* for the adsorption of lysine onto TiO<sub>2</sub> films.<sup>21b</sup>

FTIR analysis of F-prot: colloidal gold bioconjugates was also tried, but failed to show good amide bands possibly due to denaturation during drying of the samples. Hence Fluorescence spectroscopy was used to confirm the intactness of the natural conformation of this enzyme.

**Tertiary Structural studies.** The biocatalytic activity of the immobilized enzyme would, to a large extent, depend on the tertiary structure of the enzyme remaining unperturbed on the surface of colloidal gold. The tertiary structure of an enzyme can be checked by fluorescence measurements by exciting the sample at a particular wavelength (280 nm for tryptophan and tyrosine residues) and monitoring the fluorescence emission spectra between 300-500 nm.<sup>22</sup> The fluorescence of the bioconjugate solutions was studied using a Perkin Elmer Luminescence Spectrometer (model LS 50B). Fluorescence spectra of bare colloidal gold and that of buffer used were also recorded as control experiments. As expected these controls did not show any emission in the region of interest at about 336 nm. Fig. 6.8.2 A shows the fluorescence spectra recorded from solutions of 10<sup>-6</sup> M and 10<sup>-7</sup> M concentration F-prot at pH 3 (curves 1 and 3) as well as the fluorescence spectrum measured from the F-prot: colloidal gold bioconjugate solution prepared from the 10<sup>-6</sup> M F-prot starting solution (curve 2). The intensity of absorbance maxima in all three solutions occurs at about 336 nm, which indicates that the F-prot molecules in the bioconjugate solution are present in its natural configuration maintaining its tertiary structure. Therefore, even though aggregates were seen in the SEM images and inferred from the size of the gold particles estimated from XRD, fluorescence measurements clearly shown that the enzyme molecules in the aggregates maintain their tertiary structure. Control experiments in which fluorescence emission from glycine – HCl (0.05 M, pH 3) buffer at about 336 nm was monitored by excitation at 280 nm and as seen from curve 4, has no significant emission as compared to that of F-prot in solution or in the bioconjugate material. Also the fluorescence emission from bare colloidal gold solution was monitored (curve 5). The control experiments indicate that the emission takes place only from the enzyme solutions in the bioconjugate material.

Fig.6.8.2B shows the fluorescence spectrum of  $10^{-9}$  M concentrated free enzyme molecules in buffer solutions (curve 1; pH 5, 0.05 M citrate buffer). The sample was excited at 295 nm, and the emission was monitored in the range 300 to 500 nm. A broad band at 340 nm is observed and indicates intactness of the tertiary structure of endoglucanase in solution. Curve 2 shows the fluorescence spectrum of the endoglucanase: colloidal gold bioconjugate system recorded under similar excitation conditions. The nature of the curve and peak positions is quite similar to the free enzyme in solution indicating intactness of the tertiary structure of the enzyme after bioconjugate formation. Hence, via fluorescence spectroscopy of the bioconjugates one can conclude that the tertiary structure of the enzymes conjugated to colloidal gold is intact, and any changes are minimal.

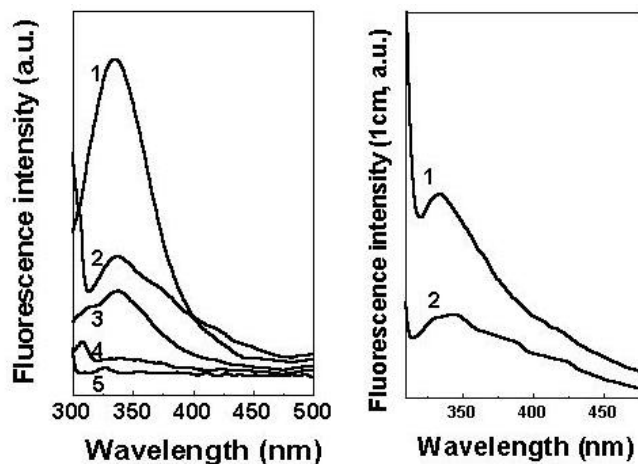


**Figure. 6.8.2:** A) Fluorescence spectra of F-prot solution at a concentration of  $10^{-6}$  M at pH 3 (curve 1), F-prot : colloidal gold bioconjugate solution at pH 3 (curve 2) prepared from the  $10^{-6}$  M concentration starting F-prot solution and F-prot solution at a concentration of  $10^{-7}$  M at pH=3 (curve 3). An estimate of the F-prot concentration in the bioconjugate solution may be made from these curves (see text for details). Control experiments wherein fluorescence spectra from glycine – HCl (0.05 M, pH 3) buffer (curve 4), and fluorescence spectra from bare gold colloidal particles (curve 5). (see text for details). B) Fluorescence spectra of  $10^{-9}$  M *endoglucanase* solution in buffer at pH 5 (curve 1) and *endoglucanase* : colloidal Au bioconjugate solution in buffer at pH 5 (curve 2).

Fluorescence spectroscopy was also used to quantify the amount of enzyme on the colloidal gold surface in the bioconjugate solution. In the case of F-prot: colloidal gold bioconjugates, a calibration curve was obtained by plotting the fluorescence intensities of different concentrations of F-prot at pH 3. The concentration of F-prot in the F-prot: colloidal gold bioconjugate system was calculated to be  $3.7 \times 10^{-7}$  M and is an important number in the estimation of the specific activity of the bioconjugate solution. However, in the case of *endoglucanase*: colloidal gold, a significant amount of fluorescence quenching of the tryptophan

residues in the enzyme was observed after bioconjugate formation. Hence, we have used an indirect method to calculate the amount of enzyme for this system. The fluorescence emission from the supernatant obtained after centrifugation and separation of the bioconjugates was compared with two different concentrations of free enzyme in buffer solutions. Knowing the initial concentration of enzyme added to the colloidal gold solution and subtracting the concentration of enzyme molecules in supernatant, we calculated the amount of enzyme in the bioconjugate to be 130  $\mu\text{g}/\text{mL}$ . Lowry's method<sup>23</sup> was also used for the estimation of amount of enzyme present in the bioconjugate material and was found to be 100  $\mu\text{g}/\text{mL}$ . This compares favorably with the amount of enzyme estimated via fluorescence measurements.

## 6.9 BIOCATALYTIC ACTIVITY MEASUREMENTS

The most important aspect in enzyme: colloid bioconjugate systems is the retention of the biocatalytic activity after adsorption onto the nanoparticle surface. This is of vital importance because of the ultimate application potential of such protein-coated particles in areas of medical diagnosis and drug delivery.

**F-prot: colloidal gold bioconjugate system.** The biocatalytic activity of the centrifuged/re-suspended F-prot-colloidal gold bioconjugate solution was determined by reaction with a solution of hemoglobin (Hb; 5 mg/ml) prepared in glycine-HCl buffer at pH 3. Since F-prot is a proteolytic enzyme that acts on proteins, proteins such as Hb are generally used for biocatalytic activity. In a typical experiment to estimate the biocatalytic activity of the bioconjugate solution, 1 mL of the solution consisting of 100  $\mu\text{L}$  of the F-prot: colloidal gold bioconjugate material and 0.9 mL of the buffer, was reacted with 1 mL of the Hb solution and the reaction mixture was incubated at 37° C for 30 min. After the incubation time, 1.7 M perchloric acid was added to the reaction solution to precipitate the remaining Hb. After 30 min, the precipitate was removed by centrifugation and the optical absorbance of the filtrate measured at 280 nm. F-prot digests hemoglobin and yields acid soluble products (tryptophan and tyrosine residues) which are readily detected by their strong UV signatures at 280 nm. From the amount of F-prot estimated from the fluorescence studies, specific activity of the enzyme was calculated. For comparison the biocatalytic activity of same concentration of F-prot in solution was recorded. To check the reproducibility of the biocatalytic activity measurements, 10 separate measurements of the F-

prot: colloidal gold bioconjugate material were performed as mentioned above and the average specific activity was calculated. The specific activity of free enzyme in solution was 6.1 units and that of the enzyme immobilized onto colloidal gold surface was  $5.5 \pm 0.4$  units. (One unit of enzyme will produce a change in absorbance at 280 nm of 0.001 per minute at pH = 3.0 and 37 °C measured as acid soluble products using hemoglobin as the substrate). The small standard deviation shows that the results are highly reproducible. A comparison of the specific activities of the free enzyme and enzyme in the bioconjugate solution shows that there is not much decrease in the activity of the enzyme molecules in the bioconjugate system. This is a significant result and shows that the enzymes in the aggregates have not lost their biocatalytic activity. This indicates that the colloidal gold particles stabilize the enzyme molecules within the aggregates.

**Endoglucanase: colloidal gold bioconjugate system.** The biocatalytic activity of endoglucanase: colloidal gold bioconjugate in solution was determined by reaction with an aqueous solution of carboxymethyl cellulose (CMC, 10 mg/mL; 0.05 M sodium-phosphate buffer, pH 7) and incubating the mixture at 60 °C for 1 h. The reducing sugar released was determined by the di-nitro-salicylic-acid (DNSA) method.<sup>24</sup> Five separate measurements of the bioconjugate solutions were performed to check the reproducibility of the data. The concentration of endoglucanase in the bioconjugate system was estimated via fluorescence measurements and by Lowry's method.<sup>23</sup> For comparison, the biocatalytic activity of an identical amount of endoglucanase molecules in solution was determined as described above. The pH dependent variation in the biocatalytic activity measurements of the bioconjugates was studied at six pH values (pH 4, 5, 0.05 M sodium citrate buffer; pH 6, 7, 0.05 M sodium phosphate buffer; pH 8, 9, 0.05 M glycine-NaOH buffer). The values obtained were comparable with that of free enzyme molecules in solution (Table 6.9.1).

**Table 6.9.1**

Comparison of enzymatic activity of *endoglucanase* molecules in solution and after immobilization onto colloidal gold particles using carboxymethyl cellulose (CMC) as the substrate.

<b>pH</b>	<b>Free enzyme in solution Percent activity (%)</b>	<b>Bioconjugate system Percent activity (%)</b>
4	85	85
5	100	100
6	85	95
7	80	81
8	60	63
9	30	35

The reproducibility of the data was confirmed by three separate experiments performed under similar conditions. It is observed from the table that the biocatalytic activity of endoglucanase both in solution as free molecules and in the bioconjugate are comparable at all pH values. Consequently, it is inferred that the active site of the endoglucanase molecules is not blocked upon conjugation with gold nanoparticles.

In addition, the biocatalytic activity of the bioconjugates at pH 7 was tested in the temperature range 40-80 °C and compared with that of identical amount of free enzyme molecules in solution under similar conditions. Three separate measurements at each temperature were performed to check the reproducibility of the data. The data are shown in Table 6.9.2 below. It is seen that the variation in bioactivity of endoglucanase in the bioconjugates with temperature closely follows the trend observed for the free enzyme molecules in solution.

**Table 6.9.2**

Comparison of enzymatic activity of endoglucanase molecules in solution and after immobilization onto colloidal gold particles as a function of temperature

<b>Temperature (°C)</b>	<b>Free enzyme in solution Percent activity (%)</b>	<b>Bioconjugate system Percent activity (%)</b>
40	73	66
50	95	90
60	100	100
70	83	70
80	36	42

The temporal stability of the bio-conjugate was monitored by incubating the bio-conjugates at 60 °C and pH 9 for different time intervals and measuring the activity. This was

compared with an identical amount of free enzyme in solution and the data obtained is shown in Fig. 6.9.1. The data shown as circles in Fig. 6.9.1 corresponds to the residual percent biological activity of the bioconjugate system as a function of time of incubation at 60°C and pH 9. A slow initial loss in the biological activity is seen with a further steady decrease to stabilize at a residual activity of ca. 47 % within 150 minutes. Free enzyme molecules in solution (Fig. 6.9.1, squares) under similar conditions show a rapid initial decrease in the biological activity followed by a steady decrease until stabilization of the residual activity at 42 % after 150 min. The half-life of the enzyme (time required for 50 % loss in biological activity) under these conditions can be estimated from Fig. 6.9.1 to be roughly 120 and 150 min for the free enzyme and bioconjugate respectively. It is clear from the two curves that the bioconjugate system is more stable to temperature effects than free enzyme molecules in solution and shows a higher residual activity at all times at the temperature of 60 °C. This does indicate that the colloidal gold particles in the bioconjugate material play an important role in stabilizing the enzyme molecules from harsh temperature conditions.

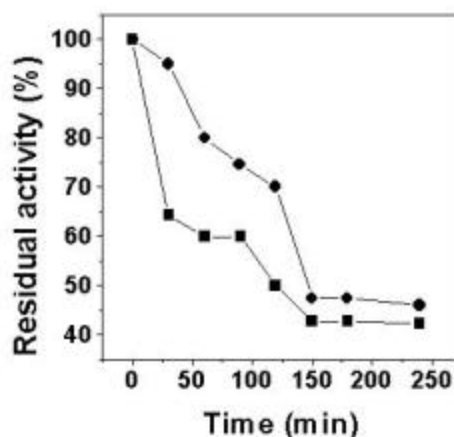


**Figure. 6.9.1:** Specific activity measured as a function of time of incubation of free *endoglucanase* enzyme at pH 9 and 60 °C (squares) and from the *endoglucanase* : Au bioconjugate under identical conditions (circles, see text for details).

## 6.10 SUMMARY

Formation of bioconjugates of the enzyme F-prot and endoglucanase with colloidal gold under enzyme friendly conditions, without enzyme modification and by use of a simple mixing protocol has been demonstrated. The binding of the enzyme with colloidal gold surface is possibly via cysteine or lysine amino acid residues on the enzyme surface. A microscopic analysis of the F-prot: colloidal gold bioconjugate material shows the presence of aggregates of

the enzyme, possibly cross-linked and stabilized by the colloidal particles. On the other hand, endoglucanase: colloidal gold system showed well-dispersed particles. The difference in the two cases might be due to variation in the pH conditions used (pH ~ 3 for F-prot, and pH ~ 5 for endoglucanase) which causes aggregation of the particles. Even though aggregation of the protein was indicated, fluorescence and biocatalytic activity measurements clearly showed that the enzyme on the surface of colloidal gold retains its native conformation and furthermore, that the specific activity of the enzyme in the bioconjugate was comparable to that of the free enzyme in solution. The biocatalytic activity of endoglucanase molecules in the bioconjugate both as a function of pH and temperature of the solution was comparable to free enzyme in solution indicating that the enzyme in the bioconjugate system is present in its natural conformation. The enzyme molecules in the endoglucanase: colloidal gold bioconjugate exhibited a small increase in temporal stability relative to that of the free enzyme in solution at elevated temperatures and suggests possible industrial application for the bioconjugates. Although much work has been done in the area of immobilization of biomolecules on the surface of colloidal polymer particles, we believe this is the first report on direct enzyme immobilization on the surface of inorganic colloidal particles, the enzyme showing excellent catalytic activity in the conjugate material. The technique is general and may be extended to other biomolecules such as nucleic acids and drugs, thus showing immense potential in the areas of drug delivery and immunoassays.

### 6.11. REFERENCES.

1. Rembaum, A.; Dreyer, W.J. *Science* **1980**, *208*, 364.
2. a) Schmitt, A.; Fernandez-Barbero, A.; Cabrerizo-Vilchez, M.; Hidalgo-Alvarez, R. *Prog. Colloid Polym. Sci.* **1997**, *104*, 144; b) Elgersma, A. V.; Zsom, R. L. J.; Norde, W.; Lyklema, J. *J. Colloid Interface Sci.* **1990**, *138*, 145; c) Kamyshny, A.; Magdassi, S. *Coll.Surf.B.*, **1997**, *9*, 147; d) Peula, J.M.; de las Nieves, F.J. *Coll.Surf.A.*, **1993**, *77*, 199; e) Peula, J.M.; de las Nieves, F.J. *Coll.Surf.A.*, **1994**, *90*, 55; f) Molina-Bolivar, J.A.; Ortega-Vinuesa, J.L. *Langmuir* **1999**, *15*, 2644.
3. a) Decher, G.; Hong, J.D. *Ber. Bunsen-Ges. Phys. Chem.*, **1991**, *95*, 1430; b) Decher, G. *Science* **1997**, *277*, 1232; c) Schmitt, J.; Decher, G.; Dressik, W.J.; Brandow, S.L.; Geer,

- R.E.; Shashidhar, R.; Calvert, J.M. *Adv.Mater.*, **1997**, *9*, 61; d) Lvov, Y.; Ariga, K.; Ichinose, I.; Kunitake, T. *J.Am.Chem.Soc.*, **1995**, *117*, 6117; e) Caruso, F.; Niikura, K.; Furlong, D.N.; Okahata, Y. *Langmuir* **1997**, *13*, 3427; f) Caruso, F.; Furlong, D.N.; Ariga, K.; Ichinose, I.; Kunitake, T. *Langmuir* **1998**, *14*, 4559; g) Caruso, F.; Mohwald, H. *J.Am.Chem.Soc.*, **1999**, *121*, 6039; h) Caruso, F.; Schuler, C. *Langmuir* **2000**, *16*, 9595; i) Lvov, Y.; Caruso, F. *Anal. Chem.*, **2001**, *73*, 4212; j) Yang, W.; Trau, D.; Renneberg, R.; Yu, N.T.; Caruso, F. *J. Colloid Interface Sci.*, **2001**, *234*, 356; k) Caruso, F. *Adv. Mater.*, **2001**, *13*, 11.
4. Evans, D.F.; Wennerstrom, H. *The Colloidal Domain*, **1999**, 2<sup>nd</sup> Ed, Wiley-VCH, USA.
  5. a) Henglein, A. *Top. Curr. Chem.* **1988**, *143*, 113; b) Mulvaney, P. *Langmuir* **1996**, *12*, 788; c) Steigerwald, M.L.; Brus, L.E.; *Acc.Chem.Res.*, **1990**, *23*, 183; d) Wang, Y.; Herron, N. *J.Phys.Chem.*, **1991**, *95*, 525; e) Kreibig, U.; Vollmer, M. *Optical properties of metal clusters.*, **1995**, Springer: Berlin; f) El-Sayed, M.A. *Acc.Chem.Res.*, **2001**, *34*, 257.
  6. a) Ghepremi, F.; Kuzyk, M. G.; Lackritz, H. S. *Prog. Polym. Sci.* **1997**, *22*, 1147; b) Colvin, V. L.; Schlamp, M. C.; Alivisatos, A. P. *Nature* **1994**, *370*, 354; c) Alivisatos, A. P. *Science* **1996**, *271*, 933; d) Thomas, J.M. *Pure.Appl.Chem.*, **1988**, *60*, 1517; e) Schon, G.; Simon, U.A. *Colloid.Polym.Sci.*, **1995**, *273*, 202.
  7. a) Hirai, H.; Wakabayashi, H.; Komiyama, M. *Chem.Lett.*, **1983**, 1047; b) Ahmadi, T.; Wang, Z.L.; Green, T.C.; Henglein, A.; El-Sayed, M.A. *Science* **1996**, *272*, 1924; c) Guzzi, L.; Horvath, D.; Paszti, Z.; Toth, L.; Horvath, Z.E.; Karacs, A.; Peto, G. *J. Phys. Chem. B*, **2000**, *104*, 3183; d) Haruta, M.; Ueda, A.; Tsubota, S.; Torres Sanches, R.M. *Catal. Today*, **1996**, *29*, 443.
  8. Niemeyer, C.M. *Angew. Chem. Int. Ed.*, **2001**, *40*, 4128.
  9. a) Dequaire, M.; Degrand, C.; Limoges, B. *Anal. Chem.*, **2000**, *72*, 5521; b) Lyon, L.A.; Musick, M.D.; Natan, M.J. *Anal. Chem.*, **1998**, *70*, 5177; c) Keating, C.D.; Kovaleski, K.M.; Natan, M.J. *J. Phys. Chem. B* **1998**, *102*, 9404; d) Keating, C.D.; Kovaleski, K.M.; Natan, M.J. *J. Phys. Chem. B* **1998**, *102*, 9414; e) Xu, H.; Bjerneld, E. J.; Kall, M.; Borjesson, L. *Phy Rev Lett.* **1999**, *83*, 4357; f) Stonehuerner, J.G.; Zhao, J.; O'Daly, J.P.; Crumbliss, A.L.; Henkens, R.W. *Biosens.Bioelectron.* **1992**, *7*, 421; g) Zhao, J.; O'Daly, J.P.; Henkens, R.W.; Stonehuerner, J.; Crumbliss, A.L. *Biosens.Bioelectron.* **1996**, *11*, 493; h) Crumbliss, A.L.;



- Perine, S.C.; Stonehuerner, J.; Tubergen, K.R.; Zhao, J.; O'Daly, J.P. *Biotech.Bioeng.* **1992**, *40*, 483.
10. a) Gole, A.; Dash, C.; Ramakrishnan, V.; Sainkar, S. R.; Mandale, A. B.; Rao, M.; Sastry, M. *Langmuir* **2001**, *17*, 1674; b) Gole, A.; Dash, C.; Sainkar, S. R.; Rao, M.; Sastry, M. *Bioconjugate Chemistry.*, **2001**, *12*, 684-690; c) Gole, A.; Vyas, S.; Phadtare, S.; Lachke, A.; Sastry, M. *Coll.Surf.B.*, In press.
11. a) Safer, D.E.; Bolinger, L.; Leigh, J.S. *J.Inorg.Biochem.*, **1986**, *26*, 77; b) Safer, D.E.; Hainfeld, J.S.; Wall, J.S.; Reardon, J.E. *Science* **1982**, *218*, 290; c) Bruchez., Jr. M.; Moronne, M.; Gin, P.; Weiss, S.; Alivisatos, A.P. *Science* **1998**, *281*, 2013; d) Chan, W.C.W.; Nie, S.M. *Science* **1998**, *281*, 2016; e) Mattoussi, H.; Mauro, J.M.; Goldman, E.R.; Anderson, G.P.; Sundar, V.C.; Mikulec, F.V.; Bawendi, M.G. *J. Am. Chem. Soc.*, **2000**, *122*, 12142; f) Alivisatos, A.P. *Pure. Appl. Chem.*, **2000**, *72*, 3.
12. a) Alivisatos, A. P.; Johnsson, K. P.; Peng, X.; Wilson, T. E.; Loweth, C. J.; Bruchez, M. P., Jr.; Schultz, P. G. *Nature* **1996**, *382*, 609; b) Mirkin, C.A.; Letsinger, R.L.; Mucic, R.C.; Storhoff, J.J. *Nature* **1996**, *382*, 607; c) Storhoff, J.J.; Mirkin, C.A. *Chem. Rev.*, **1999**, *99*, 1849; d) Storhoff, J.J.; Lazarides, A.A.; Mucic, R.C.; Mirkin, C.A.; Letsinger, R.L.; Schatz, G.C. *J.Am.Chem.Soc.* **2000**, *122*, 4640; e) Dubertret, B.; Calame, M.; Libehaber, A.J. *Nat. Biotechnol.*, **2001**, *19*, 365; f) Elghanian, R.; Storhoff, J.J.; Mucic, R.C.; Letsinger, R.L.; Mirkin, C.A. *Science* **1997**, *277*, 1078; g) Storhoff, J.J.; Elghanian, R.; Mucic, R.C.; Mirkin, C.A.; Letsinger, R.L. *J. Am. Chem. Soc.*, **1998**, *120*, 1959; h) Reynolds, R.A.; Mirkin, C.A.; Letsinger, R.L. *J. Am. Chem. Soc.*, **2000**, *122*, 3795; i) Mirkin, C.A. *Inorg. Chem.* **2000**, *39*, 2258; j) Kumar, A.; Pattarkine, M.; Bhadbhade, M.; Mandale, A.B.; Ganesh, K.N.; Datar, S.S.; Dharmadhikari, C.V.; Sastry, M. *Adv. Mater.*, **2001**, *13*, 341; k) Sastry, M.; Kumar, A.; Datar, S.; Dharmadhikari, C. V.; Ganesh, K.N. *Appl. Phys. Lett.*, **2001**, *78*, 2943; l) Willner, I.; Patolsky, F.; Wasserman, J. *Angew. Chem. Int. Ed.*, **2001**, *40*, 1861; m) Zhou, Y.; Chen, W.; Itoh, H.; Naka, K.; Ni, Q.; Yamane, H.; Chujo, Y. *Chem. Commun.*, **2001**, 2158.
13. a) Vukovic, V.V.; Nedeljkovic, J.M. *Langmuir* **1993**, *9*, 980; b) Patil, V.; Malvankar, R. B.; Sastry, M. *Langmuir* **1999**, *15*, 8197; c) Mie. G.; *Ann. Phys.* **1908**, *25*, 377; d) Creighton, J.A.; Eadon, D.G.; *J. Chem. Soc., Faraday Tras.* , **1991**, *87*, 3881; e) Henglein, A. *J. Phys.*

- Chem.* **1993**, *97*, 5764; f) Alvarez, M. M.; Khoury, J. T.; Schaaf, T. G.; Shafigullin, M. N.; Vezmar, I.; Whetten, R. L. *J. Phys. Chem B.* **1997**, *101*, 3706.
14. Stoscheck, C. M. *Met. Enzymology.* **1990**, *182*, 50.
15. Caruso, F., Furlong, D. N., Ariga, Katsuhiko., Ichinose, I., Kunitake, T. *Langmuir* **1998**, *14*, 4559.
16. Jeffrey, J.W. *Methods in Crystallography*; Academic Press : New York, **1971**.
17. Templeton, A.C.; Chen, S.; Gross, S.M.; Murray, R.W. *Langmuir* **1999**, *15*, 66.
18. a) Mackenzie, L.F.; Davies, G.J.; Schulein, M.; Withers, S.G. *Biochemistry*, **1997**, *36*, 5893; b) Sulzenbacher, G.; Schulein, M.; Davis, G. J. *Biochemistry*, **1997**, *36*, 5902.
19. White, A.; Handler, P.; Smith, E.L.; Hill, R.L.; Lehman, I.R. *Principles of Biochemistry*, Mcgraw-Hill Book Company, **1978**, 82.
20. a) Dong, A.; Huang, P.; Caughey, W.S. *Biochemistry*, **1992**, *31*, 182; b) Kumar, C.V.; McLendon, G.L. *Chem. Mater.*, **1997**, *9*, 863.
21. a) Caruso, F.; Furlong, D.N.; Ariga, K.; Ichinose, I.; Kunitake, T. *Langmuir* **1998**, *14*, 4559; b) Roddick-Lanzilotta, A.D.; Connor, P.A.; Mcquillan, A.J. *Langmuir* **1998**, *14*, 6479.
22. Eftink, M.R.; Ghiron, C. A. *Anal. Biochem.*, **1981**, *114*, 199.
23. Lowry, O.H.; Rasbrough, N.J.; Farar, A.L.; Randall, R.J. *J. Biol. Chem.* **1951**, *193*, 265.
24. Miller, G.L. *Anal. Chem.*, **1959**, *31*, 426.

# CHAPTER VII

## CONCLUSIONS

---

The salient features of the work detailed in the thesis and possible avenues for future work are briefly discussed.

---

### 7.1 SUMMARY OF THE WORK.

Nanotechnology in a broad sense deals with the study of materials in the nano dimensions. This includes the studies on colloidal particles, biomolecules, polymers etc and their interactions with each other. The establishment of efficient synthetic routes for the construction of nanometer-scale architectures/conjugates/materials is of paramount importance if the goals of molecular electronics, sensing, catalysis etc are to be realized.<sup>1</sup> Interdisciplinary work wherein different branches of basic sciences meet is currently the heart of technology. One can draw inspiration from nature, learn how it works, and mimic some of the strategies it uses, for the synthesis of novel and 'smart' materials for the betterment of life as a whole.<sup>2</sup> Prof. Stoddart<sup>1</sup> makes an interesting remark on how the advanced materials synthesized by nature mimicking techniques is different from that of the traditional techniques. He says: "It is somewhat ironic that synthetic chemists have developed *wholly unnatural methods for the synthesis of natural products, yet the wholly unnatural products* required in the quest for molecular electronic devices will be constructed using principles such as self-organization, self-assembly, self-synthesis, and self-replication, which are *natural in origin*". Furthermore, on talking about the progress in the insights gained in understanding and mimicking nature he says: "*Ultimately, chemistry has to tell a "story". The life sciences are composed of really wonderful chemical 'stories'. Chemists are just starting to write their own 'stories'. They know how to produce the 'words'. Now, they are learning how to write the 'sentences'. The 'grammar' they will use will be dictated by the nature of the noncovalent bond. The 'modern languages' are about to evolve. Materials science and the life sciences will be the beneficiaries. As a discipline, chemistry will be enriched.*"

The objective of this thesis is to develop a strategy for the synthesis of efficient biocomposites to gain fundamental insights on protein-lipid interactions on one hand and for possible technological applications on the other. This so-called area of *nanobiotechnology* wherein proteins/enzymes are immobilized onto 2-D and 3-D substrates is a central theme of this thesis. The thesis describes detailed investigations into a new approach for the formation of nanobiocomposites of proteins/enzymes and fatty lipids by a process driven by weak secondary interactions such as electrostatic, hydrophobic and hydrogen bonding interactions. It is shown that a thermally evaporated fatty lipid film, ionized under appropriate conditions, immersed into

protein/enzyme solution, leads to the diffusion of the biomolecules, which can be monitored using a host of techniques. The role of the lipid (cationic/anionic), pH of the solution, thickness of the lipid, preordering of the lipid, charge: mass ratio of the protein etc can be used to control the amount of protein loading under protein-friendly conditions. It has been shown that the protein is intercalated *within the lipid bilayers* and not on the film surface. The natural conformation of the immobilized protein is retained as evidenced by FTIR, fluorescence and biocatalytic activity measurements. The biomimetic nature of the soft lipid host, its inertness, its flexibility which enables it to adopt the contours of the protein guest are the factors primarily responsible for the intactness of the protein structure. The diffusion of the protein in the lipid matrix has been analyzed in terms of a 1-D diffusion model. The diffusivity (D) and the concentration at the interface ( $C_0$ ) values indicate that the diffusion process is governed to a large extent by electrostatic interactions between the host and the guest. The reversibility of the protein diffusion process has also been demonstrated, wherein varying the electrostatic interactions can leach the entrapped protein out. The immobilized biocatalysts show enhanced temporal, temperature and pH stability indicating the protective nature offered by the lipid matrix towards harsh environmental conditions. The biocatalysts have also been immobilized onto 3-D curved surfaces such as that of colloidal gold particles. These bioconjugates also display enhanced stability against harsh external conditions. The possibility of formation of patterned nano-biocomposites of nanoparticles and biomolecules enhances the applicability of the protocol towards the realization of a 'bio-chip' for multiple catalytic and immunosensing devices.

## 7.2 SCOPE FOR FUTURE WORK.

The interesting aspect of our protocol is the formation of protein-lipid biocomposite materials via weak secondary interactions under protein friendly conditions without the necessity of protein modification. This protocol is general and can be extended towards the immobilization of poly nucleic acids, hormones and biological cells. The facility of patterning can be extended towards the patterned immobilization of DNA, and can be used for screening genomic libraries. Multiple enzymes could also be co-immobilized either into the same lipid matrix or into patterns of lipids and could be used for the formation of desired products by a one step reaction, wherein each enzyme would specifically react with its substrate giving desired final product. Preordering

of the lipid films for enhancing the protein diffusivities could be used for enzymes for attaining enhanced biocatalytic activities. Immobilization of different antibodies onto colloidal gold surface would improve immunosensing as the concentration on the curved surfaces would be more, hence improving the output signals.

In conclusion, we have attempted to understand the fundamental principles governing the immobilization of proteins into fatty lipid films. Though electrostatic interactions are the main governing factor for protein immobilization, we believe that other secondary interactions, such as, hydrophobic and hydrogen bonding also participate in such a process. The enhanced stability of the immobilized proteins is due to the bio-friendliness, inertness and flexibility of the lipid bilayers. Through this work we have attempted to design efficient biocomposites for technological applications -which is the ultimate goal of every material scientist working in this area. At the end one interesting remark would say a lot about life and attempts towards enriching it through science.<sup>3</sup> *"Life is, in all probability, a chemical process; but living it is perhaps something that is not even fully accessible to scientific enquiry."*

### 7.3. REFERENCES.

1. a) Philip, D.; Stoddart, J.F. *Angew. Chem. Int. Ed.*, **1996**, 35, 1154; b) Whitesides, G. M. *Sci. Am.*, **1995**, Sept, 114.
2. Fendler, J. H. *Membrane mimetic chemistry*, **1982**, Wiley-Interscience, USA.
3. Ball, P. *Designing the Molecular World : Chemistry at the frontier.*, **1994**, Princeton University Press, New Jersey, USA.